AD NUMBER

AD865319

NEW LIMITATION CHANGE

TO

Approved for public release, distribution unlimited

FROM

Distribution authorized to U.S. Gov't. agencies and their contractors; Administrative/Operational Use; Dec 1969. Other requests shall be referred to Air Force Materials Lab., Attn: MAMC, Wright-Patterson AFB, OH 45433.

AUTHORITY

AFML ltr, 29 Mar 1972

AFML-TR-69-84
PART III. VOLUME I

STABILITY CHARACTERIZATION OF REFRACTORY MATERIALS UNDER HIGH VELOCITY ATMOSPHERIC FLIGHT CONDITIONS

PART III. VOLUME I: EXPERIMENTAL RESULTS OF LOW VELOCITY COLD GAS/HOT WALL TESTS

LARRY KAUFMAN
HARVEY NESOR
ManLabs, Inc.

TECHNICAL REPORT AFML-TR-69-84, PART III, VOLUME I

DECEMBER 1969

AIR FORCE MATERIALS LABORATORY
AIR FORCE SYSTEMS COMMAND
WRIGHT-PATTERSON AIR FORCE BASE, OHIO

NOTICE

When Government drawings, specifications, or other data are used for any purpose other than in connection with a definitely related Government procurement operation, the United States Government thereby incurs no responsibility nor any obligation whatsoever; and the fact that the Government may have formulated, furnished, or in any way supplied the said drawings, specifications, or other data, is not to be regarded by implication or otherwise as in any manner licensing the holder or any other person or corporation, or conveying any rights or permission to manufacture, use or sell any patented invention that may in any way be related hereto.

This document is subject to special export controls and each transmittal to foreign governments or foreign nationals may be made only with prior approval of the Air Force Materials Laboratory MAMC, Wright Patterson Air Force Base, Ohio 45433.

The distribution of this report is limited for the protection of technology relating to critical materials restricted by the Export Control Act.

Copies of this report should not be returned unless return is required by security considerations, contractual obligations, or notice on a specific document.

700 - January 1970 - CO455 - 105-2322

STABILITY CHARACTERIZATION OF REFRACTORY MATERIALS UNDER HIGH VELOCITY ATMOSPHERIC FLIGHT CONDITIONS

PART III. VOLUME I: EXPERIMENTAL RESULTS OF LOW VELOCITY COLD GAS/HOT WALL TESTS

LARRY KAUFMAN

HARVEY NESOR

FOREWORD

This report was prepared by ManLabs, Inc. with the assistance of Arthur D. Little, Inc., Acorn Park, Massachusetts (Dr. Joan B. Berkowitz-Mattuck, Project Leader). This contract was initiated under Project 7312, "Metal Surface Deterioration and Protection," Task 731201, "Metal Surface Protection," and Project 7350, "Refractory Inorganic Nonmetallic Materials," Task Nos. 735001, "Refractory Inorganic Nonmetallic Materials: Non-graphitic," and 735002, "Refractory Inorganic Nonmetallic Materials: Graphitic," under AF33(615)-3859 and was administered by the Metals and Ceramics Division of the Air Force Materials Laboratory, Air Force Systems Command, with J.D. Latva, J. Krochmal and N.M. Geyer acting as project engineers.

This report covers the period from April 1966 to July 1969.

The manuscript of this report was released by the authors in September 1969 for publication.

ManLabs personnel participating in this study included L. Kaufman, H. Nesor, H. Bernstein, E. Peters, J.R. Baron, G. Stepakoff, R. Pober, R. Hopper, R. Yeaton, S. Wallerstein, E. Sybicki, J. Davis, K. Meaney, K. Ross, J. Dudley, E. Offner, A. Macey, A. Silverman and A. Constantino.

This technical report has been reviewed and is approved.

W. G. Ramke
Chief, Ceramics and Graphite Branch
Metals and Ceramics Division
Air Force Materials Laboratory

The following reports will be issued under this contract.

Part/Volume	
I-I	Summary of Results
II-I	Facilities and Techniques Employed for Characterization of Candidate Materials
II-II	Facilities and Techniques Employed for Cold Gas/Hot Wall Tests
II-III	Facilities and Techniques Employed for Hot Gas/Cold Wall Tests
III-I	Experimental Results of Low Velocity Cold Gas/Hot Wall Tests
III-II	Experimental Results of High Velocity Cold Gas/Hot Wall Tests
III-III	Experimental Results of High Velocity Hot Gas/Cold Wall Tests
IV-I	Theoretical Correlation of Material Performance with Stream Conditions
IV-II	Calculation of the General Surface Reaction Problem

ABSTRACT

The oxidation of refractory borides, graphites and JT composites, hypereutectic carbide-graphite composites, refractory metals, coated refractory metals, metal oxide composites, and iridium coated graphites in air was investigated over the spectrum of conditions encountered during reentry or high velocity atmospheric flight, as well as those employed in conventional furnace tests. Elucidation of the relationship between hot gas/cold wall (HG/CW) and cold gas/hot wall (CG/HW) surface effects in terms of heat and mass transfer rates at high temperatures is a principal goal.

Furnace oxidation results in flowing air at 0.9 to 7.2 ft/sec for times up to four hours at temperatures between 1150° and 4200°F are presented for 30 candidate materials including the refractory borides, carbides, boride composites, boride-graphite composites (JTA), JT composites, carbide-graphite composites, pyrolytic and bulk graphite, PT graphite, coated refractory metal/alloys, oxide-metal composites, oxidation-resistant refractory metal alloys and coated graphites. Temperature limits for coated materials, viscous flow of metal-oxide composites and effects of cyclic heating and cooling exposures are reported. Results are presented for exposures in flowing argon between 3000° and 4200°F. These data are complemented by the results of oxygen pickup and gas analysis tests on JT composites, silicide coated tungsten and a series of binary and ternary iridium-base alloys which were heated by induction in oxygen-helium mixtures flowing at 0.2 ft/sec. Failure conditions were established for the silicide coating on tungsten at oxygen partial pressures of 0.031 and 0.20 atmospheres.

TABLE OF CONTENTS

LIST OF ILLUSTRATIONS

LIST OF TABLES

I. INTRODUCTION AND SUMMARY

A. Introduction

The response of refractory materials to high temperature oxidizing conditions imposed by furnace heating has been observed to differ markedly from the behavior in arc plasma "reentry simulators." The former evaluations are normally performed for long times at fixed temperatures and slow gas flows with well-defined solid/gas-reactant/product chemistry. The latter on the other hand are usually carried out under high velocity gas flow conditions in which the energy flux rather than the temperature is defined and significant shear forces can be encountered. Consequently, the differences in philosophy, observables, and techniques used in the "material centered" regime and the "environment centered, reentry simulation" area differ so significantly as to render correlation of material responses at high and low speeds difficult if not impossible in many cases. Under these circumstances, expeditious utilization of the vast background of information available in either area for optimum matching of existing material systems with specific missions or prediction and synthesis of advanced material systems to meet requirements of projected missions is sharply curtailed.

In order to progress toward the elimination of this gap, an integrated study of the response of refractory materials to oxidation in air over a wide range of time, gas velocity, temperature and pressure has been designed and implemented. This interdisciplinary study spans the heat flux and boundary layer-shear spectrum of conditions encountered during high-velocity atmospheric flight as well as conditions normally employed in conventional materials centered investigations. In this context, significant efforts have been directed toward elucidating the relationship between hot gas/cold wall HG/CW and cold gas/hot wall CG/HW surface effects in terms of heat and mass transfer rates at high temperatures, so that full utilization of both types of experimental data can be made.

The principal goal of this study is the coupling of the material centered and environment centered philosophies in order to gain a better insight into systems behavior under high speed atmospheric flight conditions. This coupling function has been provided by an interdisciplinary panel composed of scientists representing the component philosophies. The coupling framework consists of an intimate mixture of theoretical and experimental studies specifically designed to overlap temperature/energy and pressure/velocity conditions. This overlap has provided a means for the evaluation of test techniques and the performance of specific materials systems under a wide range of flight conditions. In addition, it provides a base for developing an integrated theory or modus operandi capable of translating reentry systems requirements such as velocity, altitude, configuration and lifetime into requisite materials properties as vaporization rates, oxidation kinetics, density, etc., over a wide range of conditions.

The correlation of heat flux, stangation enthalpy, Mach No., stagnation pressure and specimen geometry with surface temperature through the utilization of thermodynamic, thermal and radiational properties of the material and environmental systems used in this study was of prime importance in defining the conditions for overlap between materials-centered and environment-centered tests.

Significant practical as well as fundamental progress along the above mentioned lines necessitated evaluation of refractory material systems which exhibit varying gradations of stability above 2700°F. Emphasis was directed towards candidates for 3400° to 6000°F exploitation. Thus, borides, carbides, boride-graphite composites (JTA), JT composites, carbide-graphite composites, pyrolytic and bulk graphite, PT graphite, coated refractory metals/alloys, oxide-metal composites, oxidation-resistant refractory metal alloys, and coated graphites were considered. Similarly, a range of test facilities and techniques including oxygen pickup measurements, cold sample hot gas, and hot sample cold gas devices at low velocities, as well as different arc plasma facilities capable of covering the 50-2500 BTU/ft^{2}sec flux range under conditions equivalent to speeds up to Mach 12 at altitudes up to 200,000 feet were employed. Stagnation pressures employed ranged between 0.001 and 10 atmospheres. Splash and pipe tests were performed in order to evaluate the effects of aerodynamic shear. Based on the present results, this range of heat flux and stagnation enthalpy produced surface temperatures between 2000° and 6500°F.

This report describes the results obtained for the Cold Gas/Hot Wall tests performed at ManLabs and Arthur D. Little employing facilities described elsewhere (1)*. Low velocity testing was performed at ManLabs, Inc. under the direction of H. Nesor. Air flowing at 0.9 to 9.0 ft/sec was employed in resistance heated tube furnaces at temperatures between 1000° and 4200°F. Exposure times ranging from five minutes up to four hours were used to evaluate the behavior of the candidate materials. Post exposure metallographic examination of samples disclosed the extent of oxidation. Temperature measurement within the tube furnaces was carried out by means of optical brightness and two color pyrometry and checked by measurements of the melting temperature of several materials.

Low velocity tests of inductively heated samples were performed at Arthur D. Little under the direction of J.B. Berkowitz-Mattuck. These exposures were carried out in oxygen-helium mixtures at flow rates of 0.2 ft/sec with oxygen monitored by measuring the rate at which oxygen was removed from the stream for times up to one hour. These measurements were complemented by measurements of CO and CO_2 formation. Post-exposure metallographic measurements were employed to check and supplement the gas analysis data. Optical brightness measurements were employed to measure the surface temperature by employing suitable emittance corrections.

---

*The underscored numbers in parenthesis refer to references listed at the end of this report.

B. Summary of Results

Air oxidation test data generated in CG/HW furnace tests are presented for most of the candidate materials. Test conditions covered temperatures between 1150° and 4200°F, times from five minutes to four hours and air flow rates between 0.9 and 9.0 ft/sec. Cyclic exposures were performed for most of the candidates. Temperature limits of 3060°, 3200° and 3450°F were found for Si/RVC(B-8), Sn-Al/Ta-10W(G-19) and WSi_2/W(G-18), respectively. Supply limited oxidation at rates of 0.2-0.3 mils/sec for temperatures between 2800° and 4100°F in air at one atmosphere was noted for RVA(B-5), PG(B-6), BPG(B-7), PT0178(B-9) and AXF-5Q Poco(B-10) graphites. The arc cast hypereutectic carbides HfC+C(C-11) and ZrC+C(C-12) exhibit surprisingly constant recession levels of 50-100 mils for one hour exposures between 1200° and 4200°F. A transition from puffy to adherent oxide occurs above 3450°F for the carbides. The SiO_2 + 35 w/oW(H-24) composite was observed to flow at temperatures above 3000°F. By contrast, the SiO_2+68.5 w/o W(H-22) and SiO_2+60 w/o W(H-23) composites exhibit low oxidation rates at temperatures between 3200° and 3900°F, above which viscous flow occurs. The hypereutectic carbides HfC+C(C-11) and ZrC+C(C-12) and the SiO_2+W(H-22) and (H-23) composites are susceptible to oxidation at low temperatures (1200°-2500°F) where protective oxides do not form. KT-SiC(E-14) exhibits low recession up to 3450°F, and rapid degradation above 3500°F.

The HfB_2+20%SiC(A-4), $HfB_{2.1}$+20%SiC(A-7) and $HfB_{2.1}$+35%SiC (A-9) composites exhibit the lowest overall recessions up to 3800°F, above which complete depletion of SiC occurs and rates are comparable to $HfB_{2.1}$ (A-2) and (A-6). HfB_2 base materials show lower recession values than the ZrB_2 base materials - ZrB_2(A-3), Boride Z(A-5), ZrB_2+14%SiC+30%C(A-10) and ZrB_2+20%SiC(A-8) which are listed in order of increasing oxidation resistance. JT0992(C-HfC-SiC)(F-15) exhibits better oxidation resistance than does JT0981(C-ZrC-SiC)(F-16), which in turn is superior to JTA(C-ZrB_2-SiC)(D-13). However, the former composites show substantially higher rates than JTA (D-13) below 3000°F since they do not contain boron and the graphite can oxidize freely. Above 3000°F, JT0992(F-15) exhibits conversion depths comparable to HfB_2(A-2) and JT0981(F-16) is similarly comparable to ZrB_2(A-3). Hf-20Ta-2Mo(I-23) is as oxidation resistant as (A-3) and (F-16), but melts near 3850°F.

Kinetic studies indicate protective behavior over a two hour period at the following temperatures for: $HfB_{2.1}$(A-2)-3700°F, ZrB_2 (A-3)-3400°F, HfB_2+20%SiC(A-4) and (A-7)-3790°F, $ZrB_{2.1}$+20%SiC (A-8)-3750°F, ZrB_2+SiC+C(A-10)-3600°F, HfC+C(C-11)-4000°F, ZrC+C(C-12)-3600°F, JTA(D-13)-3250°F, KT-SiC(E-14)-3450°F, JT0992(F-15)-3520°F, JT0981(F-16)-3390°F, SiO_2+60w/oW(H-23)-3850°F, Hf-20Ta-2Mo(I-23)-3380°F. Comparison of the recessions after two hour continuous exposures with the results obtained after four, thirty minute periods interrupted by cooling cycles yielded similar results for $HfB_{2.1}$(A-2), ZrB_2 (A-3), HfB_2+20%SiC(A-4), Si/RVC(B-8), HfC+C(C-11), ZrC+C(C-12), JTA (D-13), JT0992(F-15), JT0981(F-16), WSi_2/W(G-18) and Sn-Al/Ta-10W (G-19). In each case, the exposure temperature did not exceed the two hour protection limit or failure temperature for coatings. More rapid degradation was observed for KT-SiC(E-14), SiO_2+ 68.5w/oW(H-22), SiO_2+60w/oW (H-23) and Hf-20Ta-2Mo(I-23). Seven of the candidate materials were tested

in larger tube furnaces than usually employed (2 inch vs. 7/8 inch inside diameters). $HfB_{2.1}$(A-2) and ZrB_2(A-3) recession results were independent of test facility but more rapid oxidation was observed for $HfB_{2.1}$+ 20%SiC(A-4) and (A-7), JTA(D-13), KT-SiC(E-14), JT0992(F-15), JT0981(F-16) and Hf-20Ta-2Mo(I-23) in large furnace tests. These differences are most probably due to differences in air supply.

Six materials were heated in flowing argon for one hour between 3000° and 4200°F. Negligible changes in JT0992(F-15) and JT0981 (F-16) occurred. JTA(D-13) exhibited changes in internal structure suggestive of melting in the ZrB_2-SiC phases at 4200°F. Exposure of WSi_2/W(G-18) above 3500°F resulted in melting of the coating. Testing of SiO_2+60w/oW (H-23) between 3800° and 4000°F resulted in cracking and evidence of SiO_2 sublimation. PT0178(B-9) graphite was not affected.

Oxygen pickup and gas analysis studies were performed on JTA(D-13), JT0992(F-15), JT0981(F-16), WSi_2/W(G-18) and a series of iridium-base alloys between 2900° and 4275°F and at oxygen partial pressures of 10 to 150 Torr in oxygen-helium mixtures at flow rates of 0.2 ft/sec (CG/HW). The graphite composites exhibit protective oxidation at 2900°F and linear oxidation at 3500°F, although at 2900°F, 40 Torr O_2 is required to provide a protective oxide for JTA(D-13). Thus at temperatures where protective oxidation occurs, raising the oxygen pressure can lower the rate of oxidation. However, at higher temperatures where oxidation is linear (i.e., at or above 3500°F) raising the pressure increases the rate. In testing of WSi_2/W(G-18) at an oxygen partial pressure of 10 Torr, protective oxidation is not observed above 3500°F unless a protective film is formed first by oxidation at lower temperatures. Under such conditions, protection can be retained to 3500°F. At one atmosphere, failure was noted at 3560°F. The temperature and pressure ranges over which protective oxidation of WSi_2/W (G-18) is observed are discussed in terms of initial formation of WO_3(g) and SiO_2(s) followed by preferential oxidation of silicon to form lower silicides and finally W at the oxide/alloy interface. Failure to form a protective SiO_2 layer at low oxygen pressures and the rupturing of existing SiO_2 films by SiO(g) evolution are considered as mechanisms operative during nonprotective oxidation of WSi_2/W(G-18).

Several binary and ternary iridium-base alloys were tested at 4000°F in 53% oxygen-47% helium at one atmosphere and a 0.2 ft/sec flow rate. Comparative results indicate that rhodium additions offer the greatest resistance against oxidation while platinum and rhenium confer only moderate resistance. Osmium additions reduce oxidation resistance. It should be noted that rhenium raises the iridium-carbon eutectic temperature, while platinum and rhodium lower it.

II. RESULTS OF FURNACE OXIDATION TESTS (CG/HW)

A. Introduction

Air oxidation tests have been performed for most of the candidate materials listed in Table 1. Details of the apparatus and procedures employed are given in Part II-Volume II of this series (1), and characterization data on the candidate materials are presented in Part II-Volume I (2). In general, single samples mounted on zirconia pedestals are placed into the furnace which is at room temperature. The samples are heated to test temperature in flowing argon. When temperature is reached, the argon is turned off and air is turned on. Air flow rates between 0.9 and 9.0 ft/sec at one atmosphere have been used for times from five minutes to four hours. Testing temperatures between 1150°F and 4200°F have been employed. After the required time has elapsed, the furnace power and air are turned off and argon is reintroduced during cooling of the sample. Most of the candidate materials have been subjected to cyclic heating and cooling exposures, which generally involved four - thirty minute periods at elevated temperature with intermediate furnace cooling to below 500°F between each elevated temperature cycle. The conversion depth, or extent to which oxidation takes place during exposure, was determined by post-exposure metallography. Material recessions were measured both for length and diameter of the cylindrically-shaped samples. All conversion depths reported below are the maximum value, rather than the average of the two measurements, since significant differences have been noted between longitudinal and transverse values, particularly in samples having conversion depths greater than 100 mils.

B. Oxidation Results

Oxidation data have been generated for all candidate materials listed in Table 1 with the exception of Glassy Carbon(B-11), W+Zr+Cu(G-20), W+Ag(G-21) and Ir/C(I-24). A complete tabulation of exposure conditions and recession measurements is given in Tables 2-9. Figures 1-7 show variation of maximum conversion depth with temperature* and air flow rate for these conditions. Figures 8-15 illustrate time dependence of oxidation at fixed temperature and air flow rate. In some instances, the large furnaces (2 inch inside diameter) were used to test several samples simultaneously, withdrawing each specimen after a given time interval without cooling the furnace. The results have led to the following conclusions:

1. $HfB_{2.1}$(A-2) and $HfB_{2.1}$(A-6)

Tables 2 and 5 and Figures 1, 8, 12 and 14 summarize the results obtained following CG/HW air oxidation furnace tests on hafnium diboride. One hour exposures in flowing air have been performed at temperatures between 1200°F and 4100°F. The results which are shown in Figure 1 refer to exposures conducted in the small furnaces (7/8 inch inside diameter). $HfB_{2.1}$(A-2) appears to oxidize more rapidly at temperatures below 3200°F

*Temperatures were measured with LATRONICS COLORATIO Automatic Two-Color Pyrometers or with a MILLETRON Therm-O-Scope Automatic Two-Color Pyrometer. Instruments were calibrated weekly against a tungsten filament bulb.

than $HfB_{2.1}$(A-6) and the hafnium borides having B/Me = 1.7-2.1 (3,4). Reference to Figure 1 shows that the one hour conversion depth becomes insensitive to temperature above 3600°F. The reason for this insensitivity is not clear. In all cases, the quantity of air flowing through the furnace exceeded that required to oxidize the samples by a substantial amount. It is possible, however, that the supply of oxygen available at the gas/oxide interface is limited by the transport rate or diffusion of oxygen molecules through the gas. In a case where the observed conversion depth is limited by the air velocity (i.e., where increasing air velocity increases the conversion depth), the rate is defined to be supply limited.* By contrast, if the observed oxidation rate is independent of both air velocity and temperature, the oxidation rate may be limited by diffusion of oxygen through the gas. In the present case, the conversion depth for one hour exposures of $HfB_{2.1}$(A-2) at temperatures above 3600°F does not seem strongly dependent upon air velocities between 0.9 and 7.2 ft/sec. Thus, the reaction may be diffusion limited above 3600°F. Figures 16-19 show post-exposure photomicrographs of exposure $HfB_{2.1}$(A-2), Test 1356, and $HfB_{2.1}$(A-6), Test 367. An adherent oxide and uniform conversion of boride to oxide is indicated in both cases.

Kinetic studies have been performed at temperatures between 3350° and 4000°F for times between 15 and 120 minutes. Figure 8 shows results obtained in the small furnace (7/8 inch inside diameter tube), while Figure 12 shows results obtained in the large furnace (2 inch inside diameter tube). A comparison of "small" and "large" furnace results is contained in Figure 14. These figures indicate protective behavior** between 3350° and 4000°F with little dependence on furnace size although conversion depths in the "large" furnace appear to be very slightly larger. Two hour conversion depths are relatively insensitive to temperature above 3600°F.

Test 858 (Table 2) consisted of four - thirty minute cycles at 3590°F on $HfB_{2.1}$(A-2). A conversion depth of 116 mils was obtained. This is approximately equal to the value indicated by the non-cyclic kinetic studies so that alternate heating and cooling appear to have little effect on this material. Several low temperature exposures (Tests 863, 866, 867 and 868, Table 2) were performed between 1200° and 2700°F to verify the expected low rates of oxidation under these conditions. These tests, when combined with the results illustrated in Figure 1, show that the oxidation rates of $HfB_{2.1}$(A-2) and $HfB_{2.1}$(A-6) increase with increasing temperature.

---

* This supply limit may be caused by furnace geometry and air flow rate. As a consequence it is not a unique characteristic of the material.

** The meaning of the term "protective behavior" as employed here in describing the oxidation of bulk materials implies rates which decrease with time. This term is used in contrast to "nonprotective" behavior in which the oxidation rate is constant.

2. ZrB_2(A-3)

The data for zirconium diboride are displayed in Table 2 and Figures 1, 8, 12 and 14. One hour exposures in flowing air have been performed at temperatures between 1200° and 4200°F. Recession values for ZrB_2(A-3) are in general agreement with those for ZrB_2 prepared by ManLabs and Avco under AF33(615)-3671 (3), and are somewhat larger than values obtained for hafnium diborides. An insensitivity to temperature above 3500°F is also indicated, comparable to that discussed above for $HfB_{2.1}$(A-2). Post-exposure photomicrographs are shown in Figures 20 and 21. The oxide formed on ZrB_2(A-3) tends to chip off easily and is generally not as adherent as that formed on hafnium diborides.

Kinetic studies have been performed between 3260° and 3560°F for times up to two hours. Figures 8, 12 and 14 illustrate the small furnace, large furnace, and comparative results respectively. Protective behavior is observed at temperatures up to 3400°F for one hour. At higher temperatures, and for longer times at 3400°F, behavior becomes nonprotective. Similar results are obtained in both furnaces. Four - thirty minute cycles at 3206°F (Test 935, Table 2) yield a maximum conversion depth of 40 mils which is in agreement with the two hour kinetic experiments. Low temperature exposures between 1200° and 2700°F (Tests 900, 902, 904 and 905, Table 2) indicate the expected low rates of oxidation. Combination of these results with those at higher temperatures show that zirconium diboride exhibits an increasing rate of oxidation with increasing temperature.

3. HfB_2+20%SiC(A-4), $HfB_{2.1}$+20%SiC(A-7) and $HfB_{2.1}$+35%SiC(A-9)

The results for hafnium diboride-silicon carbide composites are presented in Tables 3 and 4 and in Figures 1, 8, 12 and 14. The tables give silicon carbide depletion depths as well as diboride conversion depths. The depletion depth is the distance from the outer surface over which silicon carbide is removed during exposure. Composites containing silicon carbide are observed to form clear bubbles of silica during an exposure. These bubbles will expand and burst during a test until the silicon carbide is completely removed. Post-exposure examination of such samples reveal that a glassy oxide remains on the surface along with the white oxide formed due to diboride oxidation.

One hour exposures have been performed at temperatures between 1200° and 4200°F. These agree with results obtained under AF33-(615)-3671 (3). No real distinction can be made between the three composites, although $HfB_{2.1}$+35%SiC(A-9) may yield slightly lower recession values than the composites containing 20%SiC. The oxidation rates for the composites are markedly slower than for $HfB_{2.1}$(A-2) and (A-6) with virtually no oxidation taking place below 3200°F.* Figure 22 illustrates the variation of depletion

*Tests run at 2400°F for 150 hours indicate that $HfB_{2.1}$+20%SiC(A-7) exhibits only several mils conversion and no preferential oxidation of silicon carbide(5).

depth with time for HfB_2+20%SiC(A-4). At 3575°F, the conversion depth shows almost no time dependence up to 120 minutes. However, at 3685°F and above the depletion depth increases rapidly after one hour. Thus, after one hour exposures at temperatures above 3800°F, complete depletion of silicon carbide has occurred for 1/2 inch cylindrical samples, and recession values become comparable to pure hafnium diboride.

Figures 23-28 show post-exposure sections of the hafnium diboride-silicon carbide composites. The absence of silicon carbide in the depleted zone beneath the oxide is clearly visible. At temperatures equal to or less than 3800°F, the oxide is quite adherent to the diboride core. Above 3800°F, the oxide is found to be separated from the diboride core or cracked after cooling to room temperature. In cases where a sample has been partially depleted of silicon carbide, radial cracks are often found in the depleted zone, as illustrated in Figures 29 and 30.

Kinetic studies have been performed for HfB_2+20%SiC (A-4) in the large furnace between 3565° and 4000°F, and for $HfB_{2.1}$+20%SiC (A-7) in the small furnace between 3550° and 3900°F. The latter results are presented in Figure 8, the former in Figure 12, and a comparison is contained in Figure 14. The comparison shows somewhat lower recession values at 3900°F in the small furnace tests on (A-7), where protective behavior is observed over a two hour period. Non-protective oxidation is observed in large furnace tests on (A-4) after one hour at 3894°F. Cyclic exposures on HfB_2+20%SiC(A-4) at 3600°F and 3900°F (Tests 1061 and 952, Table 3) indicate little difference when compared with two hour kinetic results at 3600°F, but enhanced oxidation at 3900°F. Tests at temperatures between 1200° and 2700°F yielded virtually no oxidation and little depletion. These composites generally exhibit increasing oxidation rates with increasing temperature.

4. Boride Z(A-5), $ZrB_{2.1}$+20%SiC(A-8) and ZrB_2+14%SiC+30%C(A-10)

The results of furnace oxidation tests for the zirconium diboride-base composites are presented in Tables 4 and 5, and displayed in Figures 1, 2, 8 and 9. Comparison of ZrB_2(A-3) with the (A-5), (A-8) and (A-10) composites indicates comparable behavior after one hour exposures above 3800°F similar to the behavior of hafnium diboride versus its composites. Below this temperature, the silicon carbide additions become effective over one hour periods and the composites show increased resistance to oxidation relative to pure ZrB_2. $ZrB_{2.1}$+20%SiC(A-8) appears to be most resistant to oxidation followed by ZrB_2+14%SiC+30%C(A-10) and Boride Z (A-5). Post-exposure photomicrographs are shown in Figures 31-36. The (A-8) and (A-10) exposures exhibit depletion zones, uniform oxidation and adherent, glassy oxides. The (A-5) exposure shows nonuniform oxidation and a nonadherent oxide. The zirconium diboride-base composites exhibit slightly higher recession and depletion rates than the hafnium diboride-base composites.

Kinetic studies for times up to two hours have been performed in the small furnaces for ZrB_2+20%SiC(A-8) between 3515° and 3850°F and for ZrB_2+14%SiC+30%C(A-10) between 3500° and 3764°F. Protective behavior is observed after two hours at 3700°F and one hour at 3850°F for the (A-8) composite. Rapid oxidation takes place for longer times at 3850°F due to the complete loss of silicon carbide after one hour at this temperature. The (A-10) composite exhibits protective behavior for one hour at 3650°F but non-protective behavior after longer times at 3650°F or at higher temperatures. These results are illustrated in Figures 8 and 9.

Cyclic exposures were not performed on these composites. Low temperature exposures on ZrB_2+14%SiC+30%C(A-10) between 1200° and 2800°F (Tests 1259, 1260 and 1261, Table 4) indicated extremely small conversion depths and virtually no depletion. Thus, the zirconium diboride-base composites exhibit increasing oxidation rates with increasing temperature as well as higher overall oxidation rates than their hafnium diboride-base counterparts.

5. RVA(B-5), PG(B-6), BPG(B-7), PT0178(B-9) and AXF-5Q Poco(B-10) Graphites

Table 5 and Figures 2 and 3 summarize the results obtained for the graphite candidate materials. The oxidation rates for these materials are insensitive to temperature changes between 2800° and 4200°F. Little effect of flow rate is observed between 0.9 and 3.6 ft/sec. However, higher rates of oxidation are observed as the rate is increased to 7.2 and 9.0 ft/sec. These results indicate that air oxidation at 1-9 ft/sec is supply limited at a rate of 0.2-0.3 mils/sec for all of the graphite candidates with the exception of PT0178(B-9). This is due to the lower density of this material. When these results are compared with those of high velocity CG/HW tests and HG/CW arc plasma tests presented in other reports of this series (6,7,8)*, it is apparent that the oxidation rates are controlled by the testing environment to a greater extent than by the oxidation kinetics.

Post-exposure photomicrographs of the graphites are presented in Figures 37-46. The longitudinal and transverse sections shown for RVA(B-5), PG(B-6) and BPG(B-7), Figures 37-42, indicate their relative densities with the pyrolitic materials (B-6) and (B-7) having higher densities than (B-5). The longitudinal section of BPG(B-7) (Test 207, Table 5) shown in Figure 41 indicates incipient delamination. The BPG(B-7) material showed a greater frequency of this behavior than PG(B-6). Figures 43 and 44 show typical post-exposure photomicrographs of PT0178(B-9). Its random fibrous structure is clearly evident and uniform oxidation is thus observed. Figures 45 and 46 show post-exposure photomicrographs of AXF-5Q Poco(B-10). The

*An extensive discussion of this problem is given in Reference (8). CG/HW and HG/CW results are presented in References (6) and (7) respectively.

extremely fine grain size of this material is illustrated by electron micrographs, Figures 47 and 48, at 13000X. These show two levels of structure at approximately 0.05 mils and 0.002 mils.

There have been no kinetic, cyclic or low temperature studies performed on the graphite candidates.

6. Siliconized RVC Graphite, Si/RVC(B-8)

Air oxidation results for Si/RVC(B-8), consisting of a four mil coating of SiC on RVC graphite, are given in Table 6 and Figure 3. The coating provides protection for one hour at 3100°F. Above this temperature, the coating flows and failure occurs leading to graphite-type oxidation rates. Coating failures were observed for all exposures above 3100°F. Figures 49 and 50 show post-exposure photomicrographs of Test 1048 after one hour at 2806°F at an air flow rate of 1.8 ft/sec. The coating system survived these conditions.

Kinetic studies were performed at 3016° and 3102°F for times between 15 minutes and two hours. No coating failures were observed at the lower temperature, but a partial coating failure occurred during the second hour at 3102°F. Four - thirty minute cycles at 2974°F (Test 866, Table 6) did not lead to failure, but failure did occur during the fourth cycle at 3098°F (Test 1101) which agrees with the kinetic results at this temperature.

7. HfC+C(C-11) and ZrC+C(C-12)

Table 6 and Figures 4 and 9 contain the results for the hypereutectic carbide candidate materials. The results of one hour exposures between 1200° and 4200°F show little change of conversion depth with temperature. Recession values averaging 60 mils for HfC+C(C-11) and 80 mils for ZrC+C(C-12) are obtained over the entire temperature range with slight decreases in rate near 3450°F. Post-exposure examination of these materials reveals that the heavy oxide which forms is "puffy" below 3450°F. However, above this temperature a dense, adherent oxide forms. This behavior is illustrated in Figures 51-56 which show the results of Tests 973 and 987 for HfC+C(C-11) at 3279° and 4054°F, and Tests 988 and 1031 for ZrC+C(C-12) at 3058° and 3645°F. This transition in behavior (from puffy to adherent oxide) undoubtedly gives rise to the flat conversion depth vs. temperature curves shown in Figure 4. Thus, oxidation may be supply limited at low temperatures. Reference to Figures 53-56 shows that preferential oxidation of the primary graphite flakes occurs and that the oxides contain voids which correspond to the original location of the graphite flakes. No clear dependence on air flow rate was observed between 0.9 and 7.2 ft/sec for the hypereutectic carbides.

Kinetic studies performed in the small furnaces at temperatures between 2800° and 4000°F for times up to two hours reveal the very interesting result that the oxidation rate of HfC+C(C-11) decreases with increasing temperature between 2800° and 3600°F. Above 3800°F, the rate increases with temperature, as shown in Figure 9. Similar results are noted for ZrC+C(C-12) which exhibits a decrease in oxidation rate between 2800° and 3400°F, and an increase in rate above 3600°F. These observations

are consistent with the transition in the adherence of the oxide noted above. Obviously, the puffy oxide existing below 3450°F does not afford protection whereas the more dense oxide formed above 3450°F does protect the hyper-eutectic carbides and improves their resistance to oxidation. Cyclic exposures on HfC+C(C-11) and ZrC+C(C-12) (Tests 1114 and 1120, Table 6, respectively) yielded identical results to those obtained in the two hour kinetic tests.

8. JTA(C-ZrB_2-SiC)(D-13), KT-SiC(E-14), JT0992 (C-HfC-SiC)(F-15) and JT0981(C-ZrC-SiC)(F-16)

Tables 6, 7 and 8 and Figures 5, 6, 10, 13 and 15 present the data for silicon carbide and the JT-composites. At low temperatures, JT0992(F-15) and JT0981(F-16) exhibit high oxidation rates due to their high graphite content and the fact that HfC or ZrC, and SiC cannot contribute protective oxides below 2800°F. By contrast, JTA(D-13) exhibits much lower oxidation depths between 1200° and 2700°F due to the formation of B_2O_3. Based on these observations, and those preceding for the hyper-eutectic carbides, it appears that SiC additions contribute oxidation protection above 2800°F, HfC/ZrC additions supply protection above 3400°F, while the presence of boron is required to protect graphite below 2800°F. Variation of air flow rate between 0.9 and 7.2 ft/sec has little effect on JT0981(F-16). However, JTA(D-13) and JT0992(F-15) show a marked dependence on air flow rate suggesting a supply limited reaction for these composites. The results of arc plasma exposures (7) at Mach 0.3-0.5 and one atmosphere stagnation pressure at temperatures between 3500° and 4000°F are in agreement with this conclusion.

Typical post-exposure microstructures of the JT-composites are shown in Figures 57-62. The three matrix phases are clearly distinguishable in each case. X-ray diffraction analysis of the oxide coatings revealed the presence of monoclinic ZrO_2 plus some lines which could be indexed as ZrC in JTA(D-13), and only monoclinic HfO_2 and ZrO_2 in JT0992 (F-15) and JT0981(F-16).

Kinetic studies have been performed in both large and small furnaces for these materials. Figure 10 illustrates the small furnace results, Figure 13 the large furnace, and Figure 15 compares the two. It is clear that oxidation rates for the JT-composites are extremely sensitive to the testing facility. JTA(D-13) exhibits protective behavior at 3400°F and linear behavior at 3500°F in the small furnace while linear behavior at 3350°F is observed in the large furnace. JT0992(F-15) exhibits linear behavior in large furnace tests at 3616°F but protective behavior at 3600°F and borderline behavior at 3700°F in small furnace tests. JT0981(F-16) exhibits linear behavior in large furnace tests at 3573°F but borderline behavior at 3600°F in the small furnace. The higher rates of oxidation noted in the large furnace may be due to air supply or temperature differences, the former most probably being the case although this conclusion has not been validated. Samples tested for 120 minutes in both facilities, however, should not show temperature differences since pyrometers are monitoring their temperatures continuously.

Cyclic exposures of JTA(D-13) at 2894°F (Test 945, Table 7) using four - thirty minute cycles yielded a conversion depth of 14 mils as compared with 8 mils after two hours of uninterrupted exposure. Cyclic

exposures of JT0992(F-15) at 3518°F (Test 914, Table 7) and JT0981(F-16) at 3450°F (Test 842, Table 8) yielded virtually identical results to those obtained for uninterrupted tests. Consequently, it appears that cyclic exposures do not produce additional oxidation as compared with uninterrupted exposures at temperatures where protective oxidation takes place.

The results for KT-SiC(E-14) are presented in Table 6 and Figures 5, 10, 13 and 15. One hour exposures indicate rapid degradation above 3500°F. In addition, Tests 570 and 571 performed by insertion of samples into a hot furnace showed similar results. These results differ from those made during high velocity CG/HW induction heating experiments where (E-14) survived exposures at 4700°F and 150 ft/sec (6). Typical post-exposure photomicrographs are shown in Figures 63 and 64. The results of small furnace, large furnace and comparative kinetic studies shown in Figures 10, 13 and 15 indicate similar dependence on test facility as in the case of the JT-composites. Rapid oxidation is observed in the large furnace after 60 minutes at 3470°F, whereas considerably slower rates are observed after two hours at 3500°F. Cyclic exposures at 3394°F (Test 878, Table 6) indicate accelerated oxidation. In general, then, the oxidation of KT-SiC (E-14) is characterized by low rates below 3450°F, a sharp transition from protective to nonprotective behavior at that temperature, and rapid degradation above 3500°F.

9. WSi_2/W(G-18) and Sn-Aℓ /Ta-10W(G-19)

Table 8 and Figure 5 summarize the results obtained for the coated refractory metal candidate materials. The tungsten disilicide coating on tungsten affords protection up to 3500°F. Four - thirty minute cycles at 3476°F (Test 1068) do not cause coating failure. This coating was developed and evaluated by Nolting and Jeffereys who report degradation near 3600°F due to melting at the W_5Si_3-WSi_2 eutectic (9). Figures 65 and 66 show the results of Test 478 which exposed a WSi_2/W(G-18) sample to flowing air at 3325°F for one hour. The central W_5Si_3 zone shown in Figure 66 is 5.0 mils wide. Figure 67 plots the log of W_5Si_3 zone width vs. reciprocal temperature results obtained for all types of tests conducted within the program along with similar data for the growth of W_5Si_3 measured by Bartlett and Gage (11) and Mo_5Si_3 on $MoSi_2$/Mo measured by Perkins and Packer (10). The latter values were converted parabolically (10) from 30 minute to 60 minute exposures for direct comparison. The furnace test data (filled circles) are in good agreement with the results of Bartlett and Gage (11) and Perkins and Packer(10), as are results of oxygen pickup experiments (to be discussed below). However, slight deviations are noted in the results for high velocity CG/HW tests (6) and considerable deviation is observed for HG/CW arc plasma exposures (7).

The emittance values employed in correcting optical brightness temperatures at $\lambda = 0.65\mu$ to true temperatures for the latter tests was $\epsilon = 0.60$ below 3500°F in Part III-Volume II(6). The large differences observed between furnace tests and arc plasma tests (squares in Figure 67) are undoubtedly due to temperature gradients through the coating. These gradients could be as high as several hundred degrees fahrenheit (7), and would then lead to reduced diffusion rates. However, this explanation does not offer a means for understanding the relative widths observed in the high velocity CG/HW test samples (triangles in Figure 67) which were inductively heated.

Figures 68 and 69 illustrate the post-exposure microstructure obtained for Test 485 exposed at 3532°F where the WSi_2 coating failed in an irregular manner. Some coating was still left on the surface after a 60 minute exposure. Kinetic studies for up to two hours at 3450°F did not produce failures in either the small or large furnaces.

The results obtained for Sn-Al /Ta-10W(G-19) indicate that this coating system offers protection at one atmosphere for one hour up to approximately 3200°F. Above this temperature, failure of the coating occurs. These results are in general agreement with those of Perkins and Packer (11, pages 294-295). The failure mechanism appears to be loss of tin and oxidation of the $TaAl_3$ layer as illustrated in post-exposure photomicrographs, Figures 70-73. Figure 70 shows the coating after exposures at 2624°F and 3092°F. The former section shows the two mil $TaAl_3$ zone and six mil Sn overlayer which is virtually identical to the as-received material (2). The latter section is typical of results above 2800°F, i.e. losses in the $TaAl_3$ zone and Sn overlayer are encountered. Figures 72 and 73 show coating failure and oxidation of the Ta-10W substrate.

Tests 1192 and 1193 (Table 8) were performed using HfC+C(C-11) pedestals in place of ZrO_2 to verify that the Sn-Al coating failure temperature near 3200°F was not due to reaction with ZrO_2. These tests confirm the 3200°F protection limit with failure occurring at 3317°F. Cyclic exposures at 2990°F (Test 1069, Table 8) did not lead to coating failure, nor did two hour kinetic study exposures at this temperature.

10. SiO_2+68.5^W/oW(H-22), SiO_2+60^W/oW(H-23) and SiO_2+35^W/oW(H-24)

Table 9 and Figures 7 and 11 display results for the silica-tungsten composite materials. The (H-24) composite containing 35^W/oW exhibits viscous flow at temperatures above 3000°F. Low oxidation rates are noted for (H-22) and (H-23) at temperatures up to 3900°F. Above this temperature, substantial viscous flow occurs. Low temperature exposures of (H-23) between 1200° and 2700°F (Tests 1239-1243, Table 9) indicate rapid attack of the tungsten below the fusion range of SiO_2. Similar results were obtained in high velocity CG/HW tests (6) in the range from 1700° to 2700°F. Tests 1239-1242 showed cracking of the samples due to oxidation of tungsten and the growth of tungsten oxide. Post-exposure photomicrographs of these composites, Figures 74-79, illustrate depletion of tungsten from the surface. Figure 78 illustrates flow in SiO_2+35^W/oW(H-24) at 3042°F.

Figure 11 contains the results of kinetic exposures on SiO_2+60^W/oW(H-23) at 3672° and 3846°F. Although the observed recessions are low, the behavior is complicated by plastic flow of SiO_2 and surface depletion of tungsten from all samples. The width of the depleted region becomes larger with time. Cyclic exposures of four - thirty minute cycles were performed for SiO_2+68.5^W/oW(H-22) and SiO_2+60^W/oW(H-23) near 3840°F (Tests 1153 and 1144 respectively, Table 9). An increase in viscous

flow is noted relative to uninterrupted two hour exposures at the same temperature. The amount of tungsten depletion in the cyclic exposures is also greater than that observed in the uninterrupted tests.

11. Hf-20Ta-2Mo(I-23)

Results of Hf-20Ta-2Mo(I-23) alloy exposures are given in Table 9 and Figures 7, 11, 12 and 14. One hour exposures indicate a generally increasing oxidation rate up to the melting point of the alloy at approximately 3850°F. This is in general agreement with other results for this alloy (12, 13). Low temperature exposures between 1200° and 2700°F showed small recession values despite the observation by the supplier Wah Chang, that "extensive oxidation" takes place during forging in air at 1400° - 1800°F. It was estimated that a one hundred mil scale formed during working in air for one hour. Based on present results it must be concluded that the "one hundred mil scale" formed during forging results from the combined effects of working, thermal cycling and oxidation. The microstructures shown in Figures 80-83 are comparable to those observed earlier (12, 13). In all cases, the contaminated metal matrix is separated from the oxide by a "subscale" region containing stringers of tantalum. This feature is clearly illustrated in Figures 81 and 83.

The results of fifteen minute to two hour kinetic studies are presented in Figures 11, 12 and 14 for small furnace, large furnace and comparative results. Protective behavior is observed at 3479°F in small furnace exposures, but rapid attack occurs after 60 minutes at 3405°F in the large furnace. Four - thirty minute cycles at 3312°F (Test 893, Table 9) resulted in accelerated oxidation. However, at 3423°F (Test 621) the oxidation rate was not accelerated.

C. Summary of Furnace Oxidation Results

Based on the results presented above for oxidation in flowing air at one atmosphere for one hour, the candidate materials can be ranked as follows:

The coated candidate materials Si/RVC(B-8), Sn-Al/Ta-10W(G-19) and WSi_2/W(G-18) indicate temperature limitations of 3060°F, 3200°F and 3450°F respectively. KT-SiC(E-14) exhibits low oxidation rates up to 3500°F at which point a sharp increase in rate occurs. SiO_2+35w/oW (H-24) exhibits viscous flow at temperatures as low as 3000°F.

Oxidation rates for the graphite candidate materials RVA(B-5), PG(B-6), BPG(B-7), PT0178(B-9) and AXF-5Q Poco(B-10) are insensitive to temperature in the range of 2800° to 4200°F but sensitive to air flow rates between 0.9 and 9.0 ft/sec. Supply limited oxidation rates of 0.2-0.3 mils/sec are observed for the graphites in this temperature range.

In general, materials containing HfB_2 or HfC have higher temperature limits than comparable materials containing ZrB_2 or ZrC. The hyper-eutectic carbides HfC+C(C-11) and ZrC+C(C-12) exhibit constant recession levels of 50-100 mils in one hour tests at temperatures between 1200° and 4200°F, with a transition from puffy to adherent oxides above

3450°F. JT0992(C-HfC-SiC) (F-15) exhibits slightly better behavior than JT0981(C-ZrC-SiC) (F-16) which in turn exhibits better high temperature behavior than JTA(C-ZrB_2-SiC) (D-13) although the (F-15) and (F-16) composites have low temperature inversions due to the fact that they do not contain boron. Hf-20Ta-2Mo(I-23) is comparable in behavior to JT0981(F-16) between 3000° and 3800°F, but the alloy melts near 3850°F. ZrB_2(A-3) is also comparable to (F-16) and (I-23) in this range, but melts at 5585°F. $HfB_{2.1}$(A-2) and (A-6) are more resistant to oxidation than ZrB_2(A-3). $ZrB_{2.1}$+20%SiC(A-8), ZrB_2+14%SiC+30%C(A-10) and Boride Z(A-5) are ranked in order of oxidation resistance for temperatures up to 3800°F. Even the least resistant (A-5) material is superior to pure ZrB_2(A-3). However, all these composites become comparable to (A-3) above 3800°F due to rapid depletion of SiC which provides protection below this temperature. The HfB_2+SiC composites (A-4), (A-7) and (A-9) are superior to the ZrB_2 composites, and exhibit the best overall behavior for the furnace oxidation conditions studied. Below 3900°F, the SiO_2+W composites (H-22) and (H-23) also yield low recession rates, but viscous flow occurs above 3900°F and tungsten oxidation occurs below 2700°F. Above 3900°F, the hypereutectic carbides (C-11) and (C-12) become competitive with the diborides and diboride-silicon carbide composites.

A summary of the results of the small furnace kinetic studies is presented in Figure 84 which indicates the temperature limits over which protective behavior for a two hour period is observed. A simple summary would be as follows: $HfB_{2.1}$(A-2) - 3700°F, ZrB_2(A-3) - 3400°F, $HfB_{2.1}$+SiC(A-4) and (A-7) - 3790°F, $ZrB_{2.1}$+SiC(A-8) - 3750°F, ZrB_2+SiC+C(A-10) - 3600°F, HfC+C(C-11) - between 3200° and 4000°F, ZrC+C(C-12) - between 3100° and 3600°F, JTA(D-13) - 3250°F (large furnace) and 3400°F (small furnace), KT-SiC(E-14) - 3450°F (large furnace) and 3500°F (small furnace), JT0992(F-15) - 3520°F (large furnace) and 3600°F (small furnace), JT0981(F-16) - 3390°F (large furnace) and 3500°F (small furnace), SiO_2+60$^{w}/_{o}$W(H-23) - 3850°F, and Hf-20Ta-2Mo(I-23) - 3380°F (large furnace) and 3480°F (small furnace). The poor low temperature behavior of (C-11), (C-12) (F-15), (F-16) and (H-23) should be kept in mind when evaluating these results.

Comparison of the recessions after two hour continuous exposures with the results obtained following four - thirty minute periods interrupted by cooling cycles yielded similar results for $HfB_{2.1}$(A-2), ZrB_2(A-3), HfB_2+20% SiC(A-4), Si/RVC(B-8), HfC+C(C-11), ZrC+C(C-12), JTA(D-13), JT0992(F-15), JT0981(F-16), WSi_2/W(G-18) and Sn-Al/Ta-10W(G-19). In each case, the exposure temperature was below the two hour protection limit or the failure temperature for coated materials. KT-SiC(E-14), SiO_2+68.5$^{w}/_{o}$W(H-22), SiO_2+60$^{w}/_{o}$W(H-23) and Hf-20Ta-2Mo(I-23) exhibited more rapid degradation in the cyclic exposures.

Comparison of the oxidation rates in the small furnaces (7/8 inch inside diameter) and the large furnaces (2 inch inside diameter) given in Figures 14 and 15 indicate no differences for $HfB_{2.1}$(A-2) and ZrB_2(A-3). However, more rapid oxidation was observed in large furnace tests on HfB_2+20%SiC(A-4) (compared with small furnace tests on (A-7)), JTA(D-13), KT-SiC(E-14), JT0992(F-15), JT0981(F-16) and Hf-20Ta-2Mo(I-23). These differences are most probably due to differences in air supply.

III. ARGON INERT TESTS

A. Introduction

Furnace exposures (CG/HW) have been performed for selected candidate materials under conditions employed to perform air oxidation tests. However, the exposures were performed in flowing argon at 0.9 ft/sec. Test conditions covered the temperature range between 3000° and 4200°F for one hour in the small furnaces (7/8 inch inside diameter). The purpose of these tests was to determine the effect of temperature exposure in the absence of air on the behavior of some of the candidate materials. The results of the argon inert tests are summarized in Table 10. Material recession and weight change were determined by post-exposure metallography and gravimetric techniques. The candidate materials investigated were Si/RVC(B-8), PT0178(B-9), JTA(D-13), JT0992(F-15), JT0981(F-16), WSi_2/W (G-18) and SiO_2+60^{W}/oW(H-23).

B. Results of Argon Inert Test Exposures

Reference to Table 10 indicates that exposures of Si/RVC (B-8) in argon at temperatures up to 3800°F caused little change in one hour. At 4000°F, however, most of the SiC coating was removed during a one hour exposure. The temperature limit of 3060°F noted for this material in air is due to the formation of volatile oxidation products. In argon, destruction of the 4 mil SiC coating proceeds via vaporization.

Negligibly small changes in dimensions and structure were noted for PT0178(B-9), JT0992(F-15) and JT0981(F-16) at temperatures up to 4200°F in argon, as shown in Table 10. At 4200°F, JTA(D-13) resulted in an internal structure which suggests melting of the ZrB_2-SiC phases. Figures 85 and 86, showing post-exposure microstructures of Test 1200, illustrate the melting of (D-13).

Exposures of WSi_2/W(G-18) at temperatures above 3500°F resulted in melting of the coating, as was observed in air. The thickness of W_5Si_3 zones observed in Tests 1203 (3101°F) and 1205 (3288°F) after one hour were 1.28 and 2.20 mils respectively. These values are lower than those observed after exposure in air at one atmosphere. Figure 67 indicates W_5Si_3 zone widths which are nearly twice as large for air exposures as those observed in these argon inert tests.

The inert tests performed on SiO_2+60^{W}/oW(H-23) at temperatures between 3800°F and 4000°F showed evidence for SiO_2 sublimation and cracking of the specimens upon cooling.

IV. RESULTS OF OXYGEN PICKUP AND GAS ANALYSIS TESTS

A. Introduction

Samples of JTA(C-ZrB_2-SiC) (D-13), JT0992(C-HfC-SiC) (F-15), JT0981 (C-ZrC-SiC) (F-16), WSi_2/W(G-18) as well as pure iridium and iridium alloyed with other platinum group metals were inductively heated between 2900°F and 4000°F during exposure to flowing mixtures of oxygen and helium. Flow rates of 0.2 ft/sec at oxygen partial pressures of 0.013 to 0.20 atmospheres and total pressures of one atmosphere were employed. Oxidation behavior was monitored by continuously measuring the rate at which oxygen was removed from the stream. The measurements of oxygen pickup rate were complemented by continuous measurements of CO and CO_2 formation in the case of the graphite composites. A complete description of the experimental procedures is given in Part II-Volume II (1) of this series, along with a detailed discussion on calculation of recession rates from the data obtained.

B. Results

1. JTA(C-ZrB_2-SiC) (D-13)

The composition of JTA(D-13) in terms of measured weight percentages is presented elsewhere (2). Conversion of the compositional data to atom percentages (neglecting the fact that the weight data does not add up to 100%) indicates that the JTA(C-ZrB_2-SiC) (D-13) composite contains 74.4 atomic per cent carbon and 5.4a/o, 6.2a/o and 14.0a/o of silicon, zirconium and boron respectively. Phases identified microstructurally include graphite, SiC and ZrB_2 (2). Table 11 summarizes the initial weights and dimensions of the JTA samples that were oxidized and gives the conditions of temperature, pressure, time and flow rate employed in the oxidation experiments.

A derivation of the expression for S, the signal from the thermal conductivity cell, is given in Part II-Volume II (1) as:

$$S = \frac{RT}{\phi} k_1 \left[\frac{w_{CO_2}}{MCO} + \frac{w_{O,sol.}}{MO_2} - \frac{w_{CO}}{2MCO} \right] \qquad (1)$$

where w_x and M_x are the weights per unit time and molecular weights of specie x respectively, k_1 is a calibration constant and ϕ is the volume flow rate. This relation applies for carbon-containing samples such as the JT-composites. In Figure 87, the quantity

$$\frac{w_{CO_2}}{M_{CO_2}} + \frac{w_{O,\,sol}}{M_{O_2}} - \frac{w_{CO}}{2M_{CO}}$$

in moles/cm^2 is plotted against time. The data points were obtained by integrating the experimental rate curve over time, and are based on the initial

surface area. The reaction rate at 2900°F and 11.9 Torr (Sample XXVIII-28, Table 11) is apparently linear. The measured recession for this sample observed by sectioning and metallographic measurements is 17 mils from change in length and 18 mils from change in diameter. Hence, the ratio of initial to final surface area is 1.49. On the basis of a linear rate law, all the points can be corrected for surface area as shown in Figure 87. The corrected points still fall on a straight line, but of higher slope than the original curve.

The observed (uncorrected) reaction rate of JTA at 2910°F and 40.4 Torr (XXVIII-33) appears to decrease considerably with time. The measured recession of 18 mils based on length and 25 mils based on diameter corresponds to a ratio of initial to final surface area of 1.68. The deviation from linearity is still apparent in the linearly corrected points plotted in Figure 87, although it is not as pronounced as in the original data. In Figure 88, a parabolic plot of the corrected points is shown. The parabolic rate law appears to be followed to an excellent approximation over the period of observation.

Qualitatively, (Sample XXVIII-28), (2900°F and 11.9 Torr) was covered with a very thick cage-like oxide that fractured away from the sample in large chunks on cooling. JTA XXVIII-33, exposed at about the same temperature at a higher oxygen pressure, 40.4 Torr, also oxidized extensively. A thick white oxide was observed on the curved sides of the cylindrical sample, and a thinner dark grey, slightly glassy oxide was seen on the two flat faces.

The quantitative difference in behavior between XXVIII-28 and XXVIII-33 is apparent in Figure 87. At the higher pressure (XXVIII-33) the initial rate of oxidation is higher, but the rate definitely drops off with time. The total extent of oxidation corrected for surface area is equal for the two samples after approximately one hour. Extrapolation beyond one-hour would suggest greater oxidation resistance over an extended period at the higher pressure. If the effect of increased pressure is to accelerate the formation of a protective film, then one might expect to observe deviations from linearity at longer times at 10 Torr and very early at 150 Torr at the same temperature.

At a temperature of 3740°F and oxygen partial pressure of 11.9 Torr (XXVII-31), the results might have been influenced by reaction with the thoria support rods. The recession rate, calculated from a linear extrapolation of the carbon consumption data, is given in Table 11. Table 11 also gives the number of moles of O_2 used to form CO_2, CO, and solid oxides, respectively. The major product is seen to be CO.

A series of tests run at 3663°F (Tests XXIX-8, 12, 17, 20 and 22, Table 11) gave calculated recession rates as high as 500 mil/hour. Reference to Figure 5 shows that JTA(D-13) exhibits a rate near 200 mil/hour at this temperature in furnace tests.

2. JT0992(F-15)

The composition of JT0992(F-15) in terms of measured weight percentages was presented elsewhere (2). Conversion of the compositional data to atom percentages indicates that the JT0992(F-15) (C-HfC-SiC) composite contains 79.1 atomic percent carbon, 11.8 atomic percent silicon and 9.0 atomic percent hafnium. Phases identified microstructurally include graphite, SiC and HfC (2). Table 12 summarizes the oxygen pickup data for JT0992(F-15). Figure 89 shows the integrated rate curve for JT0992 (F-15) sample XXVIII-37 exposed at 2950°F and a partial pressure of 40.1 Torr of oxygen. When the ordinate is negative, the number of moles of O_2 consumed in the formation of CO exceeds the sum of the number of moles of O_2 used to form both CO_2 and solid oxides. The maximum in Figure 89 may indicate that solid surface oxide is building up and acting to retard the oxidation of carbon to CO.

In Figure 90, data obtained at 40.5 Torr at higher temperatures, 3470 and 3550°F, are plotted. The 3470°F data seem to be controlled initially by rapid evolution of CO, and ultimately, by a linear oxidation process. The strong negative peak is not seen in the 3550°F data, but the period of linear increase is followed by a plateau, where CO evolution may be causing rupture of a solid oxide film, and finally by another period of linear rate that may represent repair of a solid oxide film. The relative proportion of CO_2 in the product is much higher at 3470°F than at 2950°F for an oxygen pressure of 40 Torr (Table 12).

On the basis of the calculated recessions of 14.7 and 21.2 mils/hr., for XXVIII-47 and XXVIII-50, respectively, the ratios of initial to final surface areas are 1.25 for XXVIII-47 and 1.44 for XXVIII-50. Correction for surface area changes would remove the apparent curvature in the regions of increasing ordinate in Figure 90, and the rates at these high temperatures, around 3500°F may be taken as linear. Near 2950°F, the oxidation rate for sample (XXVIII-37) decreases with time and may be assumed to be parabolic, or possibly even logarithmic. Qualitatively, the extensive oxidative degradation near 3500°F prevented observation of meaningful weight change data after oxidation. By contrast, at 2900 and 2950°F the oxidation resistance was excellent.

3. JT0981(F-16)

The composition of JT0981(C-ZrC-SiC) (F-16) composite in terms of measured weight percentages was presented elsewhere (2). Conversion of the compositional data to atom percentages indicated that the composite contains 81.5 atomic per cent carbon, 6.6 atomic per cent zirconium and 12.2 atomic per cent silicon. Phases identified microstructurally include graphite, SiC and ZrC (2).

Table 13 summarizes the experimental data on JT0981 (F-16). The data obtained near 2935°F at 10 and 40 Torr are plotted in Figure 91; the data obtained near 3550°F at the same two pressures are plotted in Figure 92. At 10 Torr, oxidation of carbon to CO seems to be the dominant process. At 40 Torr, the number of moles of O_2 going into CO_2 and solid

oxides increases relative to that going into the formation of CO. These conclusions are also confirmed by data given in Table 13. Around 2935°F, the rate of reaction definitely decreases with time. The data of Figure 91 are replotted on a parabolic basis as

$$\left[\frac{W_{CO_2}}{M_{CO_2}} + \frac{W_{O,\,sol}}{M_{O_2}} - \frac{W_{CO}}{2M_{CO}}\right]^2$$

vs. time in Figure 93. The over-all reaction rate is seen to be dropping more rapidly with time than predicted by the parabolic rate equation, indicating a highly protective oxidation mechanism. Near 3550°F recession rates would be expected to be linear on the basis of the data in Figure 92.

4. Calculated Recession Rates for the JT-Composites

The recession rates listed in Tables 11-13 were calculated on the assumption that the rate controlling factor is the oxidation of carbon. The amount of carbon initially present in each sample can be calculated from the initial weights given in the tables and the carbon analyses listed above. The percentage of carbon converted to oxide can then be obtained from the net carbon consumption data in the tables.

If x represents the net sample recession, and if the initial volume Vo of the sample is given by:

$$Vo = 2\pi r_o^2 h_o \tag{2}$$

then the final volume V may be written as:

$$V = 2\pi (r_o - x)^2 (h_o - 2x) \tag{3}$$

The fractional decrease in volume then becomes:

$$\frac{Vo-V}{Vo} = \frac{2r_o(h_o + r_o)\,x - (h_o + 4r_o)\,x^2 + 2x^3}{r_o^2 h_o} \tag{4}$$

If we equate $\frac{Vo-V}{Vo}$ with the percentage of carbon consumed, as given in Tables 11-13, we may calculate values for x, the net sample recession. The latter results are contained in Tables 11-13 for comparison with metallographic observation.

5. WSi_2/W(G-18)

The data on WSi_2 coated W is summarized in Tables 14 and 15. Figure 94 is a plot of total oxygen consumption, in g/cm^2, vs. time for run XXVIII-55. This run was aimed at determining the failure temperature for the WSi_2/W system at 10.7 Torr. The sample was heated to 3055°F, maintained that temperature for an hour, and was then heated successively, without intermediate cooling to 3210, 3285, 3375, 3440, 3510, and 4045°F. A protective film is apparently established rapidly at 3055°F,

and subsequent growth is very slow and essentially independent of temperature up to 3285°F. At 3375°F, a definite increase in oxidation rate was noticed. At 3440°F, a pronounced increase in oxidation rate occurred immediately upon raising the temperature. However, the curvature with time indicates that the rate was beginning to slow down, and that a protective film might have been re-established, perhaps to be ruptured again by evolution of gaseous oxides formed at the oxide/coating interface. At 3510 and 4045°F, rapid linear, nonprotective oxidation, characteristic of definite failure is seen. The failure temperature at 10 Torr thus lies between 3440°F and 3510°F, probably closer to 3440°F.

Data from a 150 Torr failure run (XXVIII-58) are plotted in Figure 95. Protective oxidation, characterized by rapid build-up of a silica film, and exceedingly slow subsequent oxide growth, approximately independent of temperature is noted at 3320 and 3475°F. When the r.f. power was increased for the next step, the temperature climbed rapidly to 3805°F, and the protection was lost. The failure point at 150 Torr thus appears to be greater than 3475°F but less than 3805°F.

For run XXVIII-68, at 3280°F and 149 Torr, one would have expected, based on the results obtained with XXVIII-58, protective oxidation, and low total oxygen consumption. The actual experimental results, plotted in Figure 96 do show eventual highly protective oxidation, but only after close to 0.2 g/cm^2 of oxygen had been consumed, compared to 0.006 g/cm^2 under comparable conditions shown in Figure 95. If the coating in XXVIII-68 had pin holes or if the coating composition were W_5Si_3 or W_3Si for XXVIII-68 and closer to WSi_2 for XXVIII-58, the results might be explained. In a 3370°F run at 150 Torr shown in Figure 96 oxidation is seen to be linear and catastrophic. A decreasing temperature is probably responsible for the last points lying off the line.

In runs XXVIII-70 and XXVIII-72, also plotted in Figure 96, the oxidation is seen to be linear, indicating the continual evolution of SiO(g) and the failure to form a protective SiO_2(s) film at all. Recessions in Table 14 were calculated on the basis of the assumed reaction:

$$WSi_2 + \frac{5}{2} O_2 \rightarrow WO_3(g) + 2SiO(g) \qquad (5)$$

Table 15 summarizes the results of single exposure experiments at oxygen partial pressures of 10 Torr and 149 Torr. The above results indicated failure temperatures between 3400° and 3500°F at 10 Torr and between 3450° and 3550°F at 150 Torr. These values were obtained on samples which were exposed at a series of ascending temperatures. In the single exposure experiments, Test XXIX-43 shows the onset of failure at 3460°F at 10 Torr, while Tests XXIX-53 and 57 define the one atmosphere failure temperature at about 3500°F. Figures 97-100 show post-exposure macrophotographs of the WSi_2/W(G-18) samples as well as the appearance of the W_5Si_3 zones formed at 3370°F in one hour. Reference to Figure 67 shows that the oxygen pressure does not influence the width of the zone, and that the widths obtained in these tests agree quite well with those of Bartlett and Gage (11).

Discussion of the oxidation of WSi_2 must take into account the different mechanisms that are operative in the protective and nonprotective

ranges. The remarkable oxidation resistance of WSi_2 up to 3100°F in air or pure oxygen has been ascribed (14), (15) to the rapid formation of a slow-growing, self-healing film of pure SiO_2. The initial oxidation reaction on the bare WSi_2 surface is probably:

$$WSi_2 + \frac{7}{2} O_2 \rightarrow WO_3(g) + 2SiO_2(s) \qquad (6)$$

Once a coherent silica film has formed, further growth may depend upon diffusion of oxygen to the SiO_2/WSi_2 interface. It is generally believed that silicon is then oxidized preferentially, so that the reaction at the interface becomes:

$$WSi_2 + \frac{7}{5} O_2 \rightarrow \frac{1}{5} W_5Si_3 + \frac{7}{5} SiO_2 \qquad (7)$$

As oxidation proceeds, layers of W_3Si and eventually even pure W should develop beneath the silica film. The primary factor controlling the over-all recession of the coated system should be reaction (6), since it is much more rapid than reaction (7) and results in greater silicide consumption. If w_O is the measured oxygen consumption (g/cm^2), then $d_{(1)}$, the WSi_2 recession in mils, based on reaction (6) is given by:

$$d_{(1)} = \frac{M_{WSi_2}}{7 M_O} \left(\frac{w_O}{\rho_{WSi_2}}\right) \frac{1000}{2.54} = 90.8\, w_O \qquad (8)$$

where M is the molecular weight of X, ρ_{WSi_2} is the density of WSi_2 (9.3g/cc) and $\frac{1000}{2.54}$ is the conversion factor from cm to mils. Equation (8) has been used to calculate recession values for those experiments listed in Table 14 where rapid initial oxidation followed by a flat protective region was observed. Subsequent recession $d_{(2)}$, via reaction (7) will be given by:

$$d_{(2)} = 43.9\, w_O \qquad (9)$$

Equation (9) was used to convert oxygen consumption data to recession data for measurements made within the protective region.

Nonprotective oxidation of WSi_2 is associated with two related phenomena: (1) failure to form an SiO_2 film at all low oxygen pressures, and (2) rupture of an already existing SiO_2 film by SiO(g) evolution. Analagous behavior has been observed for pure silicon (16), and the problem has been analyzed in detail by Wagner (17). Wagner's analysis should also be applicable to silicides if the lowered silicon activity is taken into account. Silicon forms one stable solid oxide, $SiO_2(s)$, and a gaseous oxide, SiO(g). If p^*_{SiO}, the pressure of SiO(g) at the surface of a silicide of activity a_{Si}, is less than the equilibrium partial pressure $p_{SiO(eq)}$ for the reaction:

$$1/2\ Si\ (a_{Si}) + 1/2\ SiO_2(s) = SiO(g) \qquad (10)$$

the condensed oxide will not form. (In general p_x will represent the pressure of x at the solid surface.) The condition for a protective $SiO_2(s)$ film to form, or in Wagner's terminology, the point of transition between active and passive oxidation is:

$$p^*_{SiO} = p_{SiO\,(eq)} \qquad (11)$$

Since oxygen should react readily at a bare silicide surface, oxidation in the active region will be characterized by $p^*_{O_2} << p_{O_2}$ where p_{O_2} is the oxygen partial pressure in the ambient gas stream. From boundary layer theory (18), m_{O_2}, the rate of transport of oxygen towards the surface will be given by:

$$\dot{m}^-_O\,(atoms/cm^2\text{-}sec) = -\frac{2D_{O_2}\,C^o_{O_2}}{\delta_{O_2}} \qquad (12)$$

where the negative sign denotes motion towards the surface, D_{O_2} is the diffusion coefficient for O_2 molecules, $C^o_{O_2} = p_{O_2}/RT$ and δ_{O_2} is the boundary layer thickness for mass transport of O_2. Similarly, the rate of transport of oxygen away from the surface as SiO(g) is given by:

$$\dot{m}^+_O = \frac{D_{SiO}\,C^*_{SiO}}{\delta_{SiO}} \qquad (13)$$

In the steady state, there will be no net oxygen transport, and therefore, we will have

$$C^*_{SiO} = 2\,(\delta_{SiO}/\delta_{O_2})\,(D_{O_2}/D_{SiO})\,C^o_{O_2} \qquad (14)$$

Wagner approximates the ratio of the boundary layer thicknesses by: $(\delta_{SiO}\ \delta_{O_2}) = (D_{SiO}/D_{O_2})^{1/2}$. Then, setting $p^*_{SiO} = p_{SiO(eq)}$, he finally solves for the maximum ambient oxygen pressure compatible with a bare silicide surface:

$$p^o_{O_2}\,(max) \simeq 1/2\left[\frac{D_{SiO}}{D_{O_2}}\right]^{1/2} \qquad p_{SiO(eq)} \approx 0.4\,p_{SiO(eq)} \qquad (15)$$

The ratio of diffusion coefficients is estimated by Wagner as $(D_{SiO}/D_{O_2}) = 0.64$. The equilibrium pressure, $p_{SiO(eq)}$, for reaction (10) is plotted in Figure 101 as a function of temperature for various activities of silicon. Calculations were based on the data given in the JANAF Tables (19). The activity of silicon in WSi_2 is not known, but may be estimated by comparison with activities in the Mo-Si system. For $MoSi_2$, a_{Si} lies between 0.1 and 1; for Mo_5Si_3, $0.005 \leq a_{Si} \leq 0.1$, and for Mo_3Si $a_{Si} \simeq 0.004$. The activities in the W-Si system are expected to be lower by about a factor of two.

If we estimate $a_{Si} = 0.1$ for WSi_2, then at an ambient oxygen pressure of 10 Torr (0.013 atm), we find from Figure 101 that active or nonprotective oxidation should be observed on the bare silicide surface at temperatures above 3022°F, where

$$p_{SiO(eq)} = \frac{0.013}{0.4} = 0.03 \text{ atm}$$

Experimentally, passive oxidation was observed at 3055°F (XXVIII-55), active oxidation at 3355°F (XXVIII-70). At an ambient oxygen pressure of 0.2 atm, corresponding to air, active oxidation is predicted at temperatures above 3600°F.

There is a hysteresis in the transition point between active and passive oxidation. The above discussion was concerned with the failure to form a protective silica film as a function of ambient oxygen pressure. Once an $SiO_2(s)$ film has been formed, the ambient oxygen pressure may be permitted to fall well below $p^{o}_{O_2}$ (max) before oxidative protection is lost. Wagner's analysis (17) gives the lowest ambient oxygen pressure p_{O_2} (min) at which a layer of SiO_2 formed at higher pressure is stable. The final equation is:

$$p_{O_2} \text{ (min)} = 1/2\left[(1/4)^{2/3} + (1/2)^{2/3}\right] K^{2/3} \frac{D_{SiO}}{D_{O_2}} \qquad (16)$$

where K is the equilibrium constant for the reaction:

$$SiO_2(s) = SiO(g) + 1/2\ O_2(g) \qquad (17)$$

Values of $p^{o}_{O_2}$ (min) based on JANAF thermodynamic data are plotted against $10^3/T$ in Figure 102. According to Figure 102, even at 4000°F, a silica film once formed should be stable down to oxygen pressures of 4.7 Torr.

Wagner's development is concerned with the effect of reducing the oxygen pressure at constant temperature after a silica film has formed at that same temperature. A problem of equal importance in practice is the stability of a silica film with increasing temperature. If a protective SiO_2 film is grown on the surface of a silicide at some oxygen pressure, and the temperature is raised while maintaining the pressure constant, SiO(g) can be formed via reaction (17) at the silicide/oxide interface. If the equilibrium SiO(g) pressure becomes the same order of magnitude as the ambient pressure, evolution of SiO(g) and consequent film rupture may be anticipated. If $a_{Si} = 0.1$, then the SiO(g) pressure at the silicide/SiO_2(s) interface will become of the order of one atmosphere at a temperature around 3785°F. The experimental failure point was closer to 3600°F. It should be noted that eutectic melting occurs in this sytem at 3650°F.

6. Iridium-Base Alloys

The oxidation behavior of a series of eight iridium and iridium-base alloys, prepared by D. P. Harmon of Aerojet General Corp., Sacramento, California (20), was evaluated by means of the gas analysis technique (1, 21). A recorder tracing for the oxidation of an Ir-Rh-Re sample is reproduced in Figure 103. The rate of oxygen pickup by the reacting sample in g/min of oxygen consumed, is given as a function of time. Similar curves were obtained in every experiment. The rate of oxidation of all the alloys under study was observed to rapidly reach a maximum level and then to remain linear for time periods that varied from 5-30 minutes. Subsequently, the rate began to drop with time, often in the step wise manner illustrated in Figure 103. Since the oxides of the platinum metals are known to be highly volatile at the temperatures of the present series of experiments, the rate of oxidation is expected to be independent of time. Consequently, the cause of the observed decrease in rate is presently unknown. However, even the initial linear rate is low compared to the true surface reaction controlled rate. Consequently, it is possible that the apparent drop in rate with time is due to changes in the pattern of flow of metal oxides away from the surface and oxygen towards the surface.

Table 16 summarizes the experimental runs completed. Initial sample weights and dimensions and the experimental conditions maintained during oxidation are given. Sample surface temperatures were measured through an optical window with a micro-optical disappearing filament pyrometer. A combination window correction and pyrometer calibration was determined by viewing a G.E. standard lamp with the pyrometer through the same optical window. A further correction is necessary for the emittance of the oxidizing sample. In one experiment an iridium sample was heated in pure helium, flowing at a rate of 0.1 ft/sec to the point of incipient melting. The observed brightness temperature at this point was 3596°F. Application of the window correction brings the brightness temperature to 3686°F. Using the melting point of pure iridium (20), 4430°F, as the true temperature of the sample, the emittance ϵ at the melting point can be calculated from Equation 18 (22):

$$\ln \epsilon [\lambda, T] = \frac{C_2}{\lambda} \left[\frac{1}{T} - \frac{1}{T_{br}} \right] \qquad (18)$$

where λ is the wave length at which the pyrometer operates ($\lambda = 0.65\mu = 6.5 \times 10^{-5}$ cm in these experiments) C_2 is a constant equal to 2.588 cm°R; T°R, (T°F + 460) is true temperature and T_{br} °R is brightness temperature (corrected for window or other extraneous optical effects). The resulting value is $\epsilon = 0.23$. This emittance value is significantly lower than the value quoted in the literature ($\epsilon = 0.30$ at 0.65μ). As indicated in the discussion, the latter was used to calculate the corrected temperatures listed in Table 16 from observed brightness temperatures.

The recessions given in the last column of Table 16 are based on the initial (maximum) observed net oxygen consumption rates. In order to convert from oxygen consumption to metal recession it is necessary to have some information about the stoichiometry of the oxidation reaction. Furthermore, this measurement is not sensitive to the vapor species formed at the hot sample surface, but rather to the solid phases which condense from the vapor onto the cool walls of the apparatus. The distinction is important

if condensation occurs with release or take up of oxygen.

In experiment XXVIII-1 on pure Ir the measured rate of oxygen consumption is 5.62×10^{-4} g/min or 3.5×10^{-5} gm.atoms of O/min. The weight loss, assuming linearity with time is 6.80×10^{-3} g/min or 3.54×10^{-5} gm.atoms of Ir/min. Thus, the net oxidation condensation reaction observed seems to involve iridium and oxygen in the atom ratio of 1:1. The metal recession rates were calculated on this basis for all of the materials studied, assuming preferential oxidation of iridium in every case.

Table 17 summarizes the dimensional changes observed in post-exposure metallographic analysis. Although a number of these samples showed nonuniform recessions, there was no indication of preferential oxidation.

C. Discussion of Results

Near 2900°F the oxidation of JTA(D-13) was found to be linear at a pressure of 11.9 Torr and parabolic at a pressure of 40.4 Torr (Figures 87 and 88). In both cases, the calculated recessions contained in Table 11 were 19.7 mils in relatively good agreement with the observed recessions. It appears that as the pressure increases, protective oxidation takes place due to formation of an oxide coating. Thus, at 2900°F, one would expect lower one hour recessions at higher pressures. This finding is in agreement with the results of air oxidation tests 216 and 217 (Table 7) which resulted in 3 mil and 6 mil recessions after one hour at 2813°F and 3110°F. At 3740°F (Test XXVIII-31, Table 11) the oxidation rate is linear and corresponds to a computed value of 55.5 mils and observed values of 160-170 mils in one hour. These results are to be compared with supply limited rates of 200 mils in 60 minutes observed in 1 ft/sec air oxidation tests (Figure 5) and Mach 0.3, 1 atmosphere recessions of 60 mils in 30 minutes (Reference 7). The higher rate at 3740°F is due to breakdown of protective oxidation and an approach to graphite behavior. Thus, at higher oxygen pressure (Test XXVIII-74, Table 11) still higher recession rates corresponding to 500 mil/hr levels are seen. In all of these exposures, the supply of oxygen exceed the removal rate. Thus, the oxidation was not supply limited.

The present results for JT0992(F-15) in Table 12 indicate that protective oxidation occurs at 2900 and 2950°F for exposures at 10.3 and 40.1 Torr of oxygen (Figure 89). Calculated and observed rates are in general agreement with results obtained by Air Oxidation Tests (Figure 6). In addition, the observed recession levels of 1-3 mils in one hour are in keeping with arc plasma exposures at Mach 3.2 and oxygen partial pressures in the range 1-4 Torr (see Reference 7). At temperatures near 3500°F, the oxidation of JT0992(F-15) is not protective. The conversion depth at 3580°F and 149 Torr (sample XXVIII-62) corresponds to a rate near 300 mils in one hour. In all cases, the oxygen supply exceeded the quantity which reacted with the sample. The foregoing rate is higher than observed in Air Oxidation tests (Figure 6). Arc plasma tests at Mach 0.3 at one atmosphere yield recession rates of 1000 mils in 30 minutes at 3500°F (7).

The behavior of JT0981(F-16) is quite similar to JT0992(F-15) in these tests as shown in Table 13 and Figures 91 and 92. Protective oxidation is noted at 2900°F yielding rates of 1-6 mils in one hour which are comparable with the results shown in Figure 6 for oxidation in air. The JT0981(F-16) exposures reported in Table 13 were not supply limited. For WSi_2/W(G-18), at an oxygen partial pressure of 10 Torr, a protective silica film can be formed at a temperature of 3175°F. The protection is then lost when the temperature is raised to the 3600-3670°F range. At 3495 and 3560°F and 10.6 Torr, a silica film fails to form at all and the oxidation is linear due to continual evolution of SiO. At an oxygen partial pressure of 150 Torr, results were highly variable. In one experiment protective oxidation, characterized by rapid build-up of a silica film after an oxygen pickup of 0.006 g/cm^2 was noted at 3450°F, and the protection was retained at 3635°F. In another experiment at the same pressure, the protective film was not established until 0.2 g/cm^2 of oxygen had been consumed. At 3520°F, linear catastrophic oxidation was noted.

The protective oxidation of WSi_2 is discussed in terms of an initial stoichiometric reaction to form WO_3(g) and SiO_2(s), and ultimate preferential oxidation of silicon with the formation of W_5Si_3, W_3Si, and finally W at the oxide-alloy interface. The nonprotective oxidation of WSi_2 is discussed in terms of two related phenomena: (1) the failure to form an SiO_2 film at all low oxygen pressures due to the establishment of a boundary layer of SiO(g) that limits oxygen access to the surface and (2) the rupture of an already existing SiO_2 film by evolution of SiO(g) at the oxide silicide interface.

The present results indicate that one atmosphere failure occurs near 3500°F in good agreement with the air oxidation tests (Figure 5, Table 8) which suggest failure at 3500°F. Arc plasma exposures at one atmosphere and Mach 0.3 (7) showed no failures up to 3210°F. By contrast, high velocity CG/HW tests at Lockheed (6) performed at one atmosphere indicates failure at 3680°F. However, failures were noted after 5 minutes of arc plasma exposure at Mach 3.2 and 24 Torr oxygen pressure at 3635°F (7). The latter result is in fair agreement with the present 10 Torr findings.

The rates of oxidation of iridium metal reported here are compared with literature values in Table 18. The rates obtained in the present work seem to be limited by mass transport in the vapor phase. Rexer's results at 4040°F (26), oxygen pressures of 142 and 710 Torr, predict a reaction controlled rate at 400 Torr of 120 mils/hr, a factor of more than ten higher than presently observed. The influence of mass transport on the observed rates can only be checked by studying the oxidation reactions as a function of temperature, flow rate and sample size. It is quite possible that even the comparative ranking of materials might be different under true reaction controlled conditions. However, if these results are taken to be representative of the oxidation behavior independent of temperature, flow rate, etc., then Table 16 suggests that rhodium additions enhance the oxidation resistance of iridium, while platinum and rhenium confer only moderate enhancement and osmium reduces the oxidation resistance. Table 16 lists the melting temperatures of these alloys as well as their melting temperatures in the presence of carbon (20). Reference to these values indicates that while rhodium increases the oxidation resistance, it lowers the temperature of the iridium-carbon eutectic. Platinum behaves in a similar fashion. On the other

hand, rhenium additions raise the iridium-carbon eutectic temperature.

The emittance value of 0.23 determined in this work is somewhat low compared to other values in the literature. Table 19, taken from a National Bureau of Standards Compilation (22) gives 0.65μ emittance values for several of the platinum group metals and one alloy. The emittance is given as 0.30 for solid iridium, although unfortunately the temperature of measurement is not reported. More recently Wright et al. (22) have performed an extensive series of measurements of the emittance of solid iridium between 1600°F and 3600°F. Their results indicate an emittance of 0.30 at 0.65μ in static air. Accordingly, this value was employed to correct the current optical temperatures to true temperatures. The present uncertainty in the emittance of the alloys under study (all of the alloys were assumed to have emittance = 0.23 at 0.65μ) leads to the obvious inconsistency for experiment XXVIII-13 in Table 16 where in the 75Ir25Pt alloy was oxidized 50°F above its melting point.

REFERENCES

1. Kaufman, L. and Nesor, H., "Stability Characterization of Refractory Materials under High Velocity Atmospheric Flight Conditions", AFML-TR-69-84, Part II-Volume II (1969).

2. Kaufman, L. and Nesor, H., "Stability Characterization of Refractory Materials under High Velocity Atmospheric Flight Conditions", AFML-TR-69-84, Part II-Volume I (1969).

3. Clougherty, E.V., Kalish, D. and Peters, E.T., "Research and Development of Refractory Oxidation-Resistant Diborides", Progress Report No. 3, Contract No. AF33(615)-3671, May 1967.

4. Kaufman, L., Clougherty, E.V. and Berkowitz-Mattuck, J.B., Tr. AIME (1967) 239 458.

5. Clougherty, E.V., private communication.

6. Perkins, R., Kaufman, L. and Nesor, H., "Stability Characterization of Refractory Materials under High Velocity Atmospheric Flight Conditions", AFML-TR-69-84, Part III-Volume II (1969).

7. Kaufman, L. and Nesor, H., "Stability Characterization of Refractory Materials under High Velocity Atmospheric Flight Conditions", AFML-TR-69-84, Part III-Volume III.

8. Kaufman, L. and Nesor, H., "Stability Characterization of Refractory Materials under High Velocity Atmospheric Flight Conditions", AFML-TR-69-84, Part IV-Volume I.

9. Elliot, R.P., "Constitution of Binary Alloys", First Supplement, McGraw-Hill Book Co., New York, N.Y., 1965, p.822.

10. Perkins, R.A. and Packer, C.M., "Coatings for Refractory Metals in Aerospace Environments", AFML-TR-65-351, September 1965.

11. Bartlett, R.W. and Gage, P.R., "Investigation of Mechanisms for Oxidation Protection and Failure of Intermetallic Coatings for Refractory Metals", ASD-TDR-63-753 Part II, July, 1964.

12. Kaufman, L. and Clougherty, E.V., "Investigation of Boride Compounds for Very High Temperature Applications", RTD-TDR-63-4096 Part III, March, 1966.

13. Berkowitz-Mattuck, J.B., Kaufman, L., Clougherty, E.V. and Hopper, R., "Oxidation of Hf-Ta Alloys", (1967) 239 750-753.

14. Berkowitz-Mattuck, J.B., "Kinetics of Oxidation of Refractory Metals and Alloys, 1000°-2000°C, ASD-TDR-62-203, Part II, March (1963).

15. Cadd, J.D., "Advancement of Protective Coating Systems for Columbium and Tantalum Alloys", AFML-TR-65-203, April 1965.

16. Kaiser, W. and Breslin, J., J. Applied Physics (1958) 29 1292.

17. Wagner, C., J. Applied Physics (1958) 29 1295.

18. Baron, J.R., Reference (12) p. 245.

19. JANAF Thermochemical Tables, Dow Chemical Co., Midland, Michigan.

20. Harmon, D.P., "Iridium Base Alloys and Their Behavior in the Presence of Carbon", AFML-TR-66-290, October 1966.

21. Berkowitz-Mattuck, J.B., J. Electrochem. Soc. (1966) 113 908-914.

22. Temperature, Its Measurement and Control in Science and Industry, Rheinhold Publishing Co., New York, N.Y. (1941) Appendix, Table 16, p. 1313. (See also T.R. Wright et al. "The Fabrication of Iridium and Iridium-Alloy Coatings on Graphite by Plasma-Arc Deposition and Gas-Pressure Bonding", AFML-TR-68-6 Battelle Memorial Institute, Columbus, Ohio, (February 1968).

23. Criscione, J.M. et al., "High Temperature Protective Coatings for Graphite", ML-TDR-64-173 Part III, October 1965.

24. Krier, C.A. and Jaffee, R.I., J. Less Common Metals (1963) 5 411.

25. Kuriakose, A.K., Kent, K. and Margrave, J.L. in Reference (23).

26. Rexer, J. in Reference (23).

27. Alcock, C.B. and Hooper, G.W., Proc. Roy. Soc. (1960) A254 551.

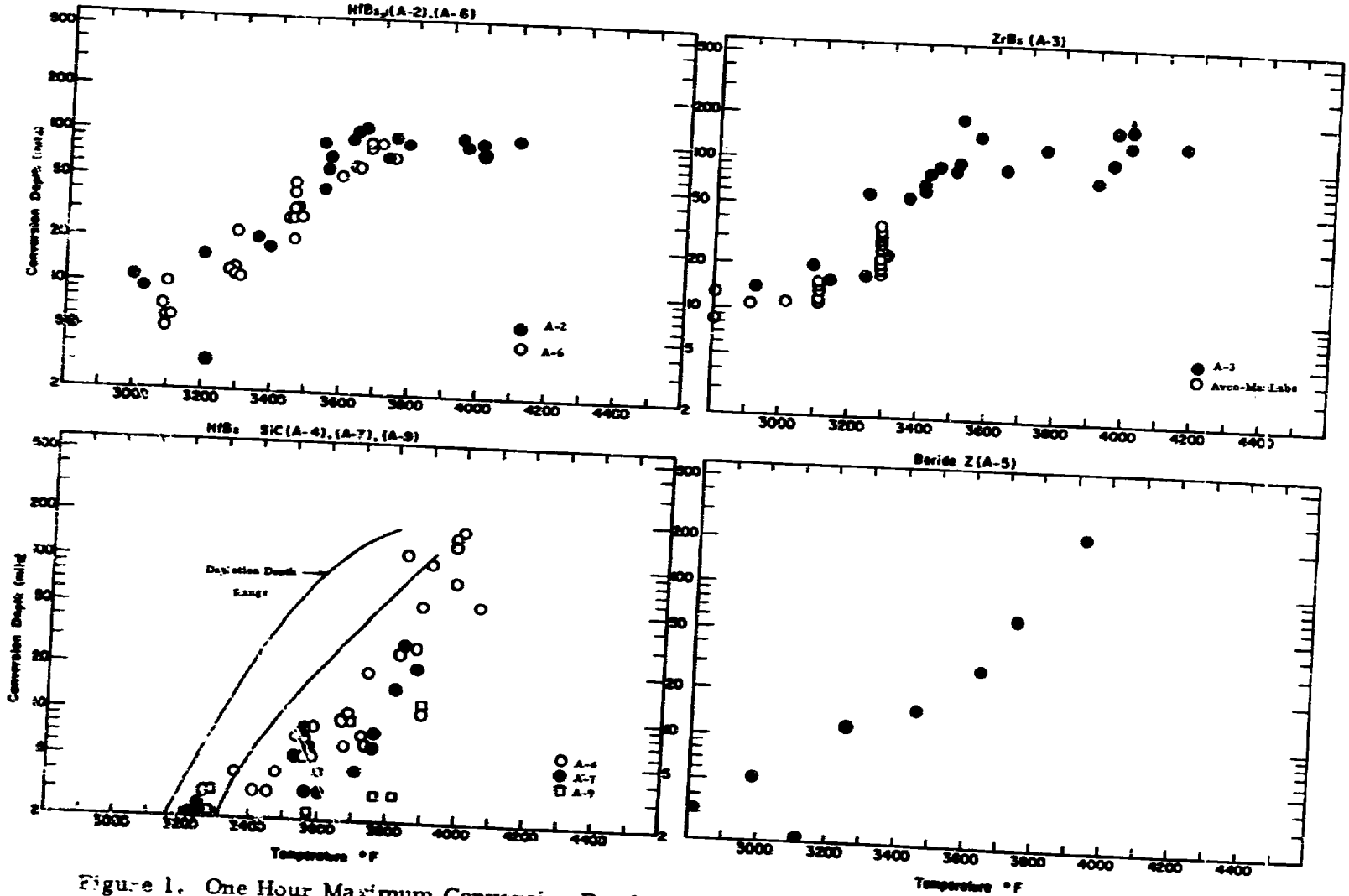

Figure 1. One Hour Maximum Conversion Depths for HfB_2 (A-2) and (A-6), ZrB_2 (A-3) and (Avco-ManLabs), HfB_2 + SiC (A-4), (A-7) and (A-9) and Boride Z (A-5) as a Function of Temperature in Flowing Air at 0.9-7.2 ft/sec.

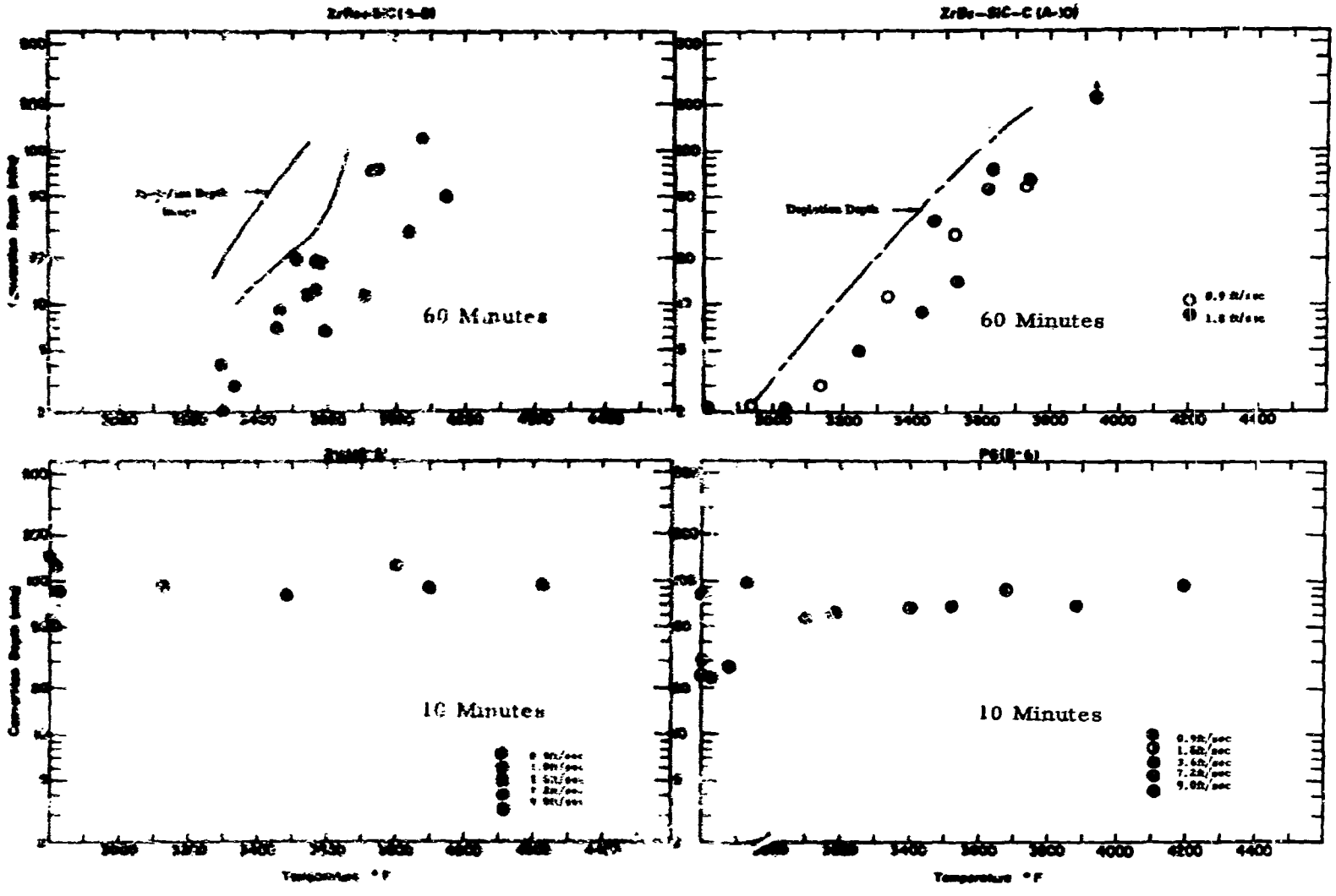

Figure 2. Maximum Conversion Depths for ZrB_2 + SiC(A-8), ZrB_2 + SiC + C(A-10), RVA(B-5) and PG(B-6) as a Function of Temperature in Flowing Air at 0.9-9.0 ft/sec. (Times as indicated).

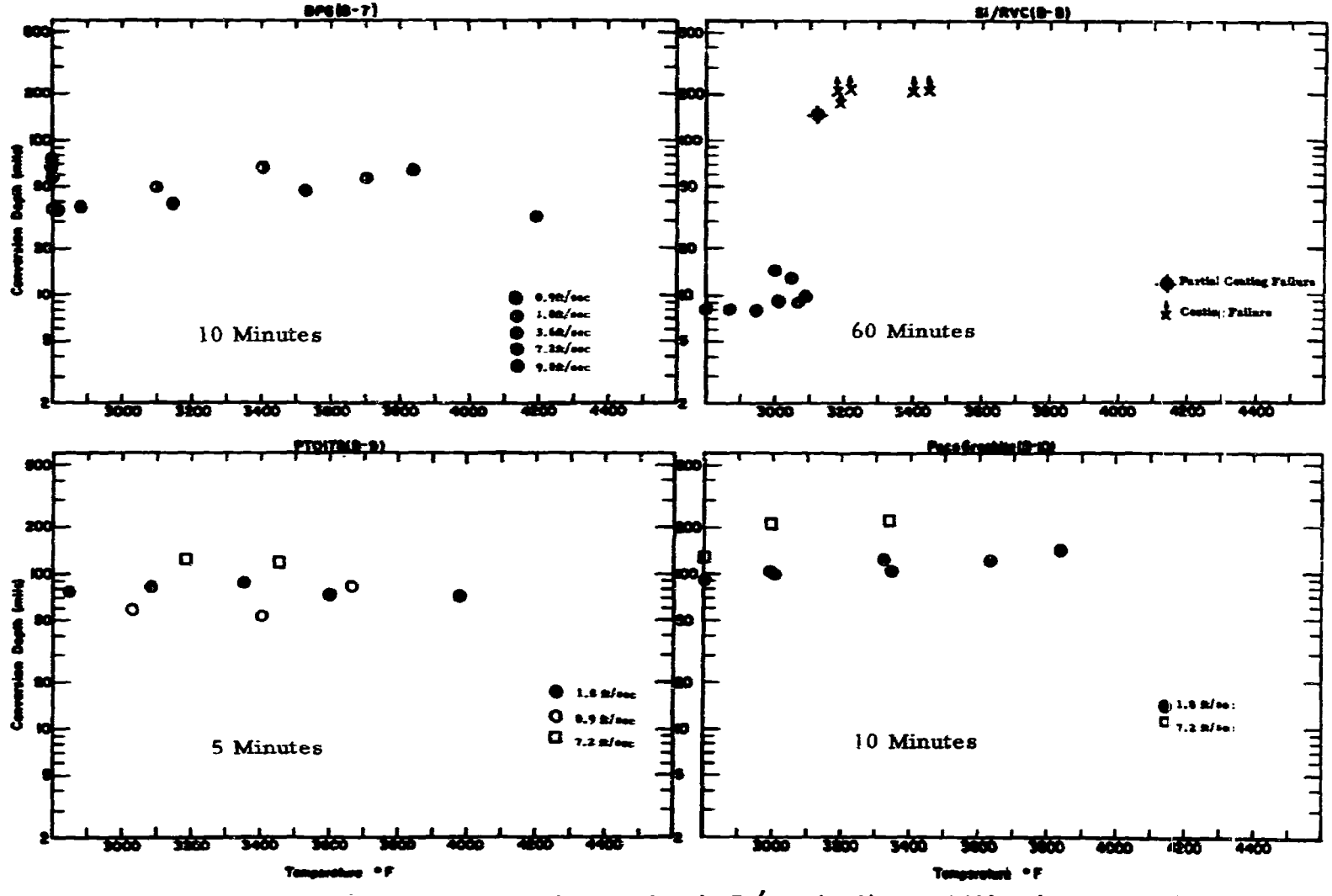

Figure 3. Maximum Conversion Depths for BPG(B-7), Si/RVC(B-8), PT0178(B-9) and Poco Graphite (B-10) as a Function of Temperature in Flowing Air at 0.9-9.0 ft/sec. (Times as indicated).

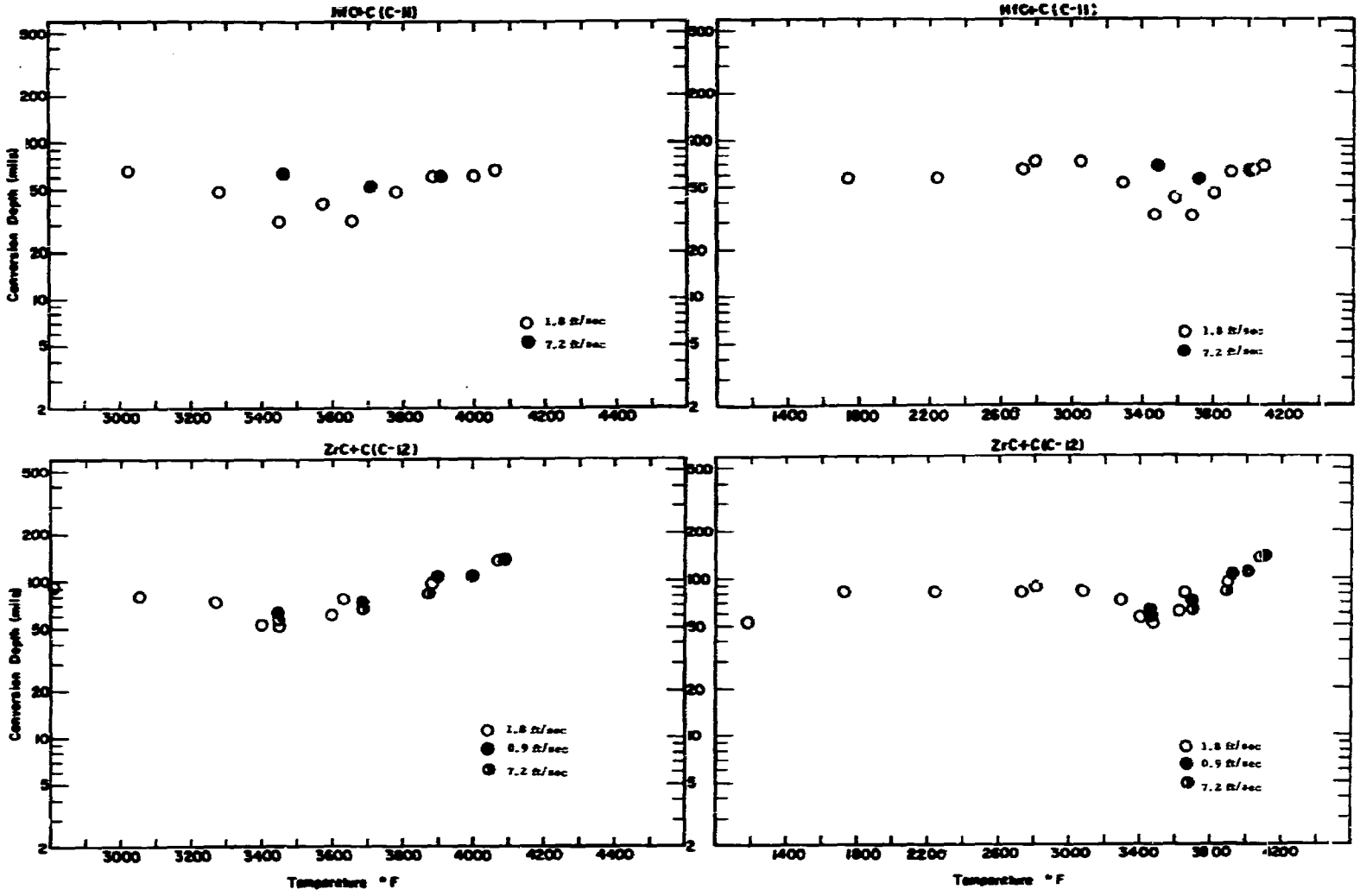

Figure 4. One Hour Maximum Conversion Depths for HfC+C(C-11) and ZrC+C(C-12) as a Function of Temperature in Flowing Air at 0.9-7.2 ft/sec.

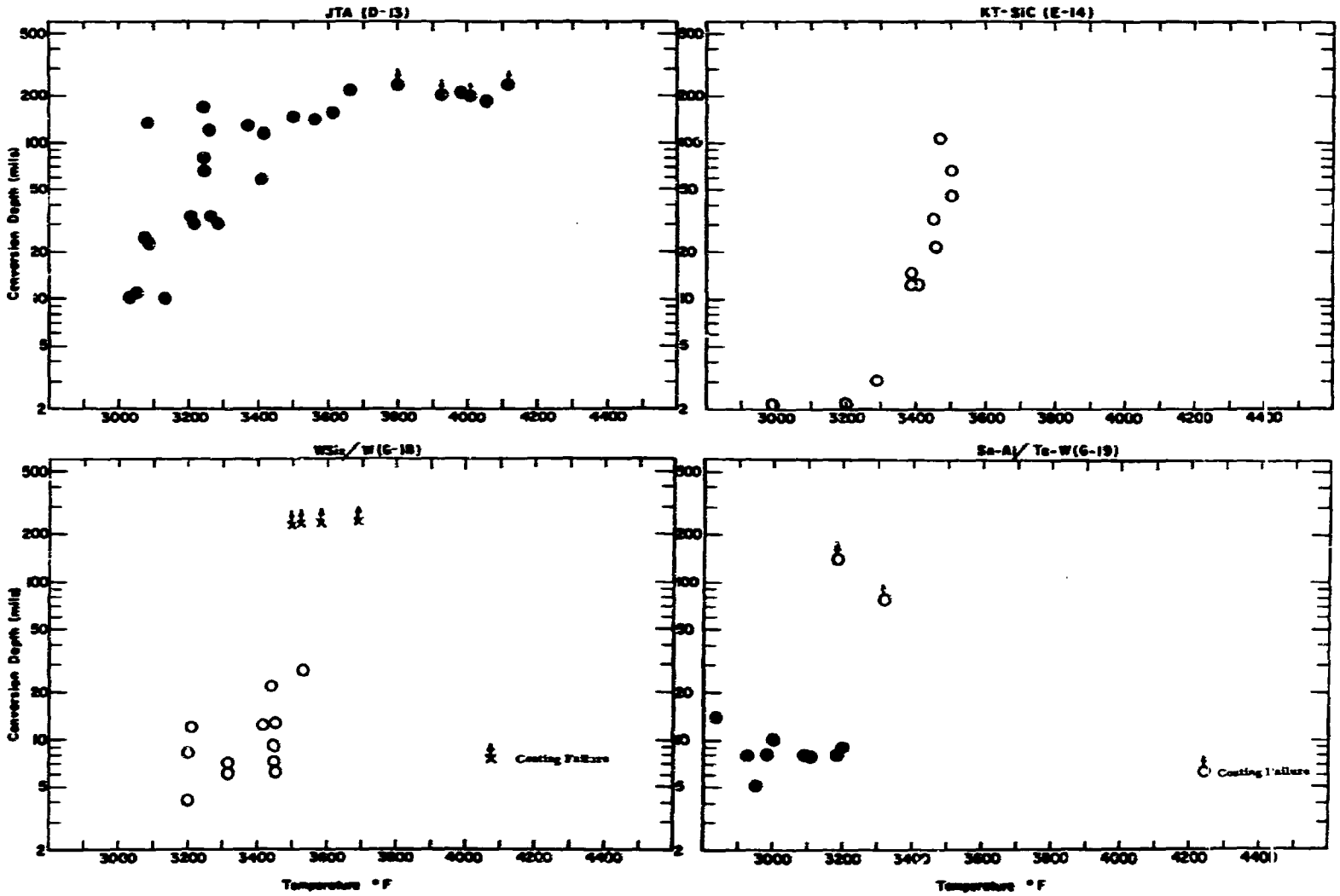

Figure 5. One Hour Maximum Conversion Depths for JTA(D-13), KT-SiC(E-14), WSi_2/W(G-18) and Sn-Al/Ta-W(G-19) as a Function of Temperature in Flowing Air at 1.8 ft/sec.

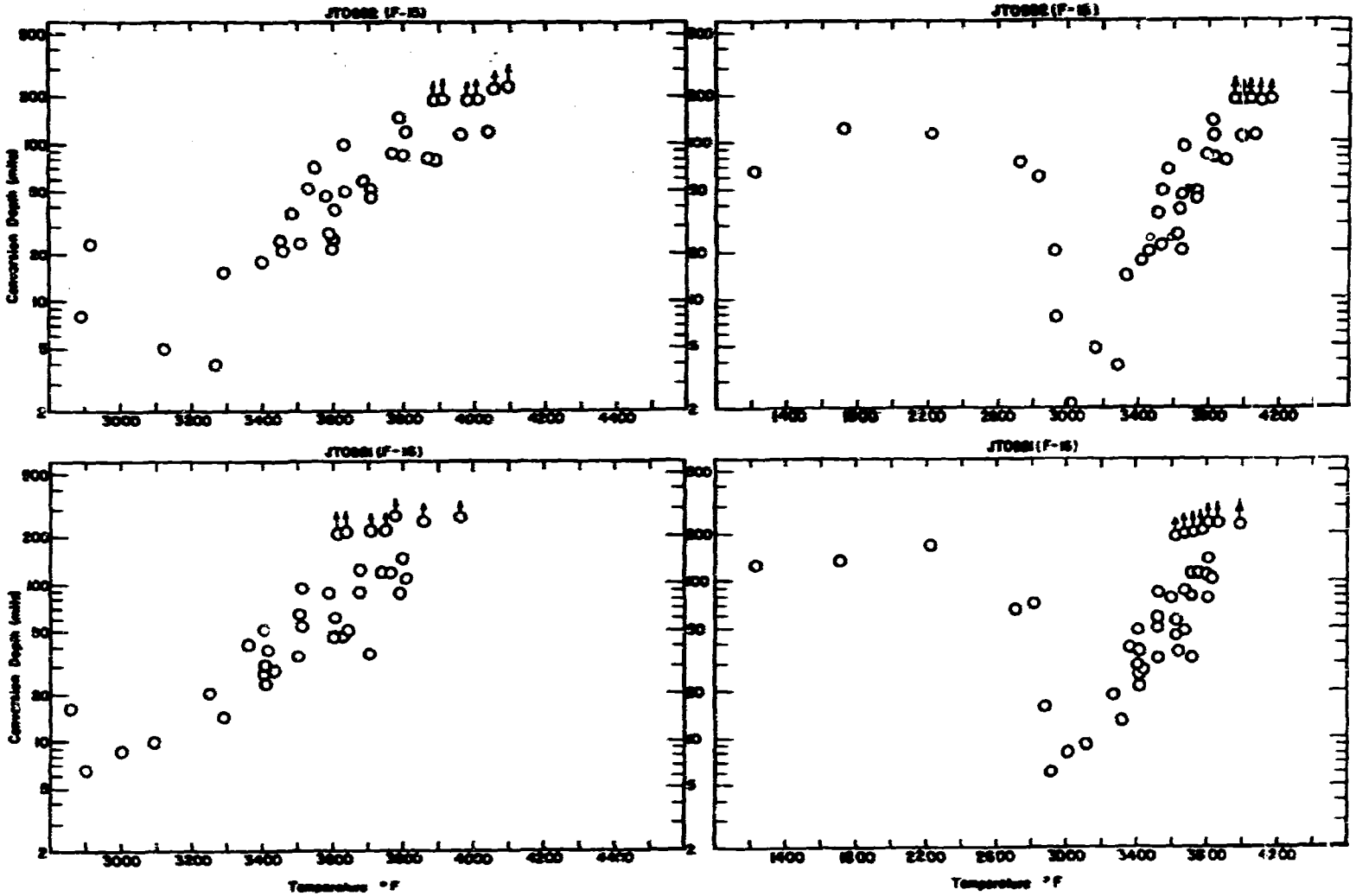

Figure 6. One Hour Maximum Conversion Depths for JT0992(F-15) and JT0981(F-16) as a Function of Temperature in Flowing Air at 1.8 ft/sec.

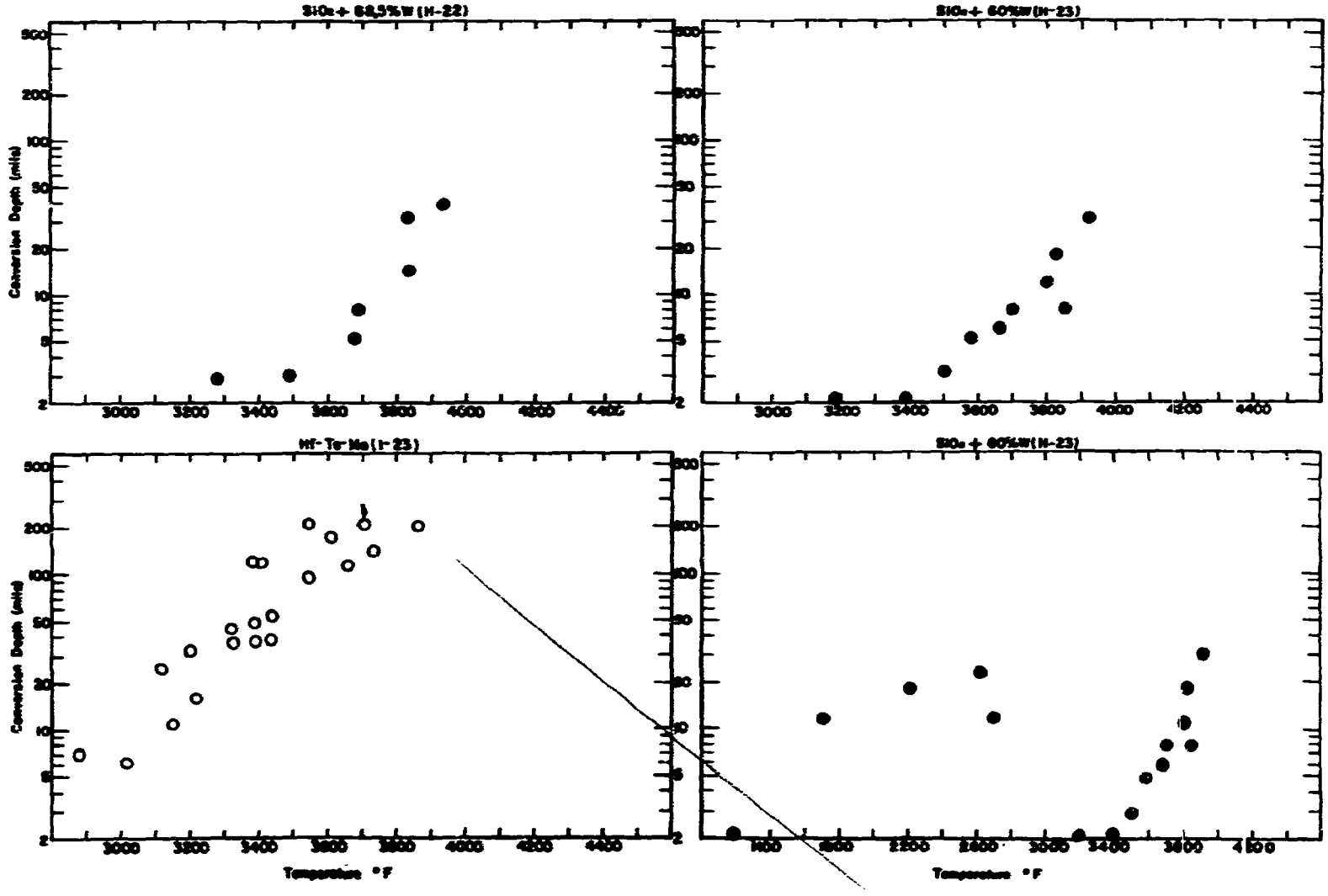

Figure 7. One Hour Maximum Conversion Depths for SiO_2 + W(H-22) and (H-23) and Hf-Ta-Mo(I-23) as a Function of Temperature in Flowing Air at 1.8 ft/sec.

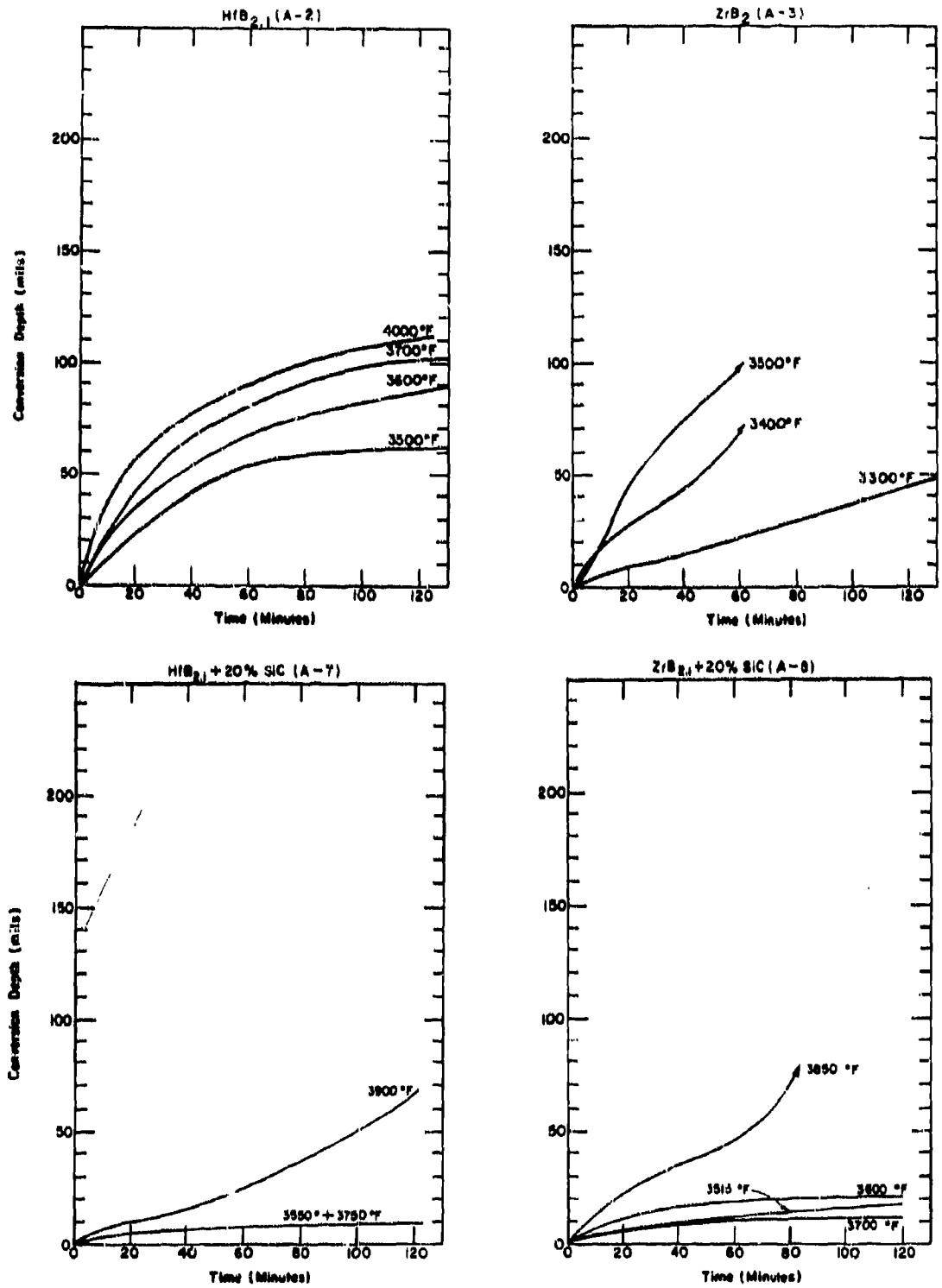

Figure 8. Conversion Depths for $HfB_{2.1}$(A-2), ZrB_2(A-3), $HfB_{2.1}$+20% SiC(A-7) and $ZrB_{2.1}$+20%SiC(A-8) as a Function of Time in Flowing Air at 1.8 ft/sec (Small Furnace).

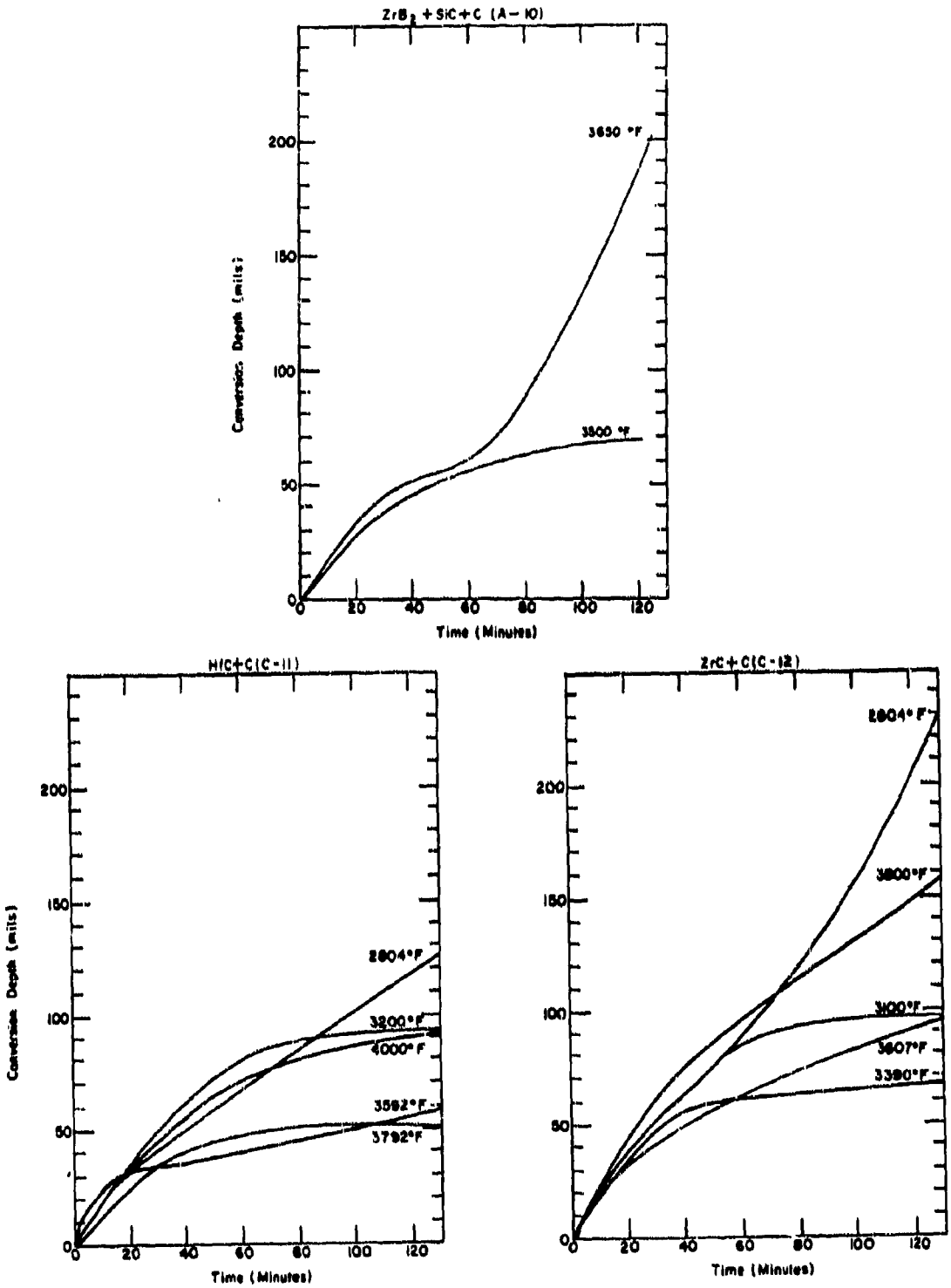

Figure 9. Conversion Depths for ZrB_2+SiC+C(A-10), HfC+C(C-11) and ZrC+C(C-12) as a Function of Time in Flowing Air at 1.8 ft/sec (Small Furnace).

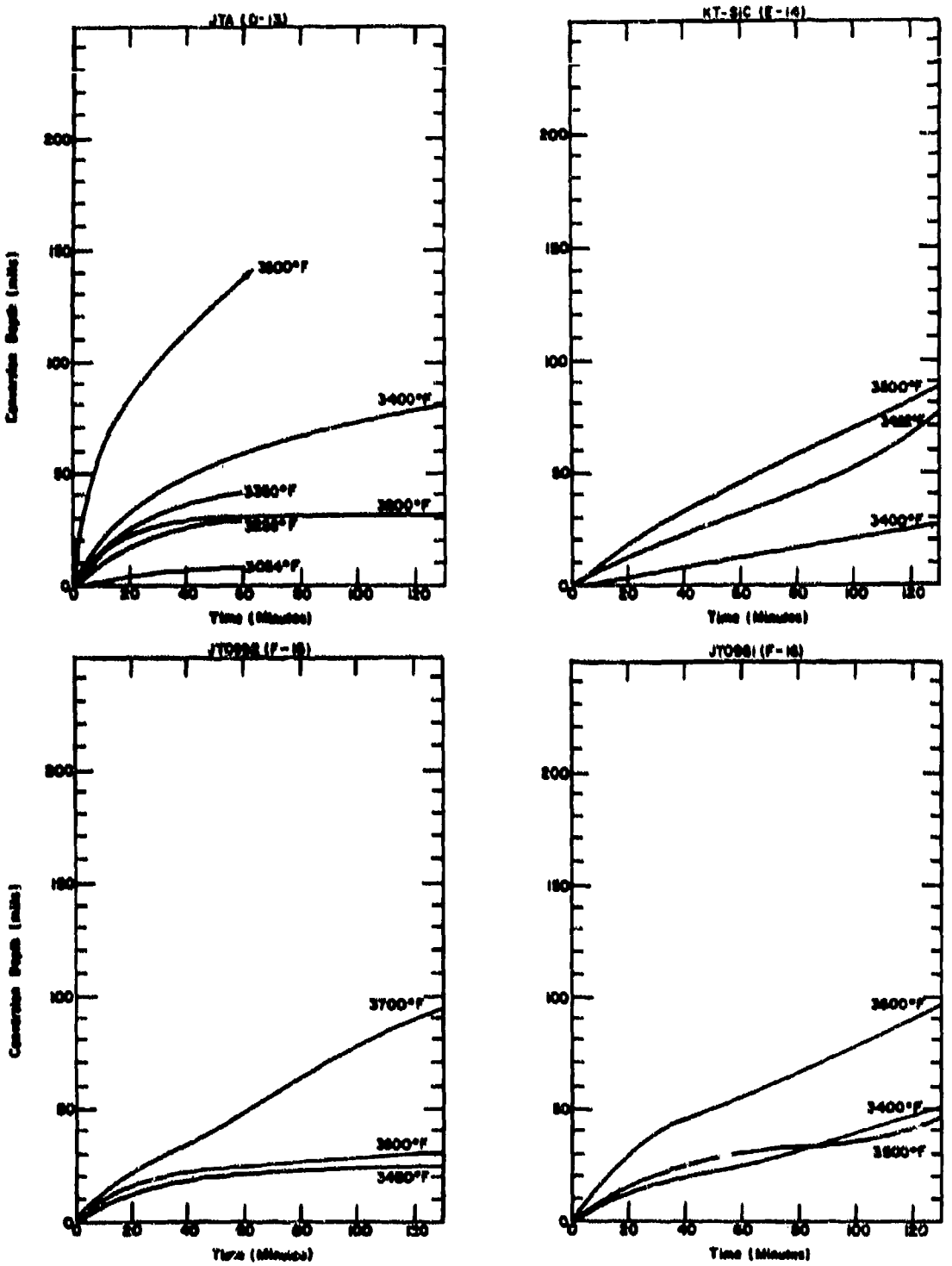

Figure 10. Conversion Depths for JTA(D-13), KT-SiC(E-14), JT0992 (F-15) and JT0981(F-16) as a Function of Time in Flowing Air at 1.8 ft/sec. (Small Furnace).

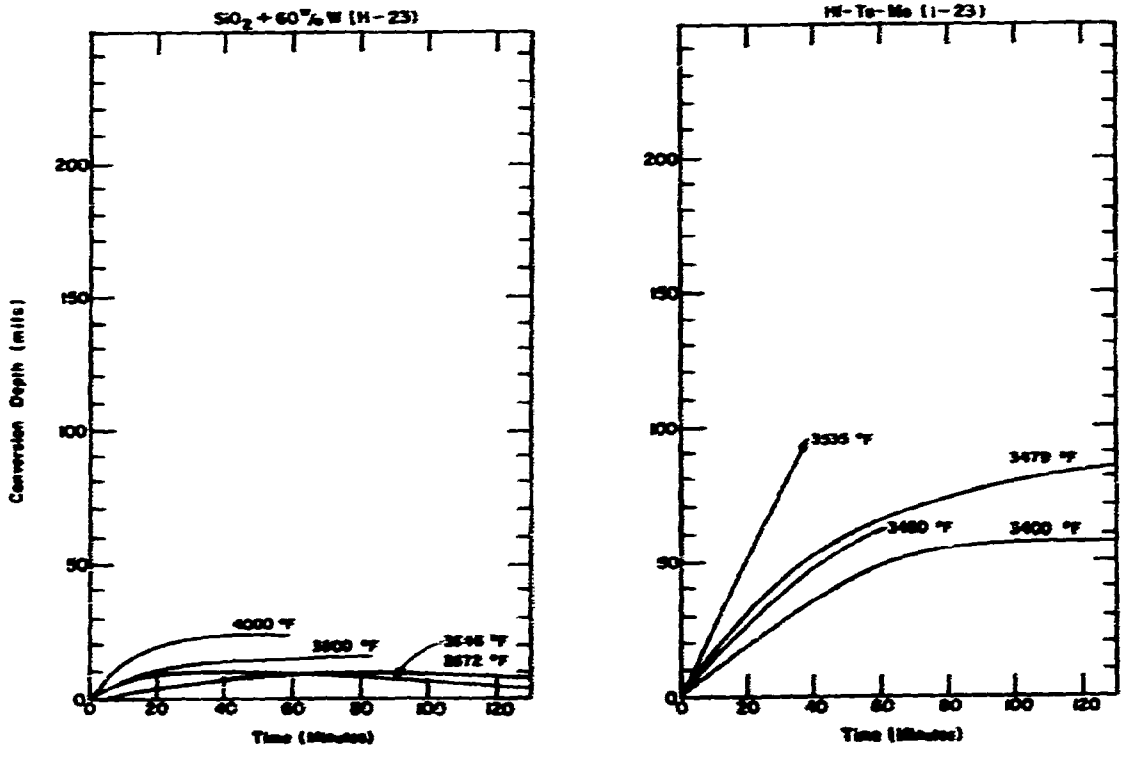

Figure 11. Conversion Depths for SiO_2+60w/oW(H-23) and Hf-Ta-Mo(I-23) as a Function of Time in Flowing Air at 1.8 ft/sec (Small Furnace).

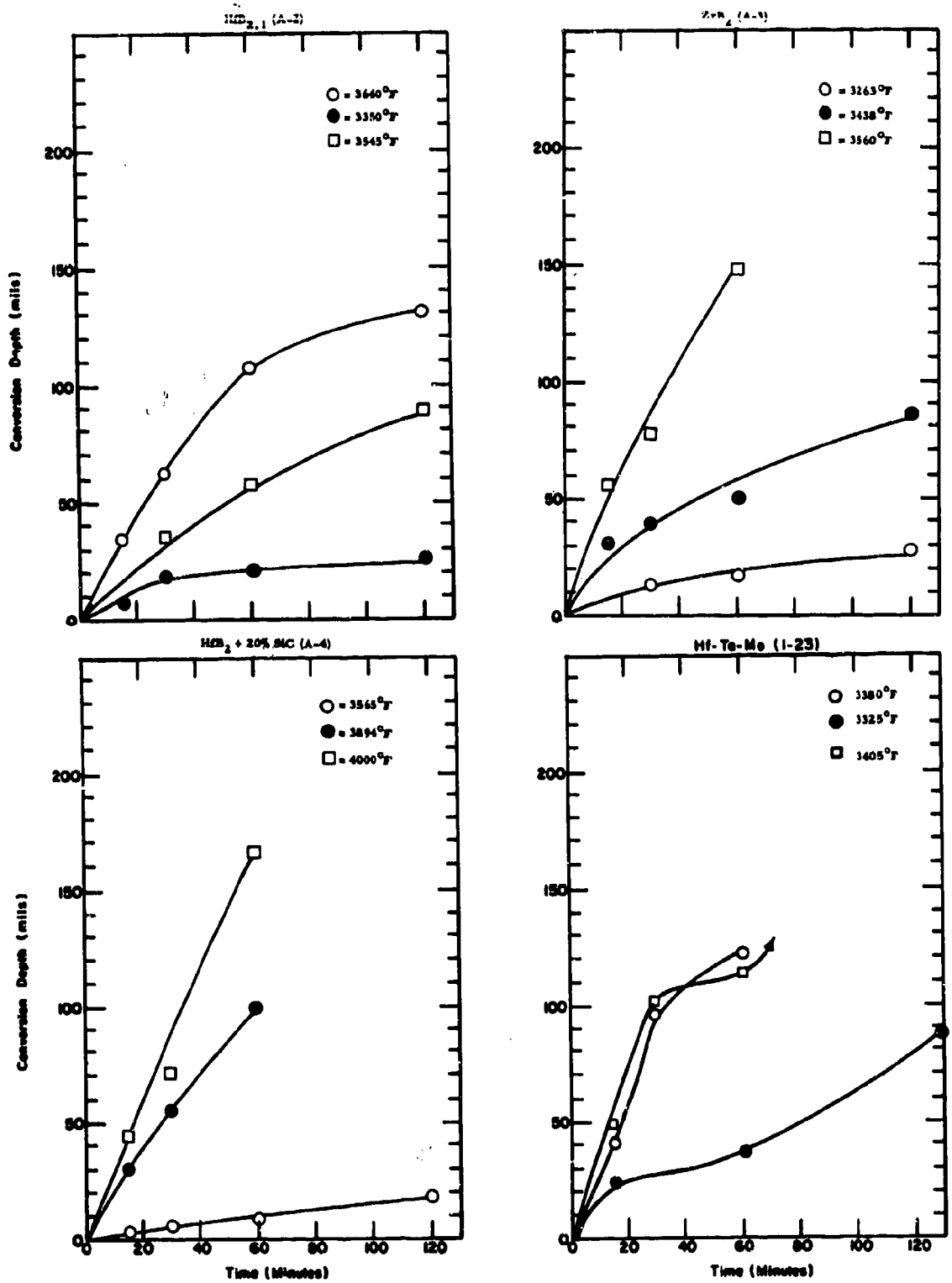

Figure 12. Conversion Depths for $HfB_{2.1}$ (A-2), ZrB_2 (A-3), HfB_2 + 20%SiC (A-4) and Hf-Ta-Mo (1-23) as a Function of Time in Flowing Air at 1.8 ft/sec. (Large Furnace).

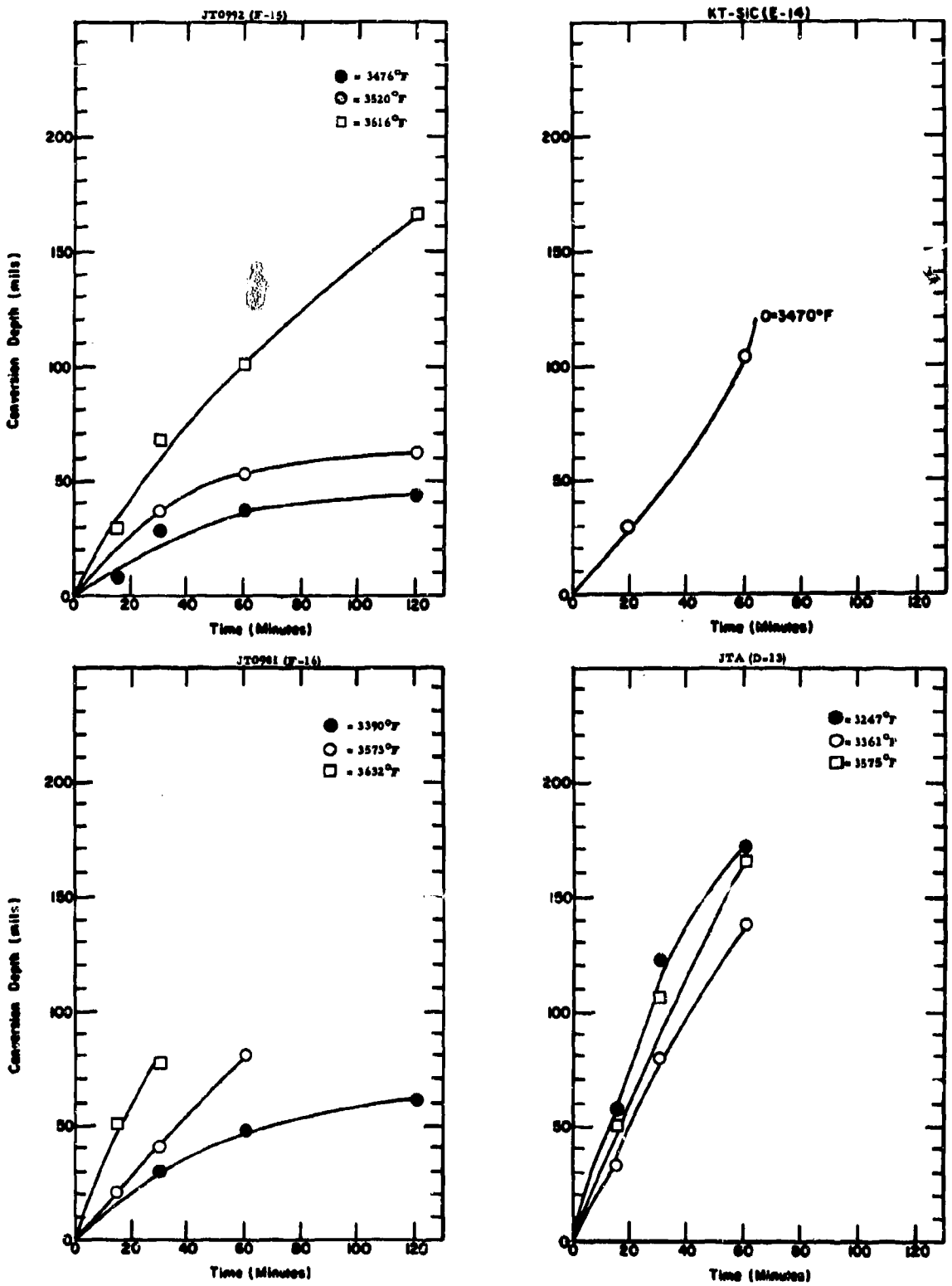

Figure 13. Conversion Depths for KT-SiC(E-14), JT0992(F-15), JT0981(F-16) and JTA(D-13) as a Function of Time in Flowing Air at 1.8 ft/sec. (Large Furnace).

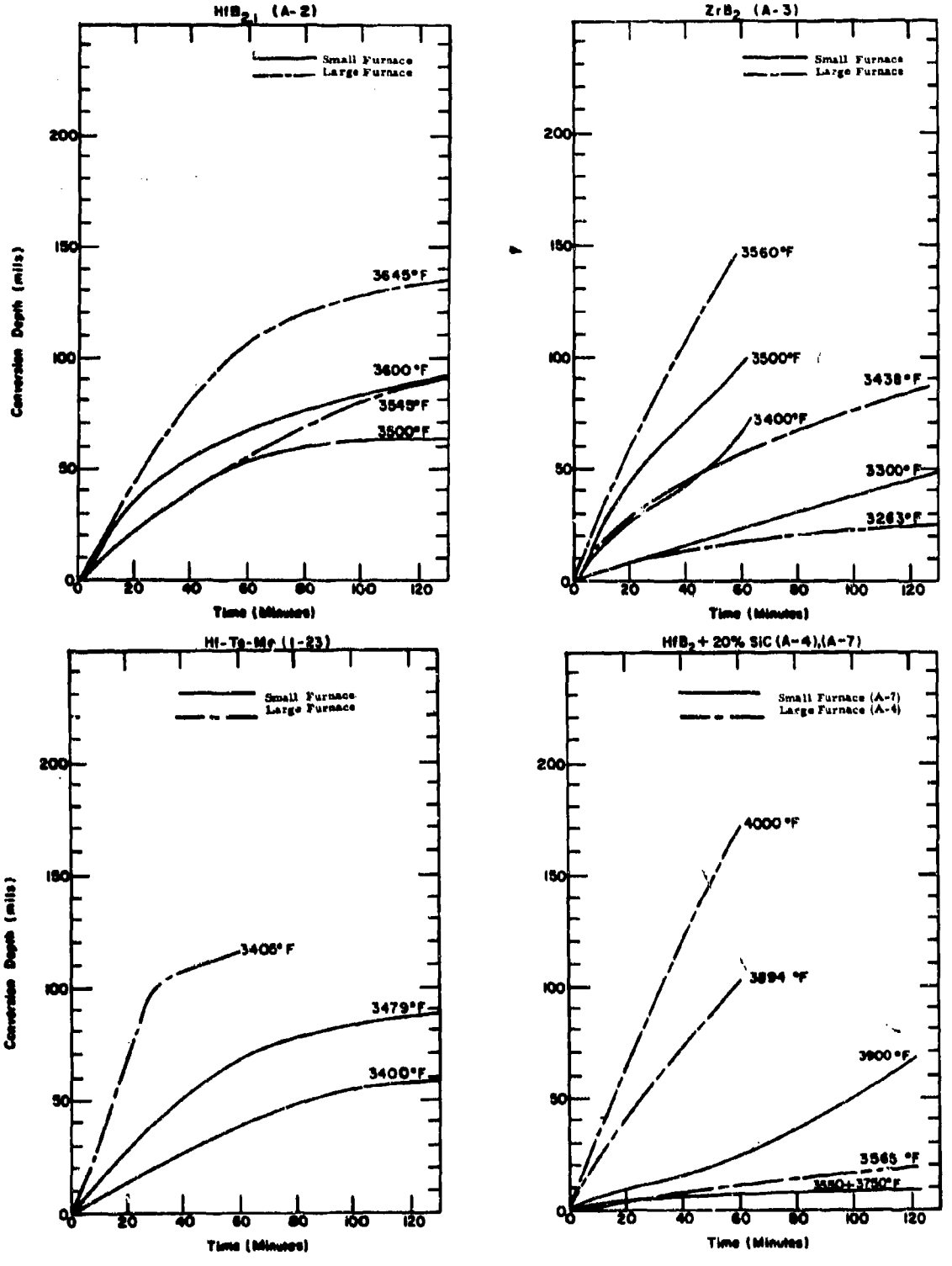

Figure 14. Comparison of Small and Large Furnace Conversion Depths for $HfB_{2.1}$(A-2), ZrB_2(A-3), HfB_2+20%SiC(A-4)(A-7) and Hf-Ta-Mo(I-23) as a Function of Time in Flowing Air at 1.8 ft/sec.

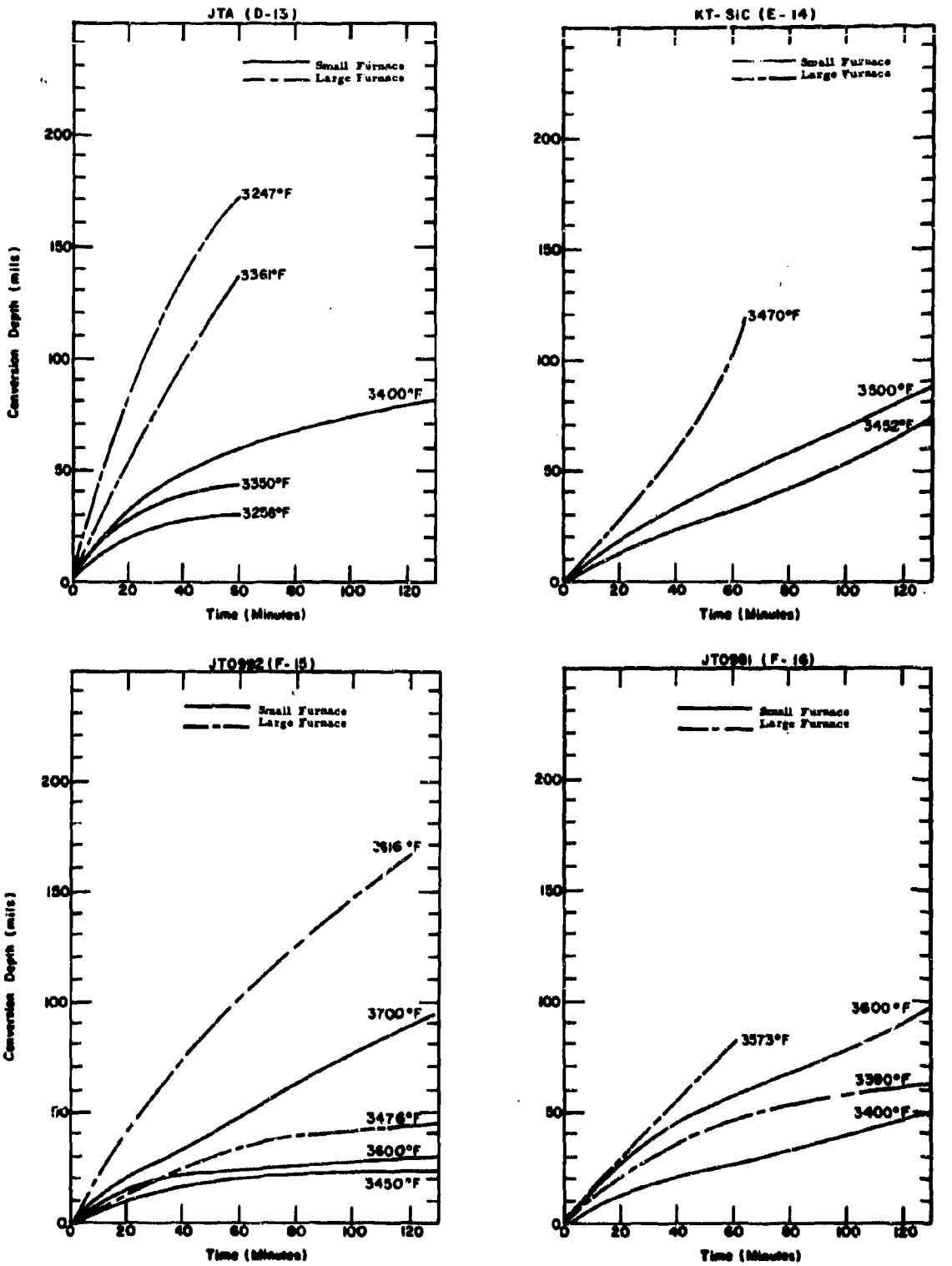

Figure 15. Comparison of Small and Large Furnace Conversion Depths for JTA(D-13), KT-SiC(E-14), JT0992(F-15) and JT0981(F-16) as a Function of Time in Flowing Air at 1.8 ft/sec.

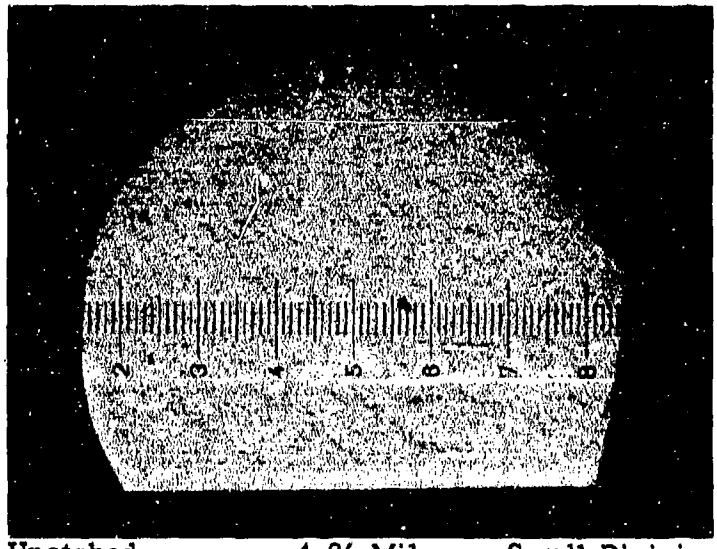

Plate No. 1-9052

Unetched 4.86 Mils per Small Division

Figure 16. Test 1356, $HfB_{2.1}$ (A-2) after 60 Minutes in Flowing Air at 3700°F, Transverse Section.

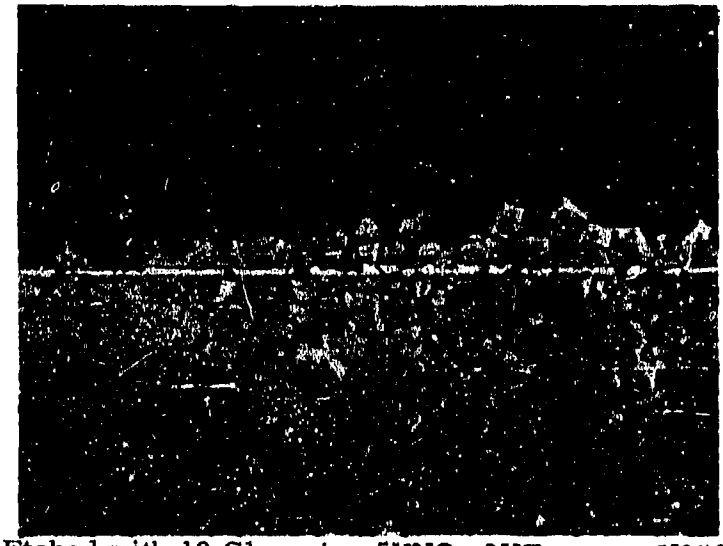

Plate No. 1-9053

Etched with 10 Glycerine $5HNO_3$ 3HF X250

Figure 17. Test 1356, $HfB_{2.1}$ (A-2) after 60 Minutes in Flowing Air at 3700°F, Transverse Section.

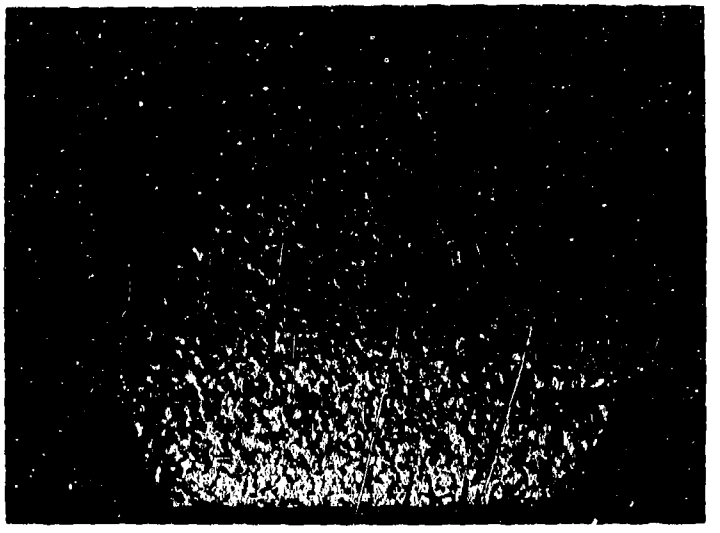

Plate No. 1-2429

Unetched 4.86 Mils per Small Division

Figure 18. Test 367, $HfB_{2.1}$(A-6) after 60 Minutes in Flowing Air at 3450°F, Transverse Section.

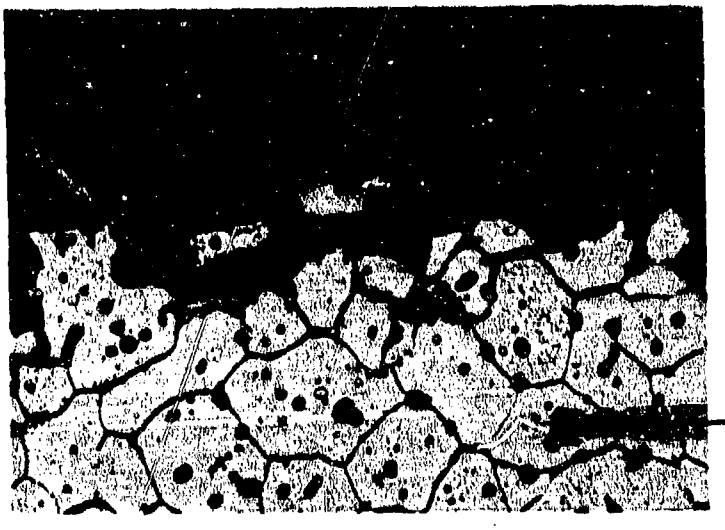

Plate No. 1-2427

Porosity

Etched with 10 Glycerine $5HNO_3$ 3HF X250

Figure 19. Test 367, $HfB_{2.1}$(A-6) after 60 Minutes in Flowing Air at 3450°F, Interface of Longitudinal Section.

Plate No. 1-8650

Unetched 4.86 Mils per Small Division

Figure 20. Test 1323, ZrB_2(A-3) after 60 Minutes in Flowing Air at 3300°F, Longitudinal Section.

Plate No. 1-8651

Etched with Glycerine $5HNO_3$ 3HF X250

Figure 21. Test 1323, ZrB_2(A-3) after 60 Minutes in Flowing Air at 3300°F, Interface of Longitudinal Section.

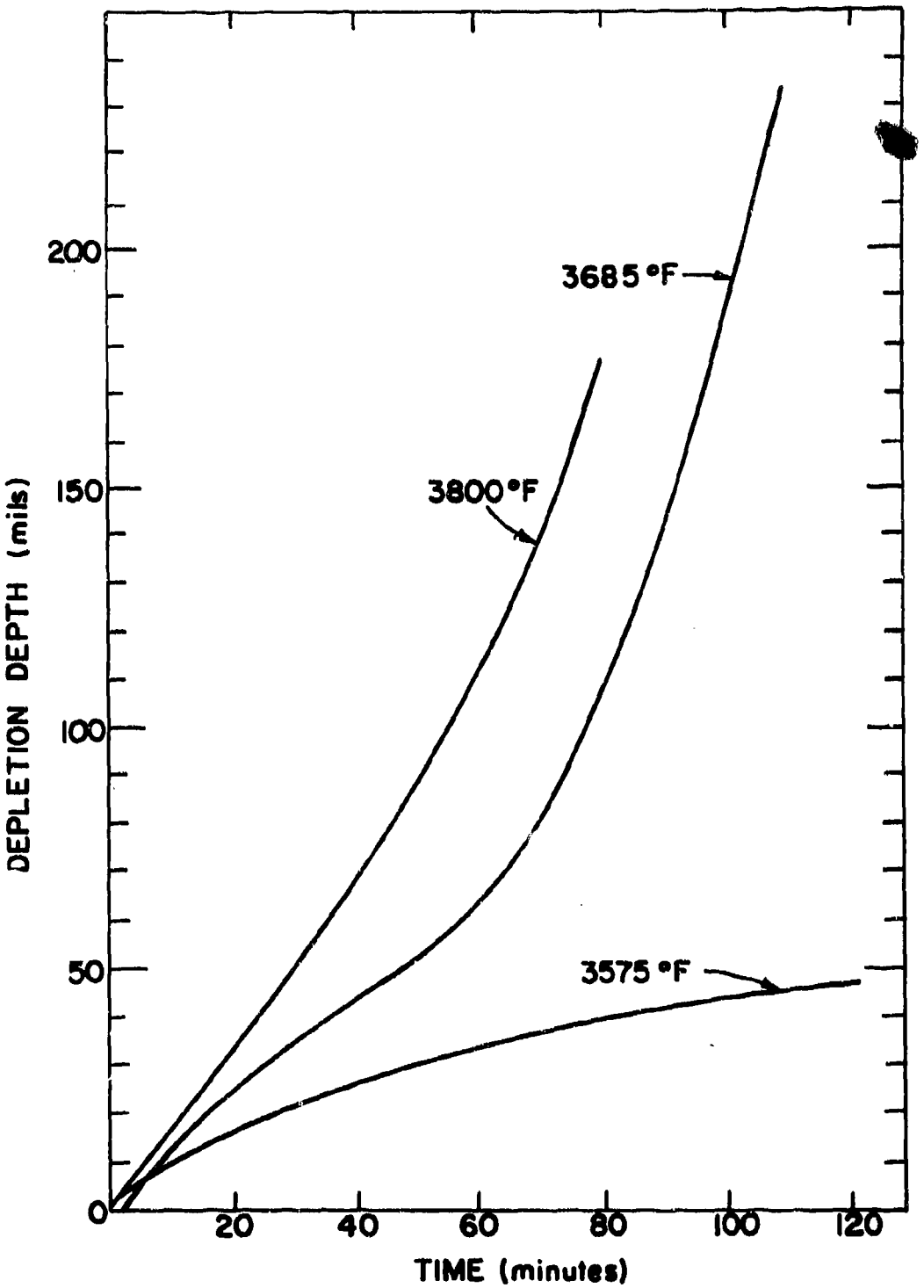

Figure 22. Depletion Depths for HfB_2+20%SiC(A-4) as a Function of Time in Flowing Air between 3575°F and 3795°F.

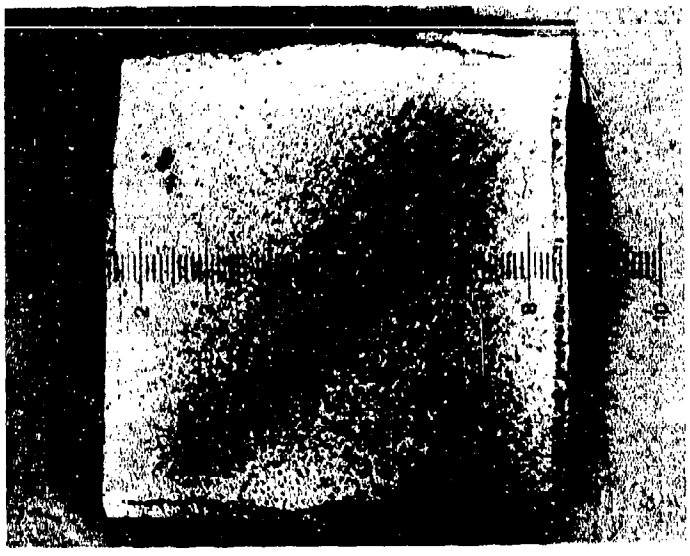

Plate No. 1-6062

Unetched 4.86 Mils per Small Division

Figure 23. Test 966, HfB_2+20%SiC(A-4-2) after 60 Minutes in Flowing Air at 3353°F, Longitudinal Section.

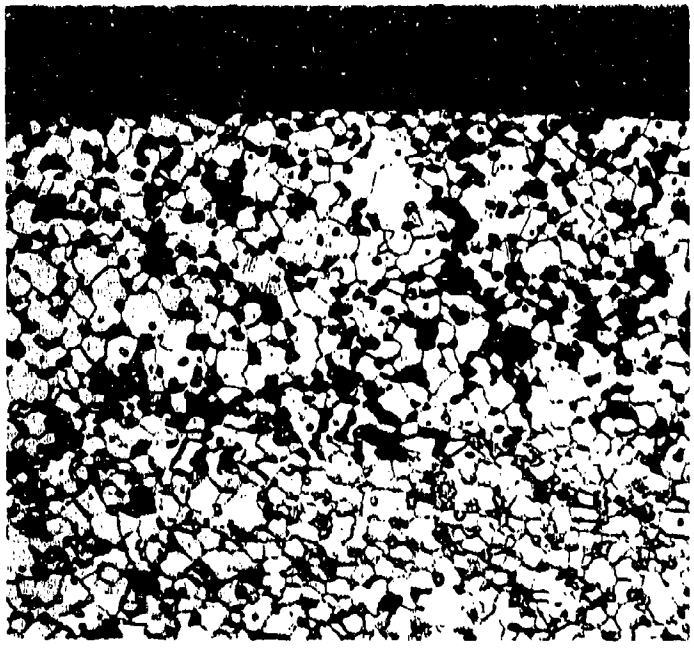

Plate No. 1-6063

Etched with 10 Glycerine 5 HNO_3 3HF X250

Figure 24. Test 966, HfB_2+20%SiC(A-4-2) after 60 Minutes in Flowing Air at 3353°F, Interfaces of Longitudinal Section.

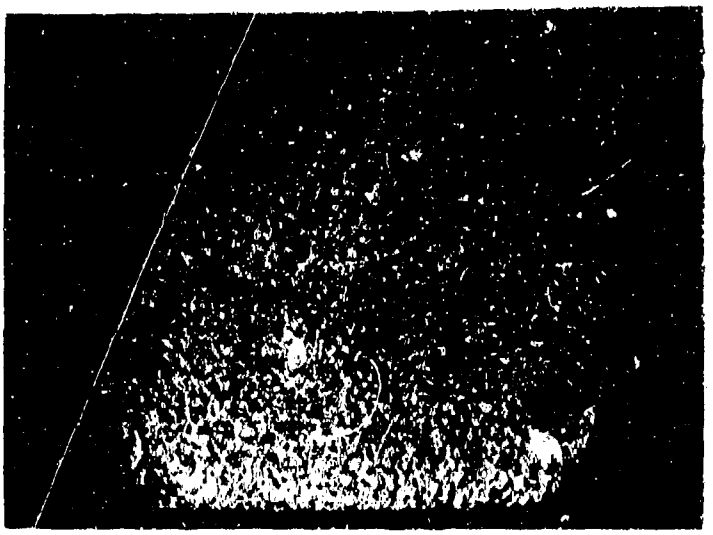

Plate No.
1-2428

Unetched 4.86 Mils per Small Division

Figure 25. Test 367, $HfB_{2.1}$ (A-6) after 60 Minutes in Flowing Air at 3450°F, Transverse Section.

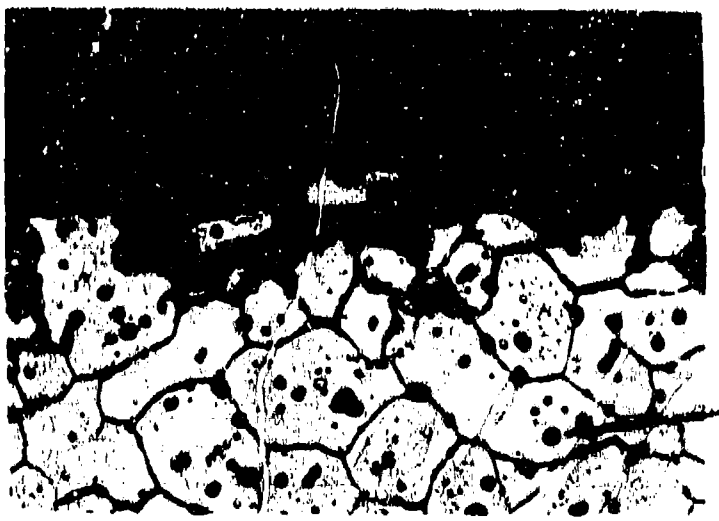

Plate No.
1-2427

Etched with 10 Glycerine
5HNO_3 3HF X250

Figure 26. Test 367, $HfB_{2.1}$ (A-6) after 60 Minutes in Flowing Air at 3450°F, Interface of Longitudinal Section.

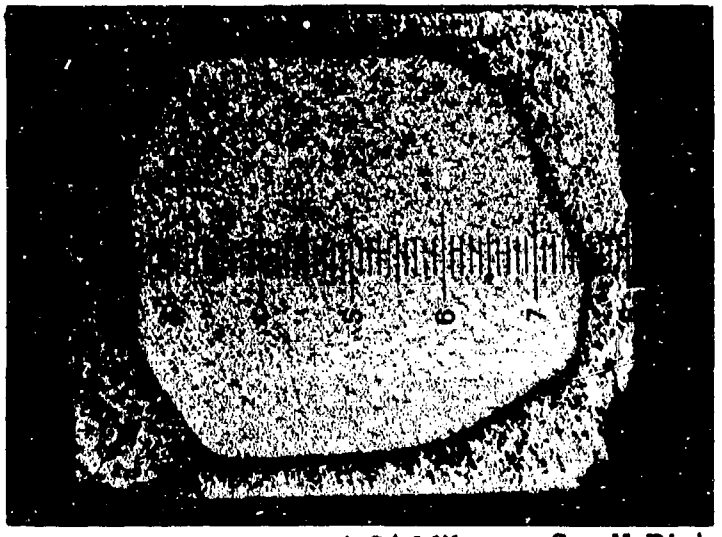

Plate No. 1-2505

Unetched 4.86 Mils per Small Division

Figure 27. Test 383, HfB_2 + 35%SiC(A-9) after 60 Minutes in Flowing Air at 3560°F, Longitudinal Section.

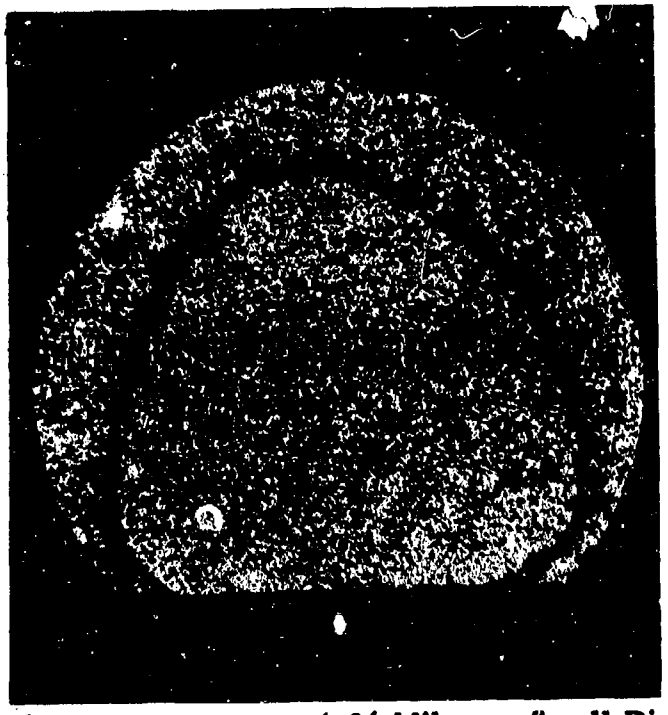

Plate No. 1-2510

Unetched 4.86 Mils per Small Division

Figure 28. Test 383, HfB_2 + 35%SiC(A-9) after 60 Minutes in Flowing Air at 3560°F, Transverse Section.

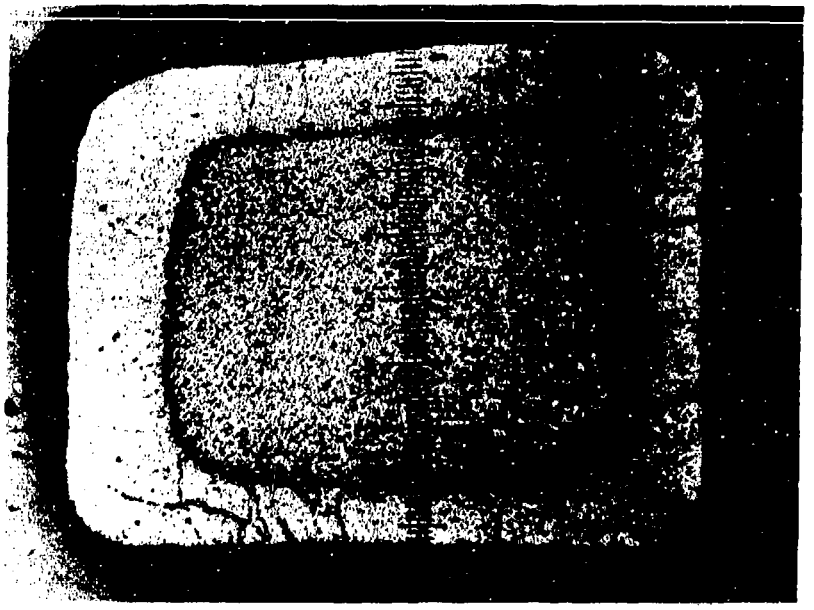

Plate No.
1-2312

Unetched 4.86 Mils Per Unit ~X8

Figure 29. HfB_2 + SiC (A-4), OX-334 (60 Min. at 3794°F) Longitudinal Section. Conversion Depth 7 Mils. Depth of SiC Depleted Zone 60 Mils.

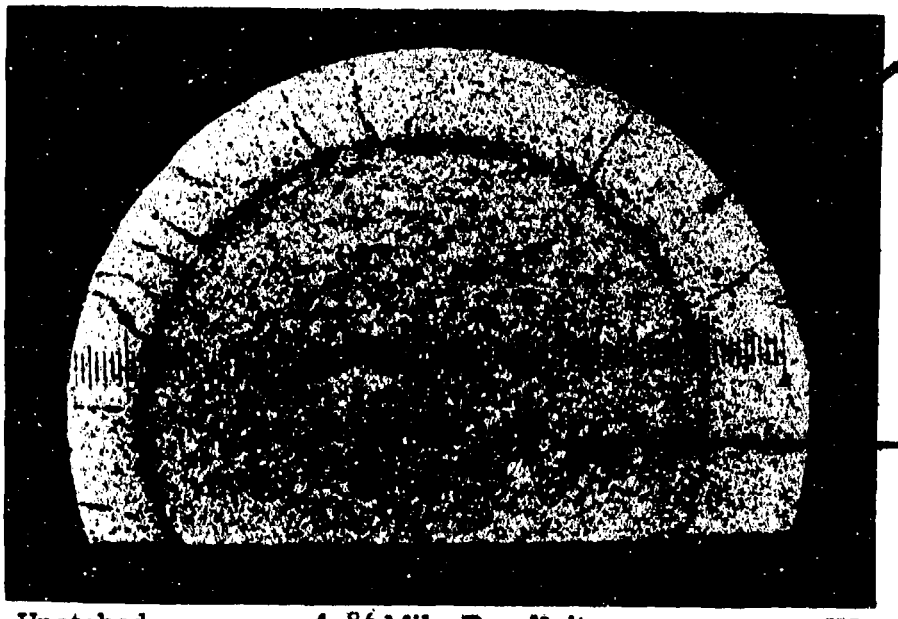

HfB_2
(SiC depleted)

Plate No.
1-2315

HfB_2 + SiC

Unetched 4.86 Mils Per Unit ~X8

Figure 30. HfB_2 + SiC (A-4), OX-334 (60 Min. at 3794°F) Transverse Section. Conversion Depth 5 Mils. Depth of SiC Depleted Zone 67 Mils.

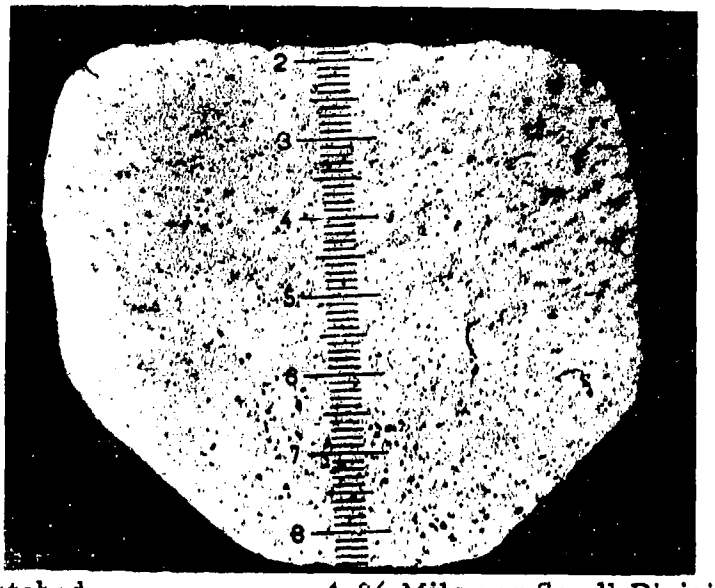

Plate No. 1-7316

Unetched 4.86 Mils per Small Division

Figure 31. Test 1174, Boride Z (A-5) after 60 Minutes in Flowing Air at 3628°F, Longitudinal Section.

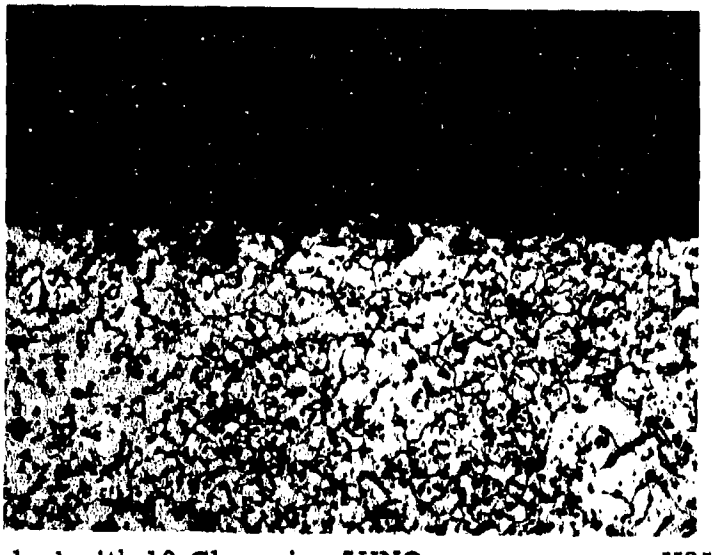

Plate No. 1-7318

Etched with 10 Glycering $5HNO_3$ X250

Figure 32. Test 1174, Boride Z(A-5) after 60 Minutes in Flowing Air at 3628°F, Interface of Transverse Section.

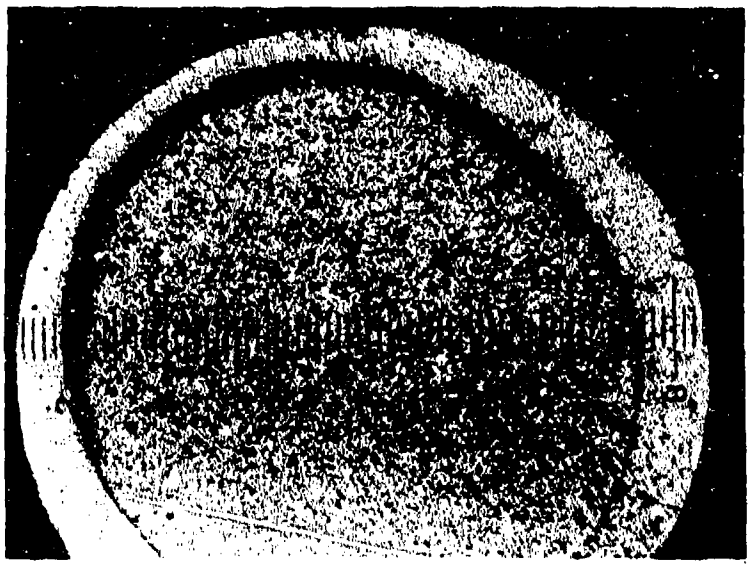

Plate No. 1-2843

Unetched 4.86 Mils per Small Division

Figure 33. Test 437, ZrB_2 + 20%SiC(A-8) after 60 Minutes in Flowing Air at 3540°F, Transverse Section.

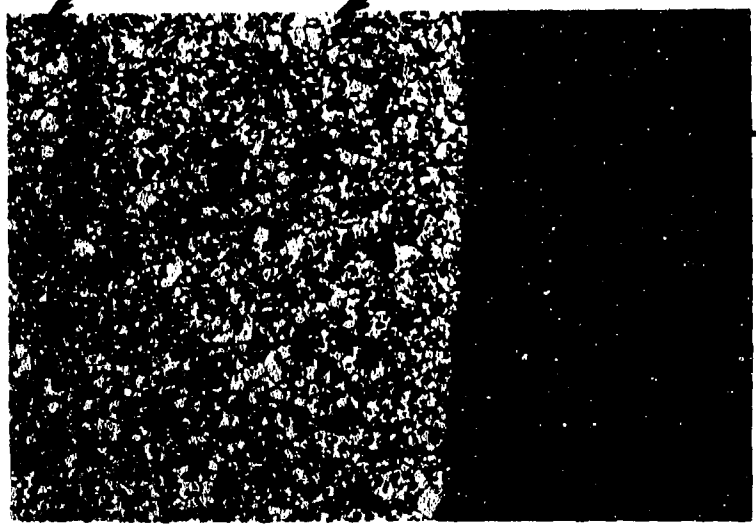

Plate No. 1-2842

Etched with 10 Glycerine 5HNO_3 3HF X100

Figure 34. Test 437, ZrB_2 + 20%SiC(A-8) after 60 Minutes in Flowing Air at 3540°F, Interfaces of Transverse Section.

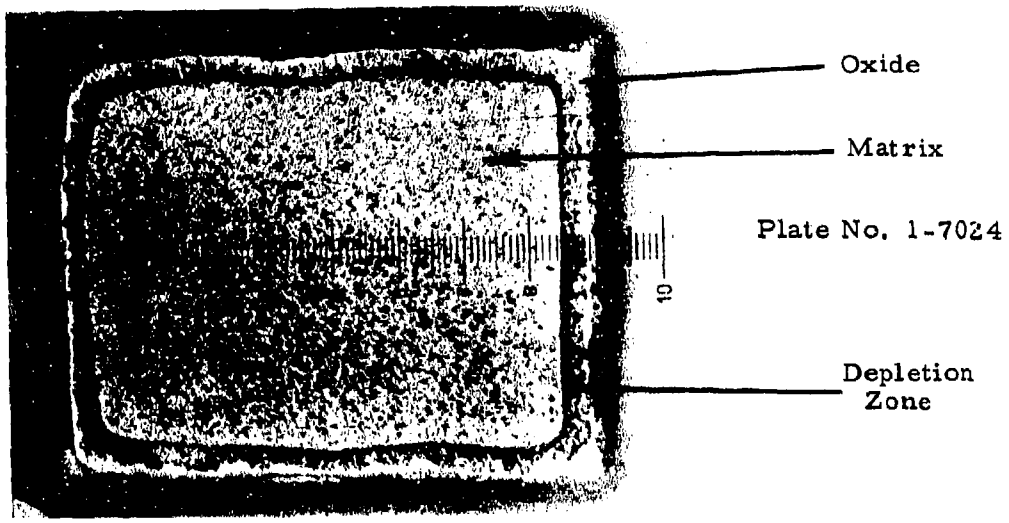

Unetched 4.86 Mils per Small Division

Figure 35. Test 1134, ZrB_2 + 14%SiC + 30%C(A-10) after 60 Minutes in Flowing Air at 3427°F, Longitudinal Section.

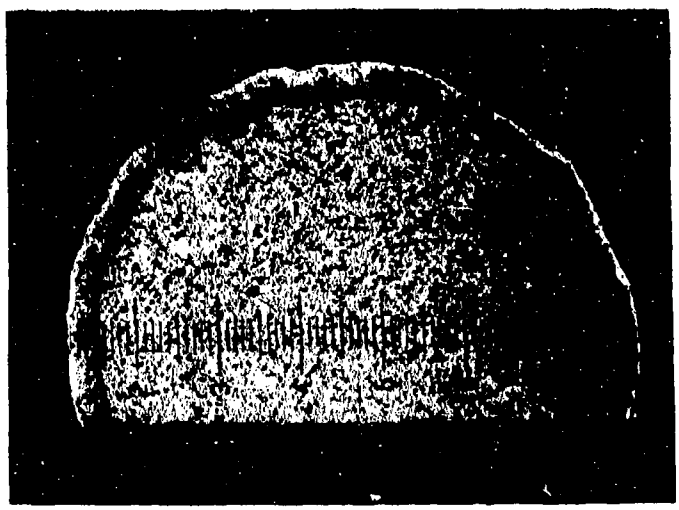

Plate No. 1-7027

Unetched 4.86 Mils per Small Division

Figure 36. Test 1134, ZrB_2 + 14%SiC + 30%C(A-10) after 60 Minutes in Flowing Air at 3427°F, Transverse Section.

Plate No.
1-1582

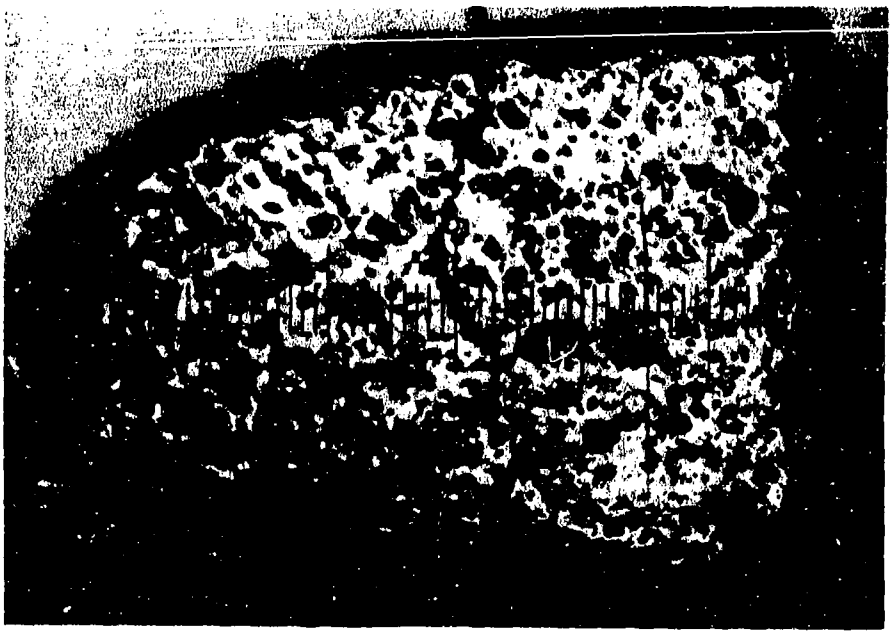

Unetched 4.86 Mils Per Unit ~X15

Figure 37. RVA Graphite (B-5), OX-198 (10 Min. at 2813°F) Longitudinal Section. Recession 105 Mils.

Plate No.
1-1584

Unetched 1.97 Mils Per Unit ~X20

Figure 38. RVA Graphite (B-5) OX-198 (10 Min at 2813°F) Transverse Section. Recession 137 Mils.

Plate No.
1-1592

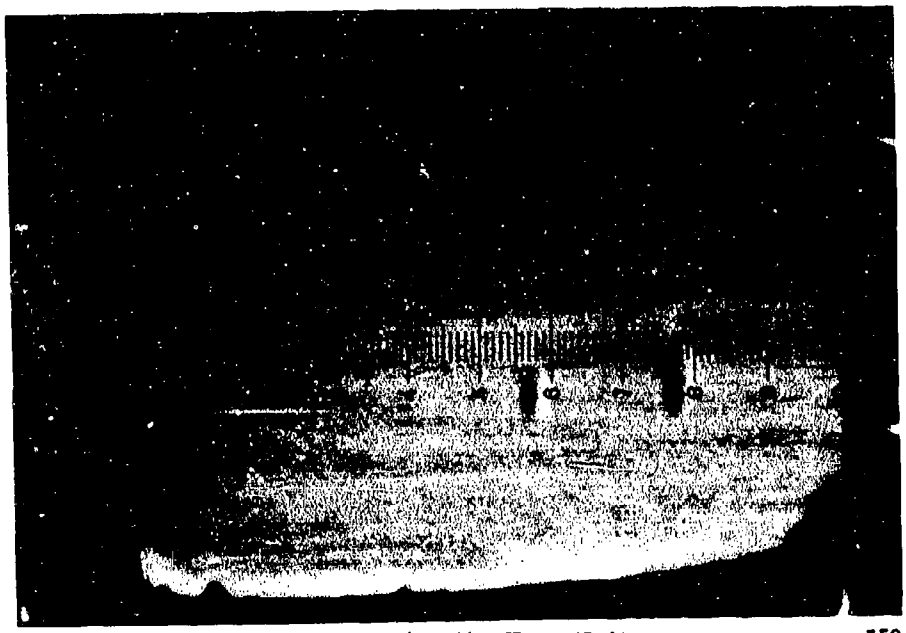

Unetched 4.86 Mils Per Unit ~X8

Figure 39. Pyrolytic Graphite (B-6), OX-200 (10 Min. at 2876°F) Longitudinal Section. Recession 19 Mils.

Plate No.
1-1594

Unetched 4.86 Mils Per Unit ~X11

Figure 40. Pyrolytic Graphite (B-6), OX-200 (10 Min. at 2876°F) Transverse Section. Recession 27 Mils.

Plate No.
1-1622

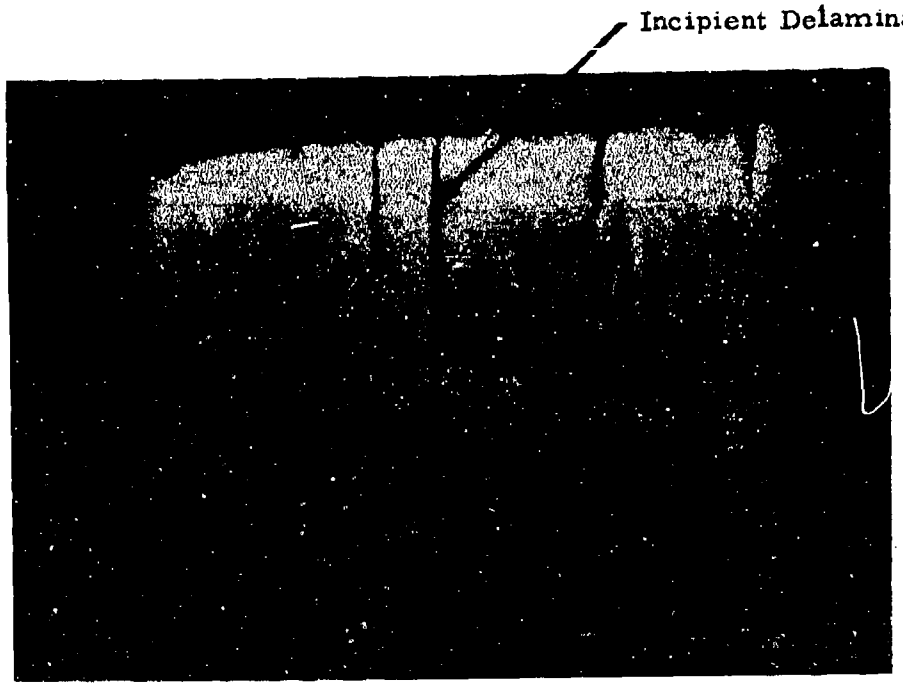

Unetched 4.86 Mils Per Unit ~X8

Figure 41. Boron Pyrolytic Graphite (B-7) OX-207 (10 Min. at 2804°F) Longitudinal Section. Recession 19 Mils.

Plate No.
1-1624

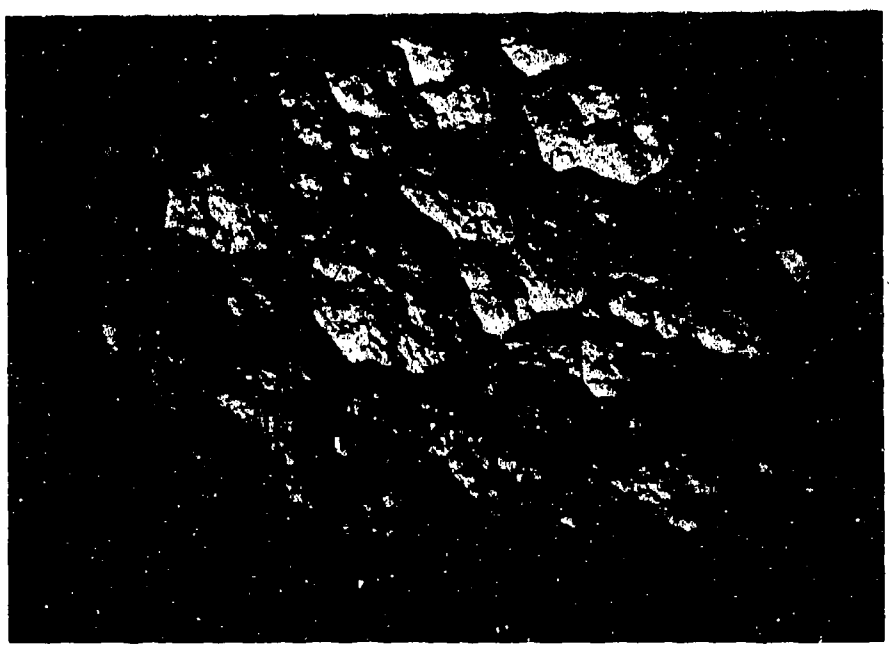

Unetched 4.86 Mils Per Unit ~X11

Figure 42. Boron Pyrolytic Graphite (B-7) OX-207 (10 Min. at 2804°F) Transverse Section. Recession 36 Mils.

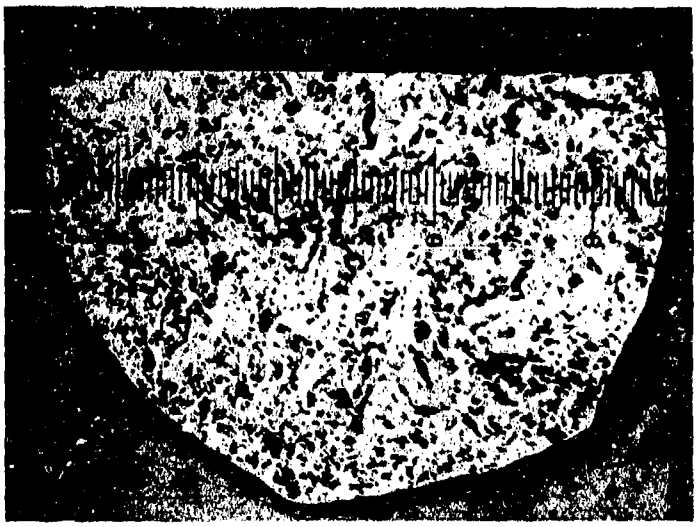

Plate No. 1-6830

Unetched 4.86 Mils per Small Division

Figure 43. Test 1099, PT0178(B-9) after 5 Minutes in Flowing Air at 3402°F, Transverse Section.

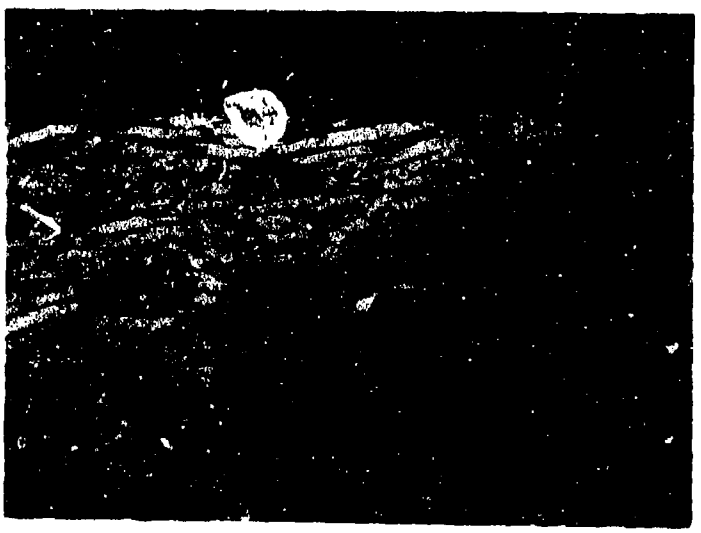

Plate No. 1-6828

Unetched X250

Figure 44. Test 1099, PT0178(B-9) after 5 Minutes in Flowing Air at 3402°F, Interface of Longitudinal Section.

Plate No. 1-6745

Unetched 4.86 Mils per Small Division

Figure 45. Test 1074, AXF-5Q Poco Graphite (B-10) after 10 Minutes in Flowing Air at 3835°F, Longitudinal Section.

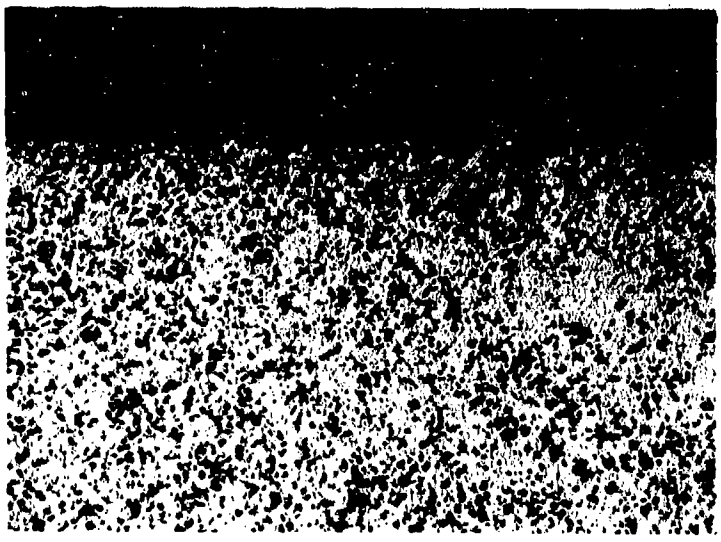

Plate No. 1-6746

Unetched X250

Figure 46. Test 1074, AXF-5Q Poco Graphite (B-10) after 10 Minutes in Flowing Air at 3835°F. Interface of Longitudinal Section.

Plate No. 3813C

Unetched X13,000

Figure 47. Microstructural Characteristics of AXF-5Q Poco Graphite (B-10). 1.5% Parlodion Replica Shadowed with Chromium at 60° Angle.

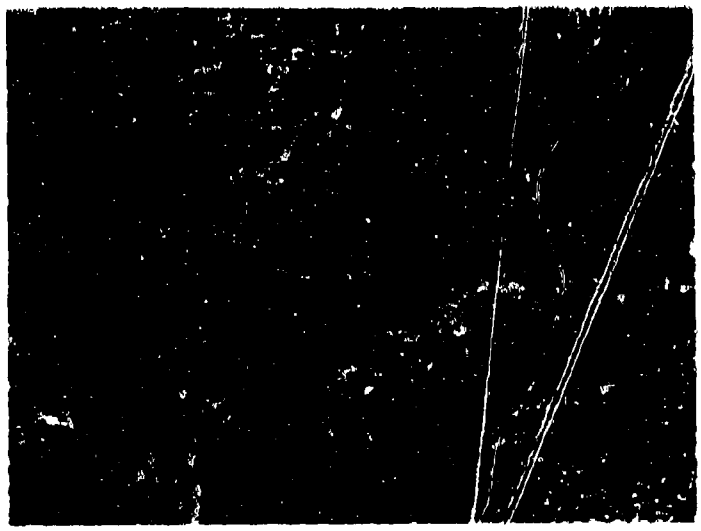

Plate No. 3813D

Unetched X13,000

Figure 48. Microstructural Characteristics of AXF-5Q Poco Graphite (B-10). 1.5% Parlodion Replica Shadowed with Chromium at 60° Angle.

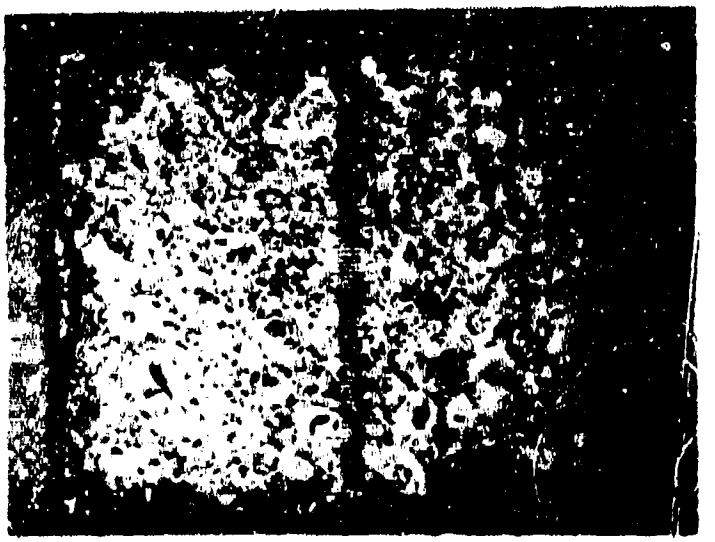

Plate No. 1-6361

Unetched 4.86 Mils per Small Division

Figure 49. Test 1048, Si/RVC(B-8) after 60 Minutes in Flowing Air at 2806°F, Longitudinal Section.

Plate No. 1-6362

Unetched X250

Figure 50. Test 1048, Si/RVC(B-8) after 60 Minutes in Flowing Air at 2806°F, Interface of Longitudinal Section. Coating Did Not Fail.

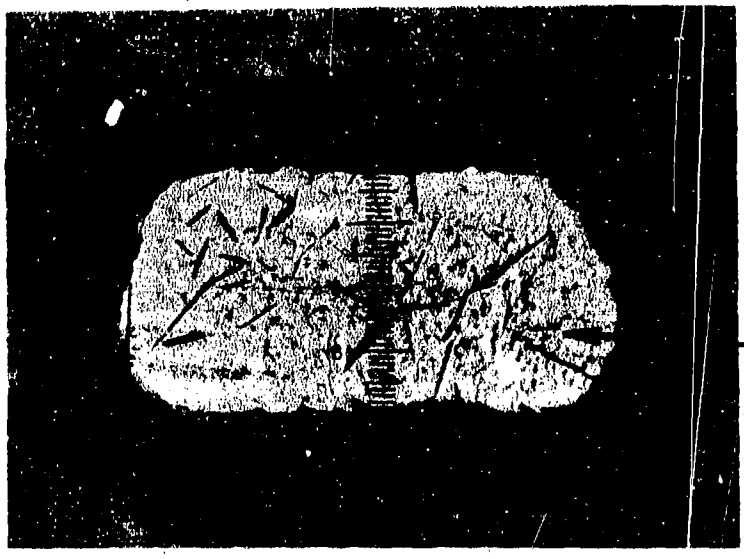

Plate No. 1-5992

Carbide

Oxide

Unetched 4.86 Mils per Small Division

Figure 51. Test 973, HfC + C(C-11) after 60 Minutes in Flowing Air at 3279°F, Longitudinal Section.

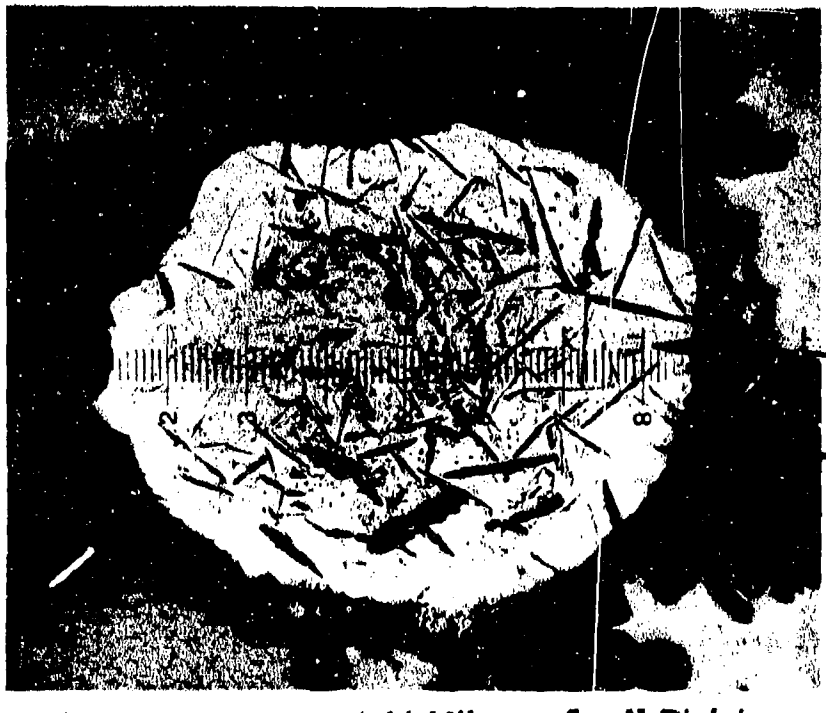

Plate No. 1-6159

Carbide

Oxide

Unetched 4.86 Mils per Small Division

Figure 52. Test 988, ZrC + C(C-12) after 60 Minutes in Flowing Air at 3058°F, Transverse Section.

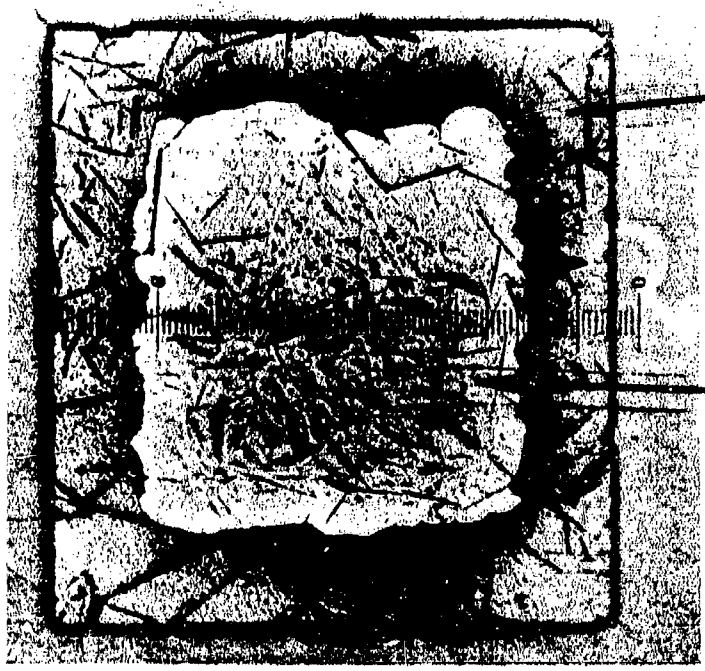

Unetched 4.86 Mils per Small Division

Figure 53. Test 987, HfC + C(C-11) after 60 Minutes in Flowing Air at 4054°F, Longitudinal Section.

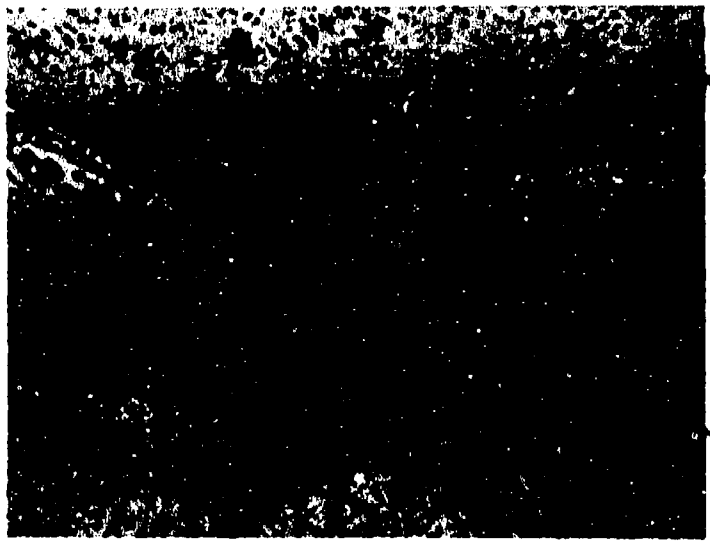

Unetched X250

Figure 54. Test 987, HfC + C(C-11) after 60 Minutes in Flowing Air at 4054°F, Interface of Longitudinal Section.

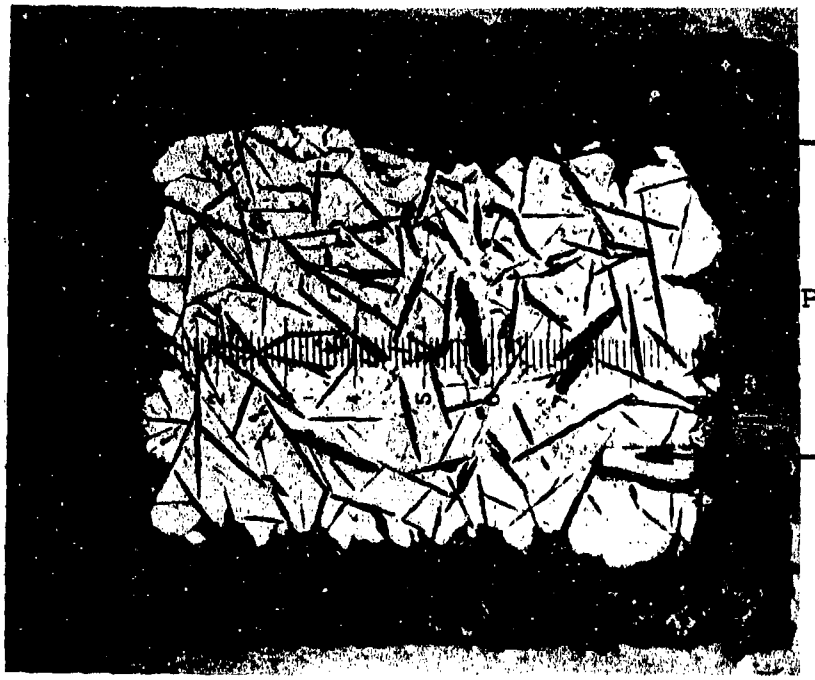

Unetched 4.86 Mils per Small Division

Figure 55. Test 1031, ZrC + C(C-12) after 60 Minutes in Flowing Air at 3645°F, Longitudinal Section.

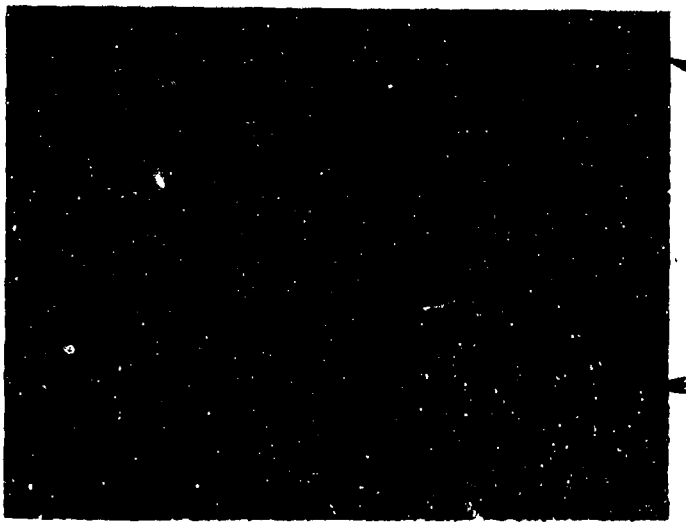

Unetched X250

Figure 56. Test 1031, ZrC + C(C-12) after 60 Minutes in Flowing Air at 3645°F, Interface of Longitudinal Section.

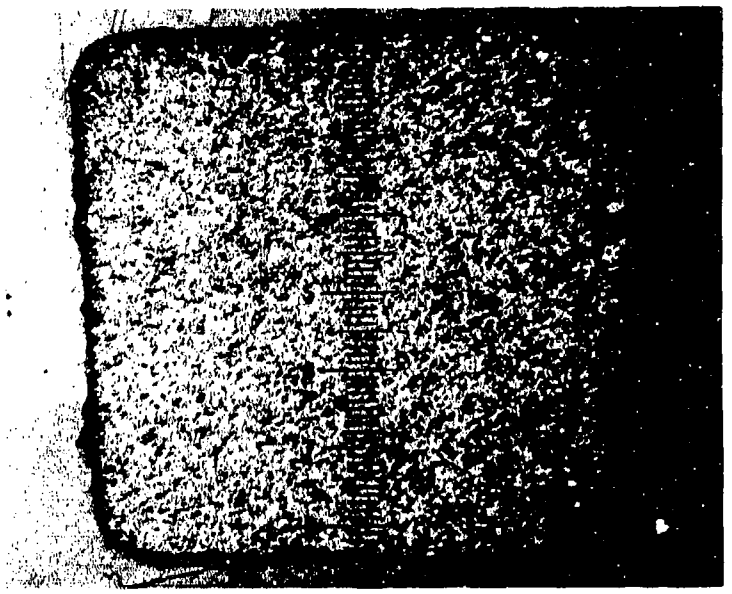

Plate No. 1-6807

Unetched 4.86 Mils per Small Division

Figure 57. Test 1090, JTA(D-13) after 60 Minutes in Flowing Air at 3350°F, Longitudinal Section.

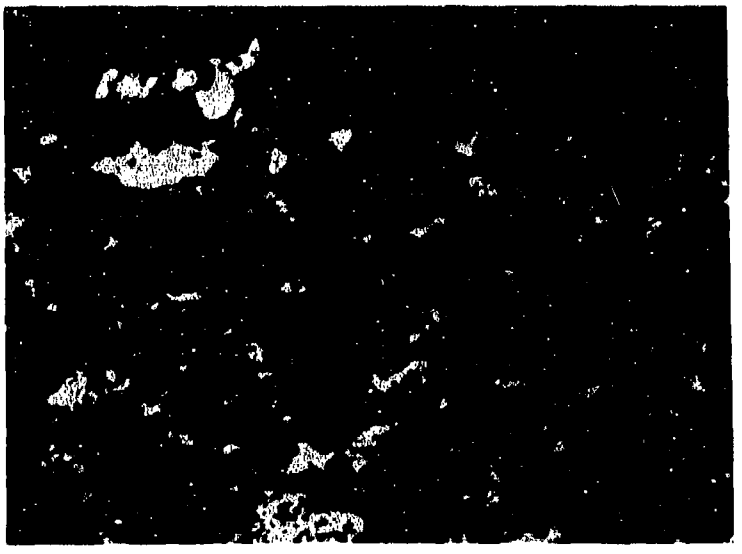

Plate No. 1-6808

Unetched X250

Figure 58. Test 1090, JTA(D-13) after 60 Minutes in Flowing Air at 3350°F, Interface of Longitudinal Section.

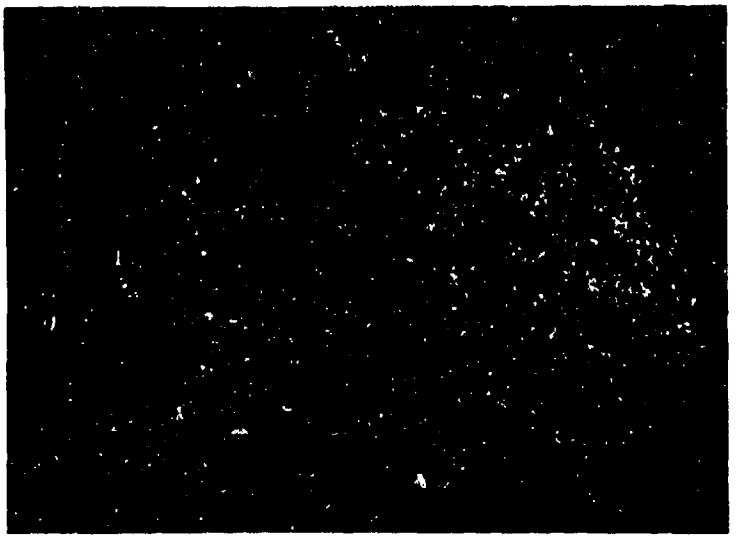

Plate No. 1-8947

Unetched 4.86 Mils per Small Division

Figure 59. Test 1378, JT0992(F-15) after 60 Minutes in Flowing Air at 3450°F, Transverse Section

Plate No. 1-8948

Unetched X250

Figure 60. Test 1378, JT0992(F-15) after 60 Minutes in Flowing Air at 3450°F, Interface of Transverse Section.

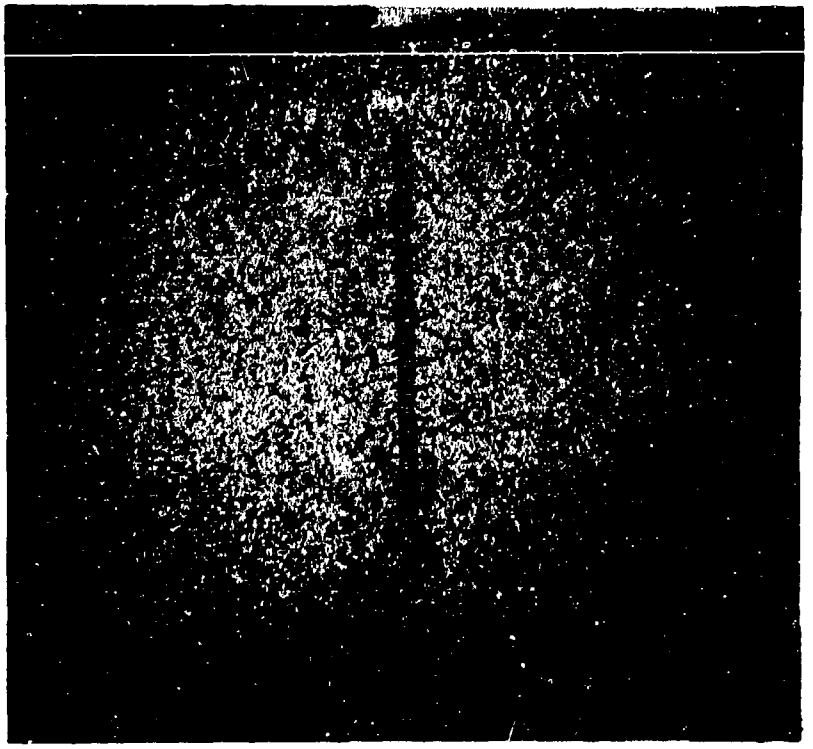

Plate No. 1-4389

Unetched 4.86 Mils Per Small Division

Figure 61. Test 734, JT0981(F-16) after 60 Minutes in Flowing Air at 3668°F, Longitudinal Section.

Plate No. 1-4390

Unetched X250

Figure 62. Test 734, JT0981(F-16) after 60 Minutes in Flowing Air at 3668°F, Interface of Longitudinal Section.

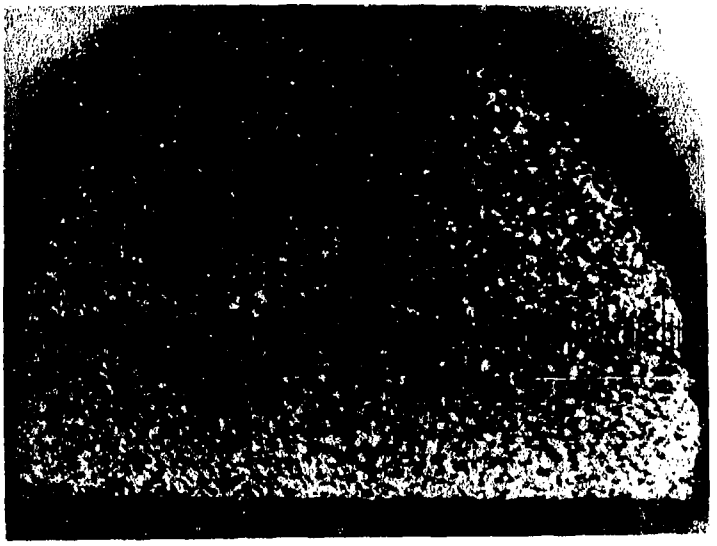

Plate No. 1-7332

Unetched 4.86 Mils per Small Division

Figure 63. Test 1177, KT-SiC(E-14) after 60 Minutes in Flowing Air at 3371°F, Transverse Section.

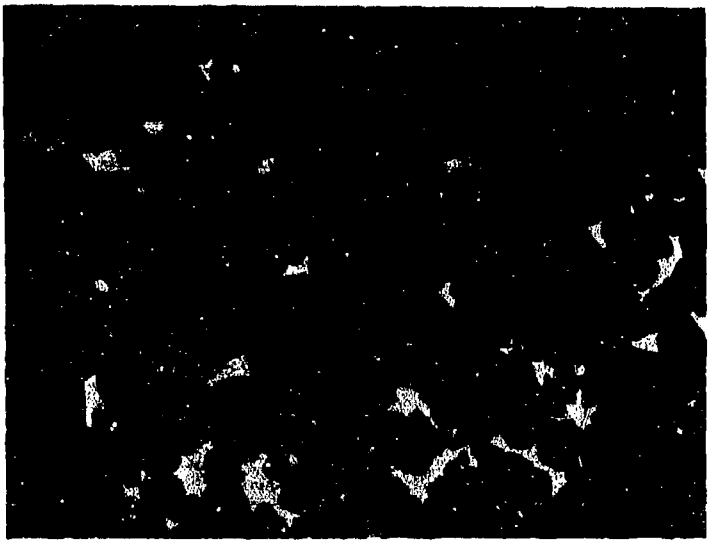

Plate No. 1-7333

Etched Electrolytically with 5%KOH Solution X250

Figure 64. Test 1177, KT-SiC(E-14) after 60 Minutes in Flowing Air at 3371°F, Interface of Transverse Section.

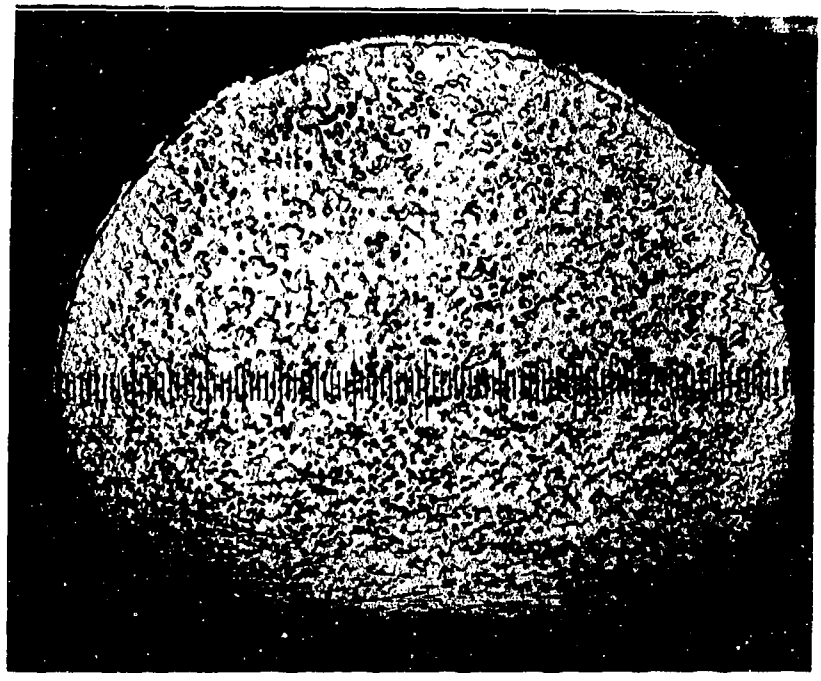

Plate 1-3157

Etched with Murakamis' Reagent Approximately X10

Figure 65. Test 478, WSi_2/W (G-18) after 60 Minutes in Flowing Air at 3325°F. Transverse Section, 4.86 Mils/Unit.

Plate 1-3156

Etched with Murakamis' Reagent X250

Figure 66. Test 478, WSi_2/W (G-18) after 60 Minutes in Flowing Air at 3325°F. Transverse Section, W_5Si_3 Zone Width Equals 5.0 Mils.

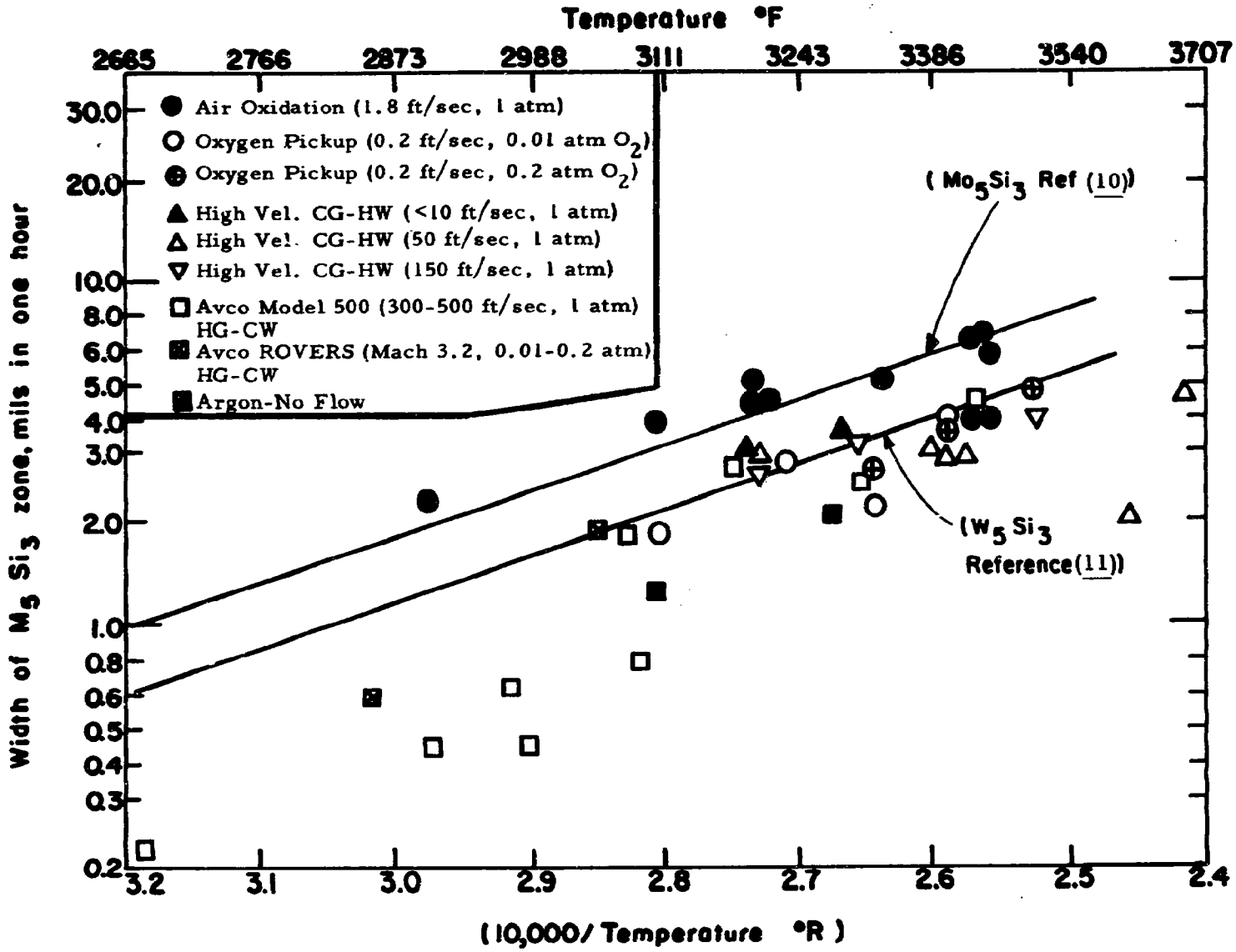

Figure 67. Growth of W_5Si_3 Zone on WSi_2/W(G-18) as a function of Flow Rate and Pressure Compared with the results of Bartlett and Gage (11) for W_5Si_3 and Perkins and Packer for Mo_5Si_3 (10).

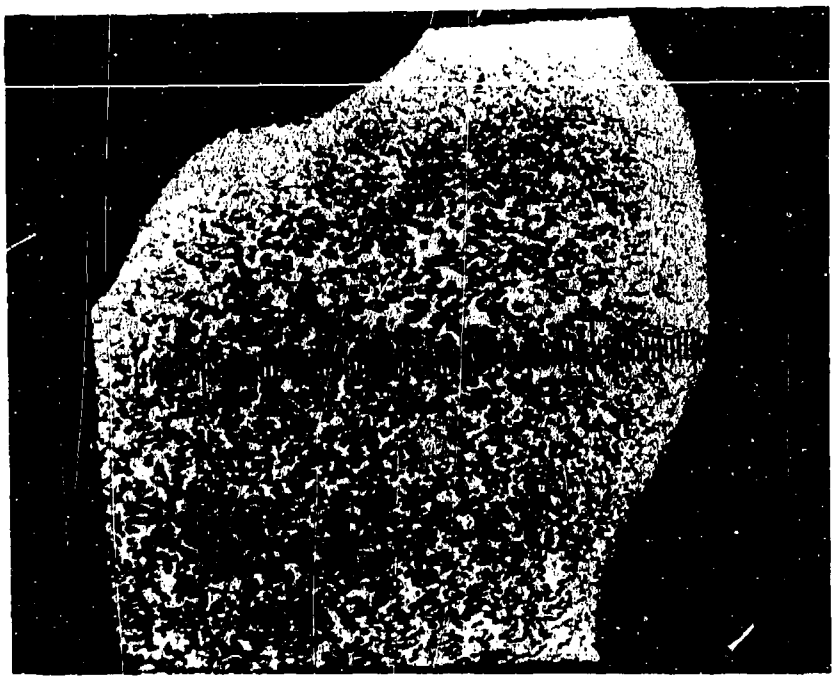

Plate 1-3191

Etched with Murakamis' Reagent Approximately X8

Figure 68. Test 485, WSi_2/W(G-18) after 60 Minutes in Flowing Air at 3532°F. Longitudinal Section, 4.86 Mils/Unit.

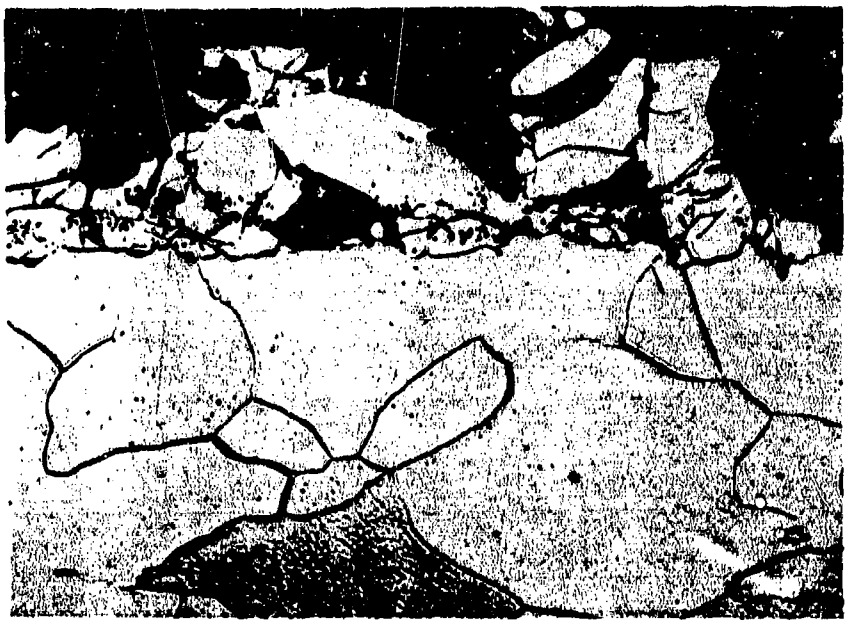

Coating

Plate 1-3192

Tungsten

Etched with Murakamis' Reagent 250X

Figure 69. Test 485, WSi_2/W (G-18) after 60 Minutes in Flowing Air at 3532°F, Longitudinal Section.

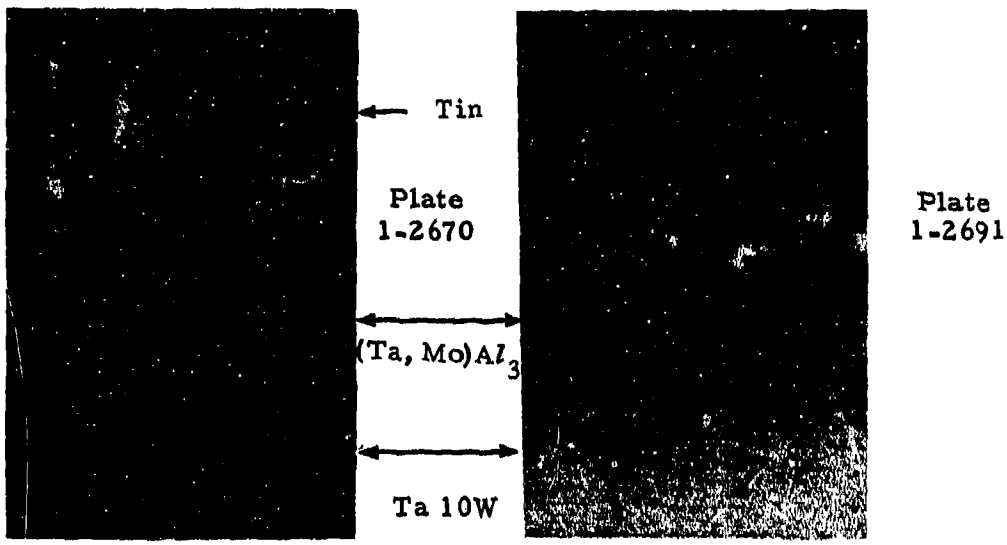

Etched with 30 cc Lactic Acid, 10 cc HNO_3, 5 cc HF X250

Figure 70. Test 390 (left) and Test 400, Sn-Al/Ta-10W after One Hour Exposures in Flowing Air at 2624°F and 3092°F. Interface of Longitudinal Section.

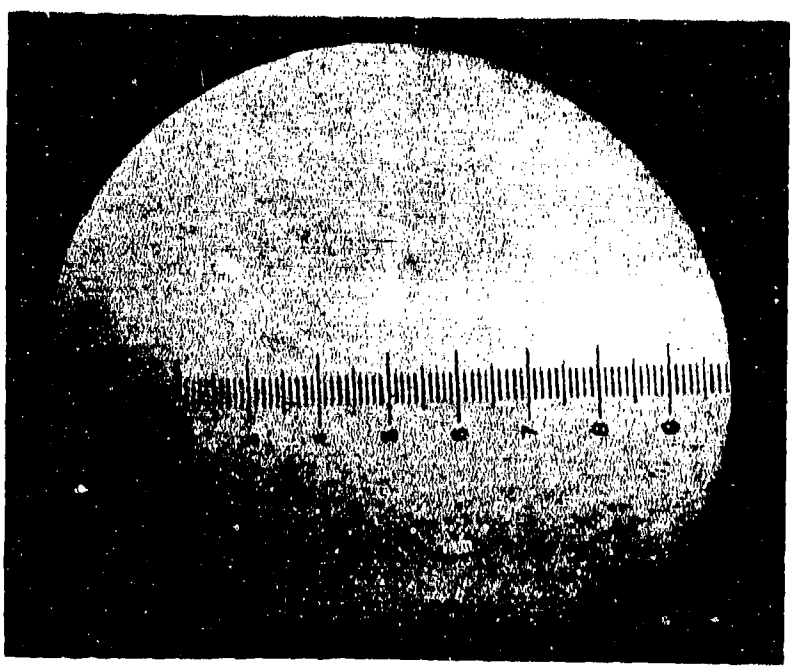

Unetched Approximately X9

Figure 71. Test 400, Sn-Al/Ta-10W after One Hour Exposure in Flowing Air at 3092°F. Transverse Section, Original Diameter 516 Mils, Final Diameter 506 Mils, 4.86 Mils/Unit.

Plate -12878

Unetched

Approximately X10

Figure 72. Test 439, Sn-Al/Ta-10W(G-19) after One Hour in Flowing Air at 3173°F. Longitudinal Section Initial Length 522 Mils, Final Length 342 Mils, 4.86 Mils/Unit.

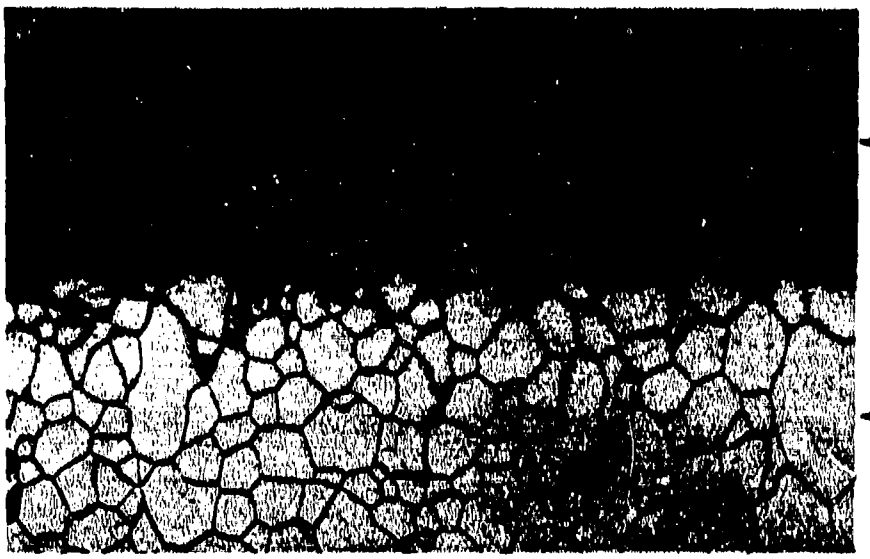

Plate 1-2879

Etched with Murakamis' Reagent

X250

Figure 73. Test 439, Sn-Al/Ta-10W(G-19), after One Hour in Flowing Air at 3173°F. Longitudinal Section, Interface Showing Oxide and Ta-10W after Coating Failure.

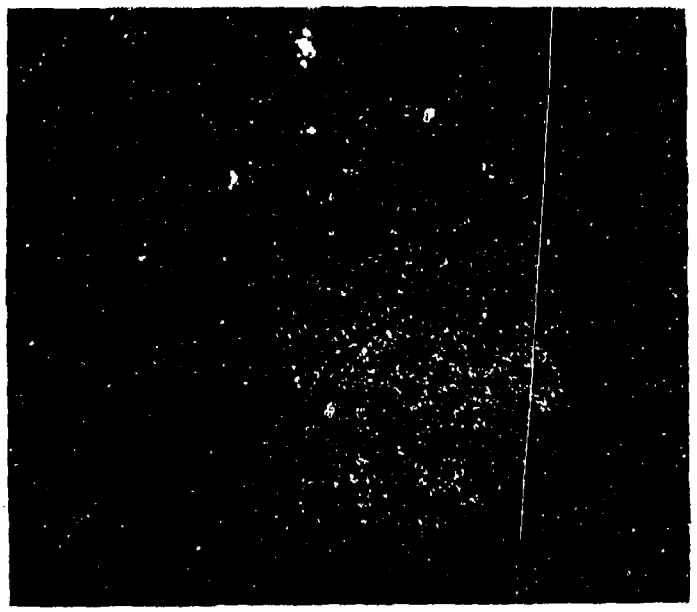

Plate No. 1-6341

Unetched 4.86 Mils Per Small Division

Figure 74. Test 1038, SiO_2 + 68.5%W(H-22) after 60 Minutes in Flowing Air at 3691°F, Longitudinal Section.

Plate No. 1-6342

Unetched X250

Figure 75. Test 1038, SiO_2 + 68.5%W(H-22) after 60 Minutes in Flowing Air at 3691°F, Interface of Longitudinal Section.

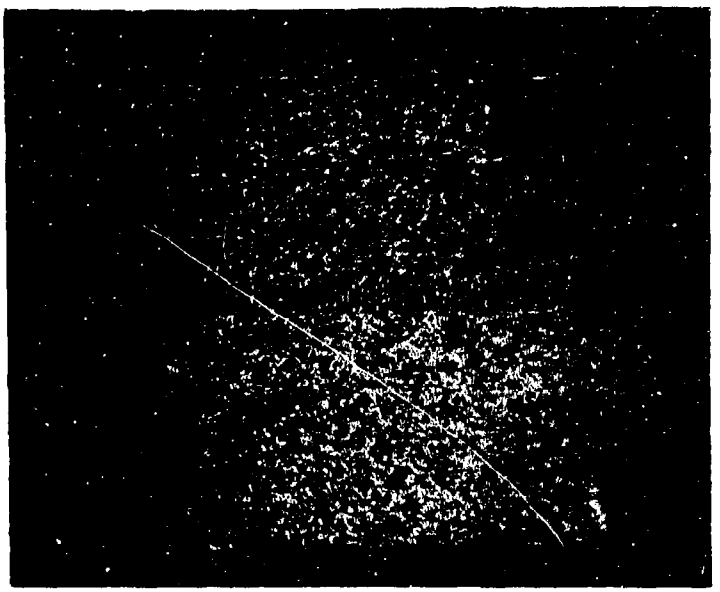

Plate No. 1-6346

Unetched 4.86 Mils per Small Division

Figure 76. Test 1042, SiO_2 + 60%W(H-23) after 60 Minutes in Flowing Air at 3819°F, Longitudinal Section.

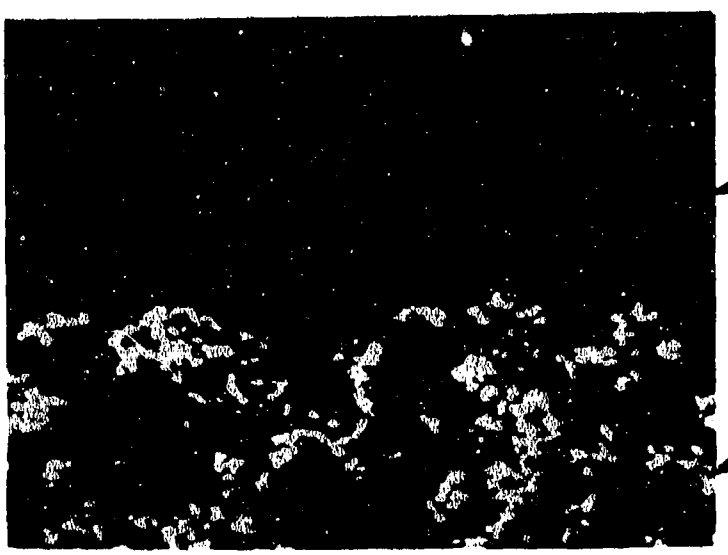

Plate No. 1-6347

Unetched X250

Figure 77. Test 1042, SiO_2 + 60%W(H-23) after 60 Minutes in Flowing Air at 3819°F, Interface of Longitudinal Section.

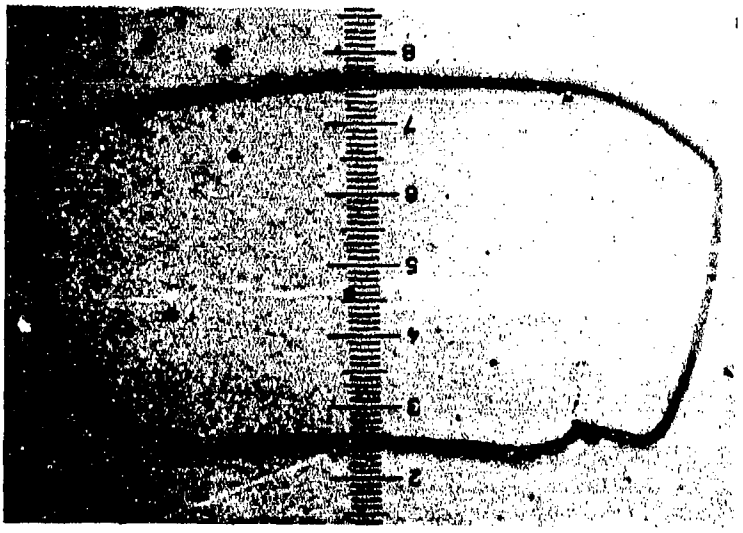

Plate No. 1-6390

Unetched 4.86 Mils per Small Division

Figure 78. Test 1047, SiO_2 + 35%W(H-24) after 60 Minutes in Flowing Air at 3042°F, Longitudinal Section.

Plate No. 1-6391

SiO_2

Tungsten Particles

Unetched X250

Figure 79. Test 1047, SiO_2 + 35%W(H-24) after 60 Minutes in Flowing Air at 3042°F, Interface of Longitudinal Section.

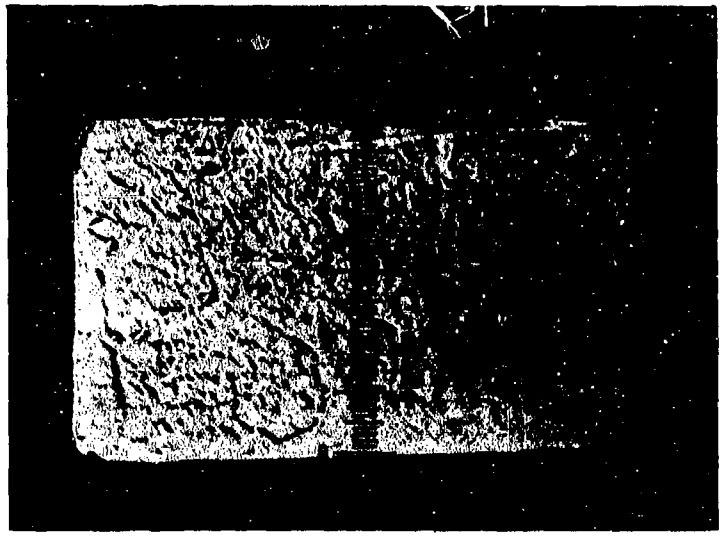

Plate No. 1-6215

Unetched 4.86 Mils per Small Division

Figure 80. Test 1007, Hf-20Ta-2Mo(I-23) after 30 Minutes in Flowing Air at 3400°F, Longitudinal Section.

Plate No. 1-6217

Etched with 15 Glycerine 5HNO_3 HCl 3HF X250

Figure 81. Test 1007, Hf-20Ta-2Mo(I-23) after 30 Minutes in Flowing Air at 3400°F, Interface of Longitudinal Section, Suboxide at Top, Tantalum Stringers are Light Phase.

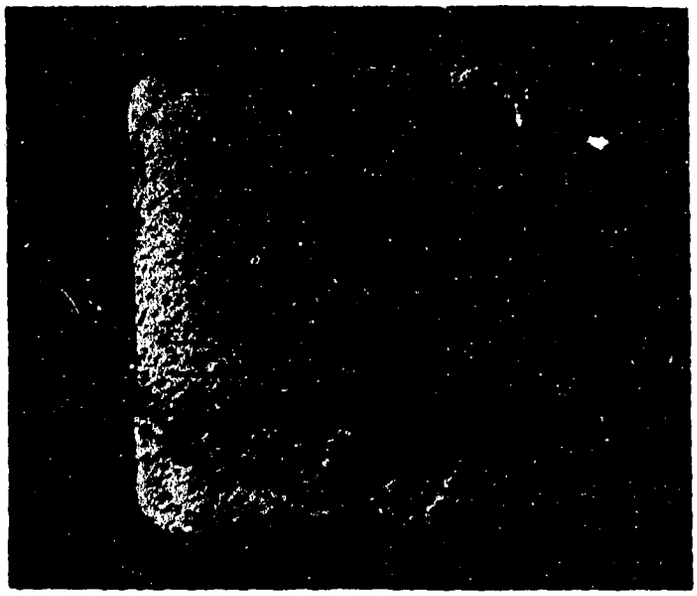

Plate No. 1-6495

Unetched 4.86 Mils per Small Division

Figure 82. Test 1056, Hf-20Ta-2Mo(I-23) after 30 Minutes at 3479°F, Longitudinal Section.

Suboxide

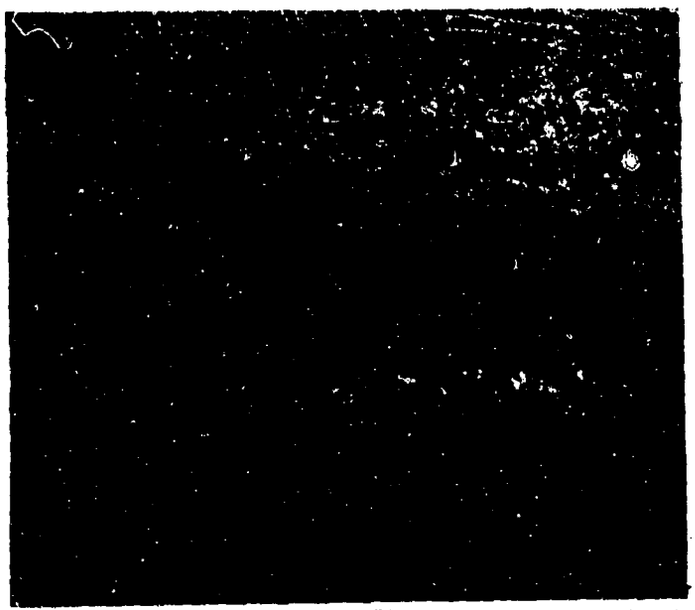

Plate No. 1-6496

Oxide

Etched with 15 Glycerine 5HNO_3 HCl 3HF X250

Figure 83. Test 1056, Hf-20Ta-2Mo(I-23) after 30 Minutes at 3479°F, Interface of Longitudinal Section, Suboxide with Tantalum Stringers at Top.

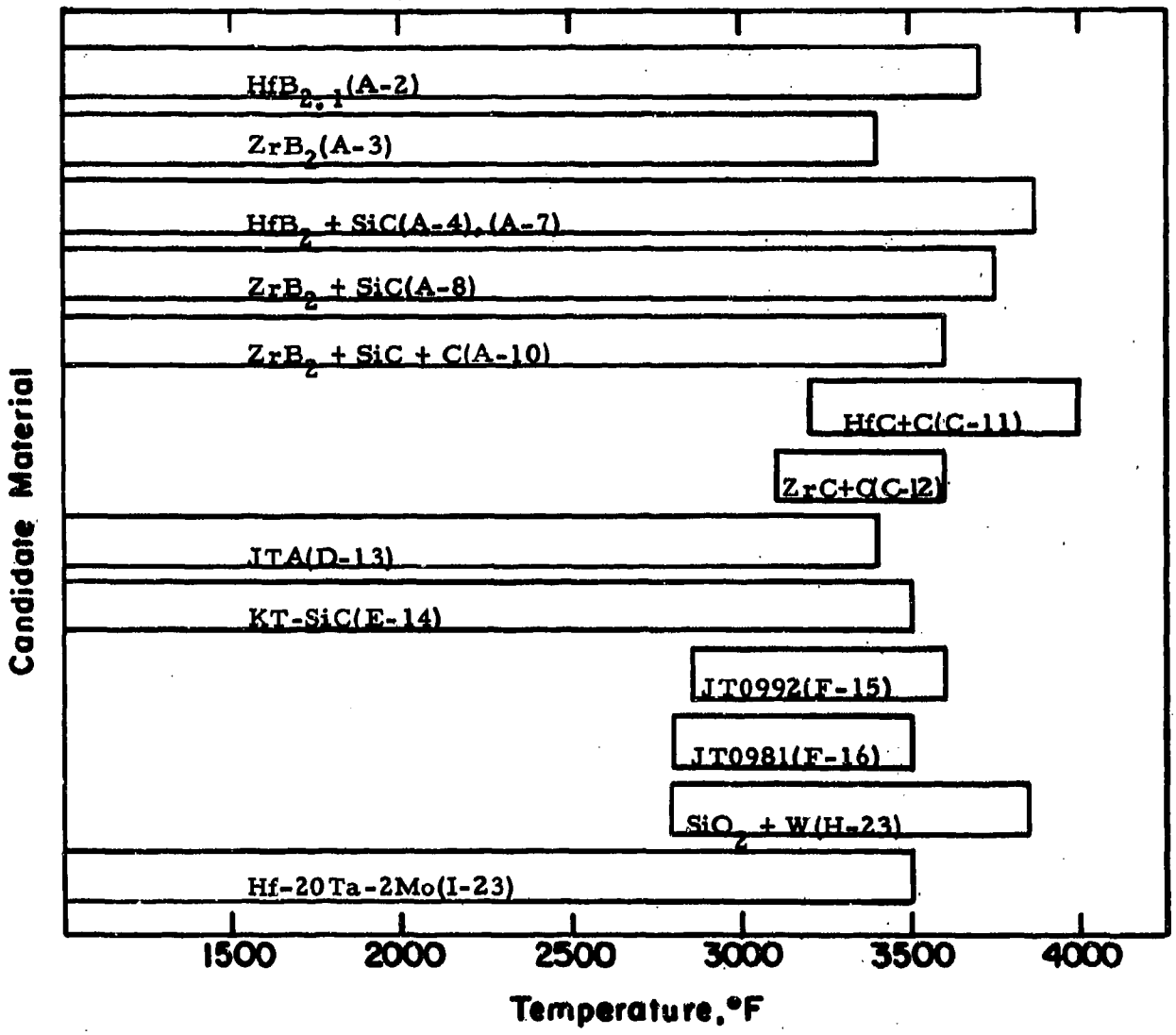

Figure 84. Two Hour Protection Limits For The Candidate Materials.

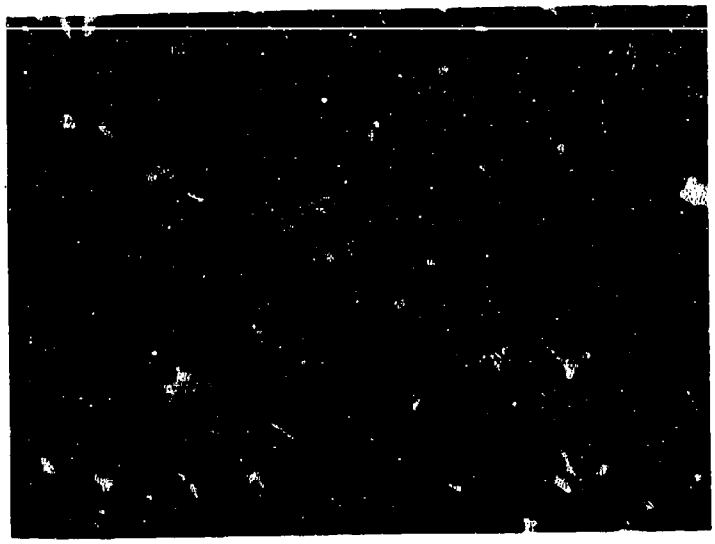

Plate No. 5089

Unetched X500

Figure 85. Inert Test No. 1200, JTA(D-13) After 60 Minutes in Flowing Argon at 4200° F, Longitudinal Section.

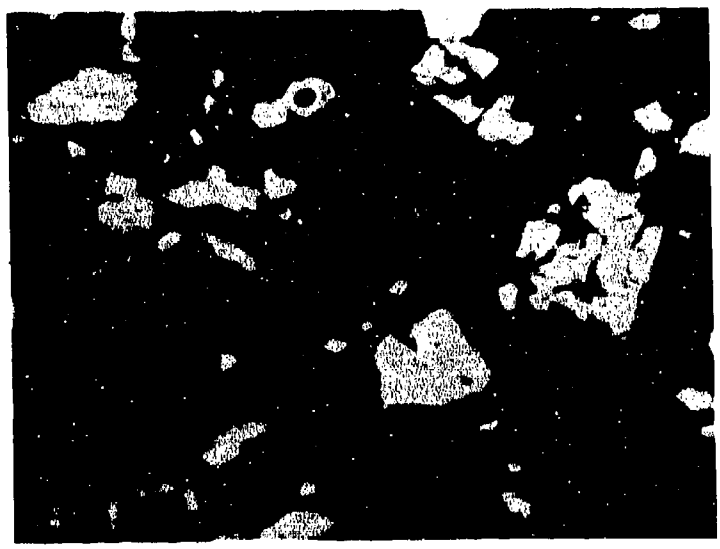

Plate No. 5093

Unetched X500

Figure 86. Inert Test No. 1202, JTA(D-13) After 60 Minutes in Flowing Argon at 4176°F, Longitudinal Section.

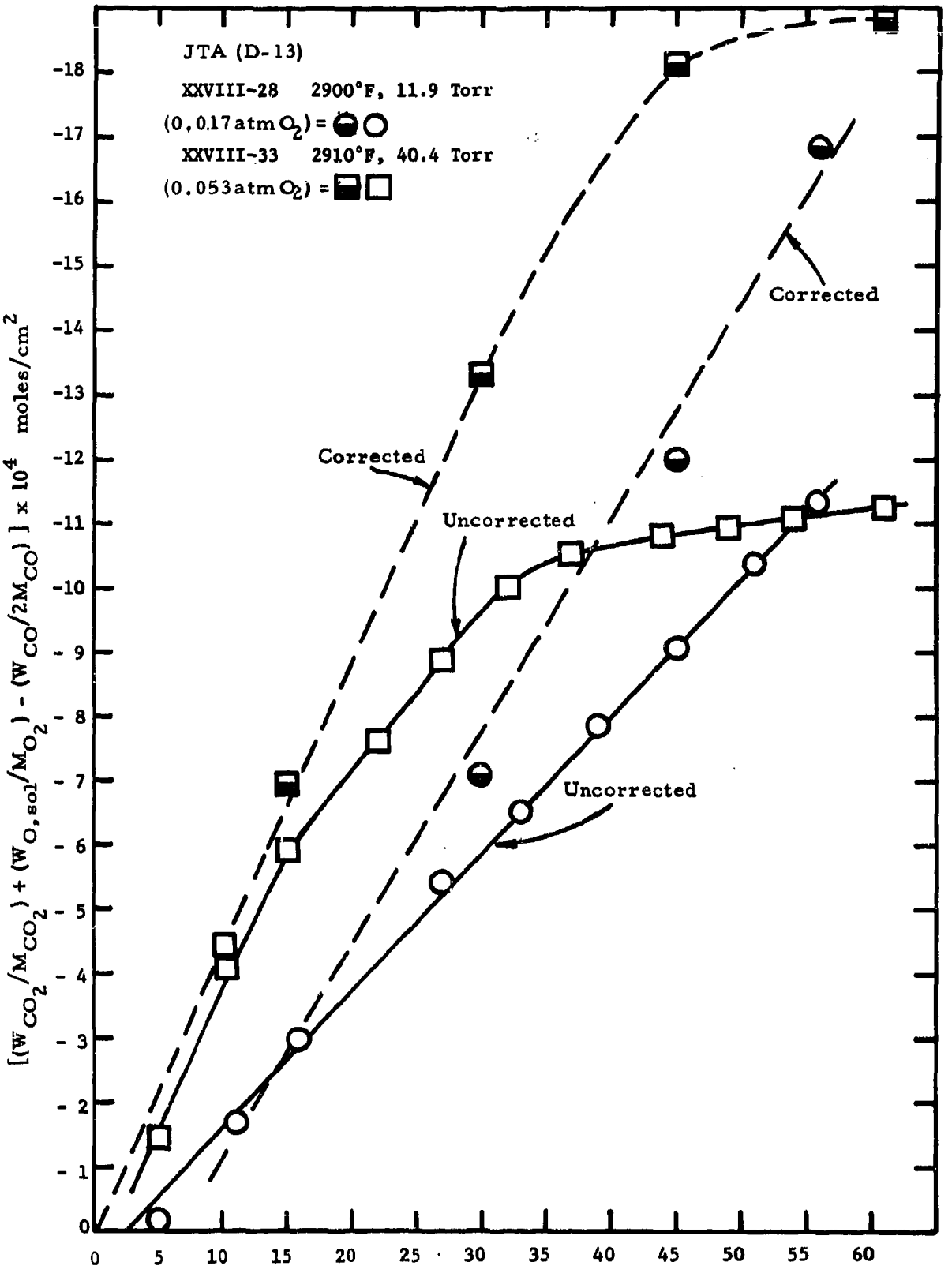

Figure 87. Oxidation of JTA (C-ZrB_2-SiC) (D-13) Composite as a Function of Time at 2900°F, Showing Correction Due to Surface Area Changes.

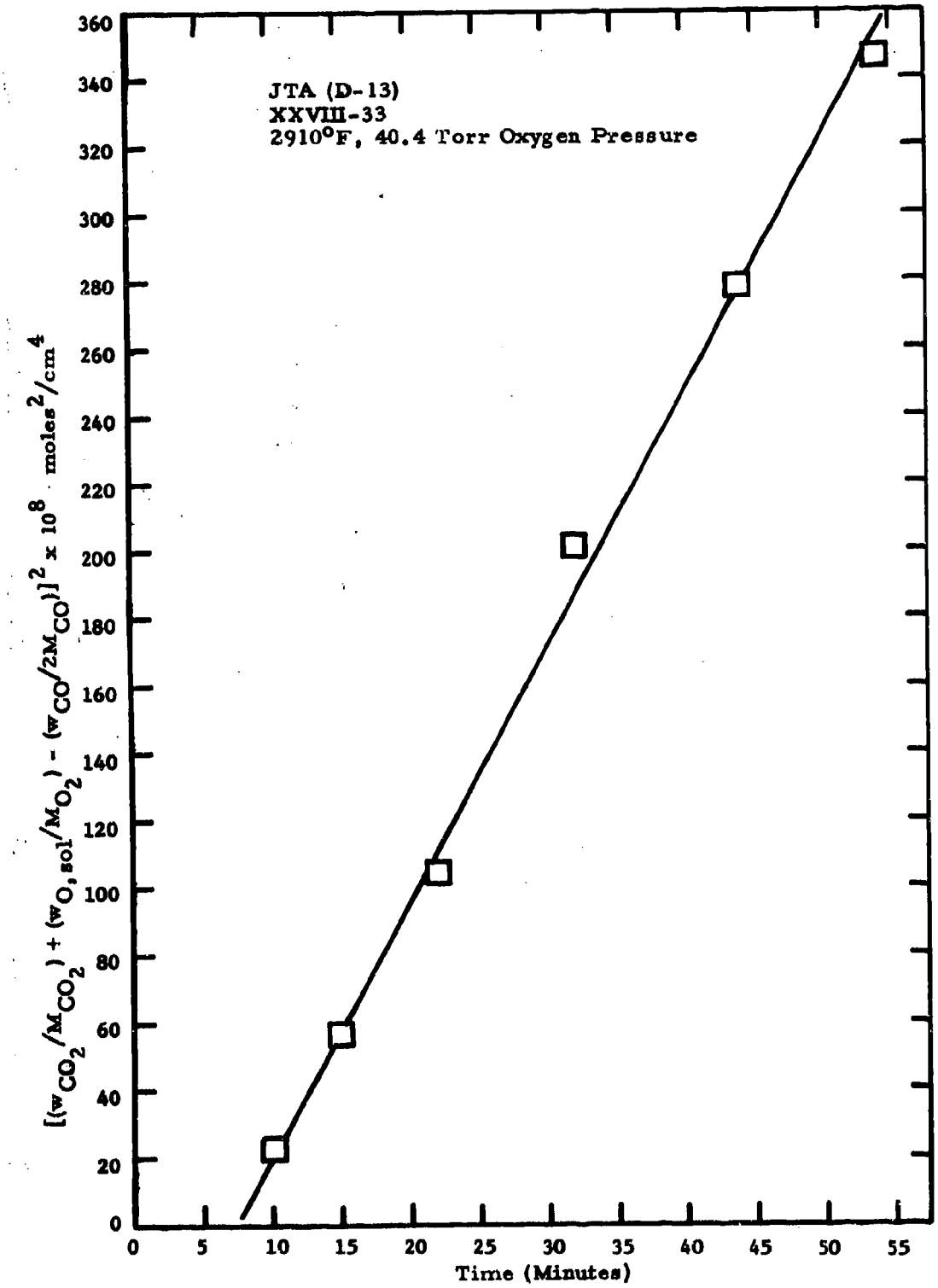

Figure 88. Parabolic Representation of the Oxidation of JTA (C-ZrB_2-SiC) (D-13) Composite at 2900°F.

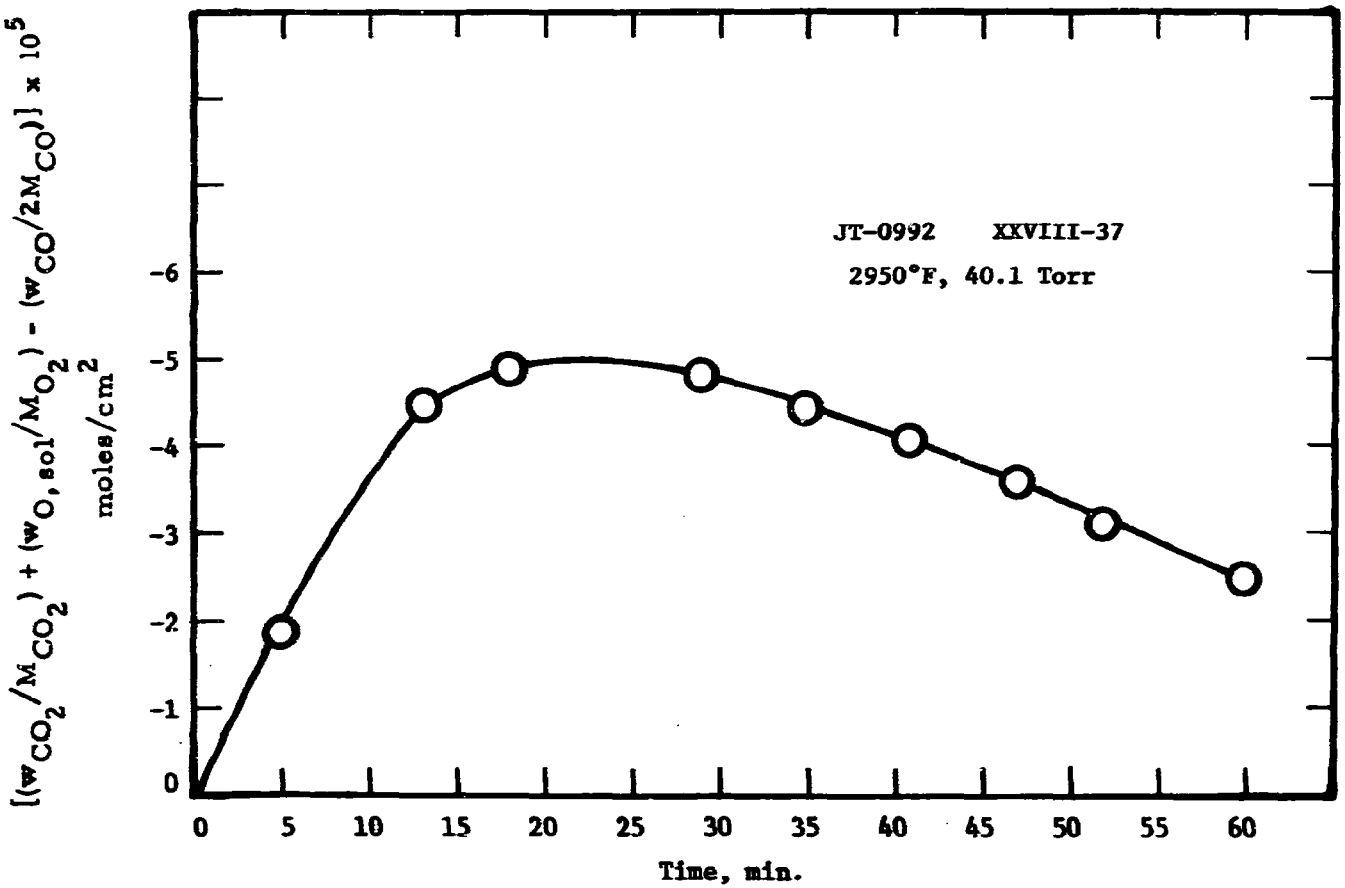

Figure 89. Oxidation of JT0992 (C-H+C-SiC) (F-15) Composite as a Function of Time at 2950°F.

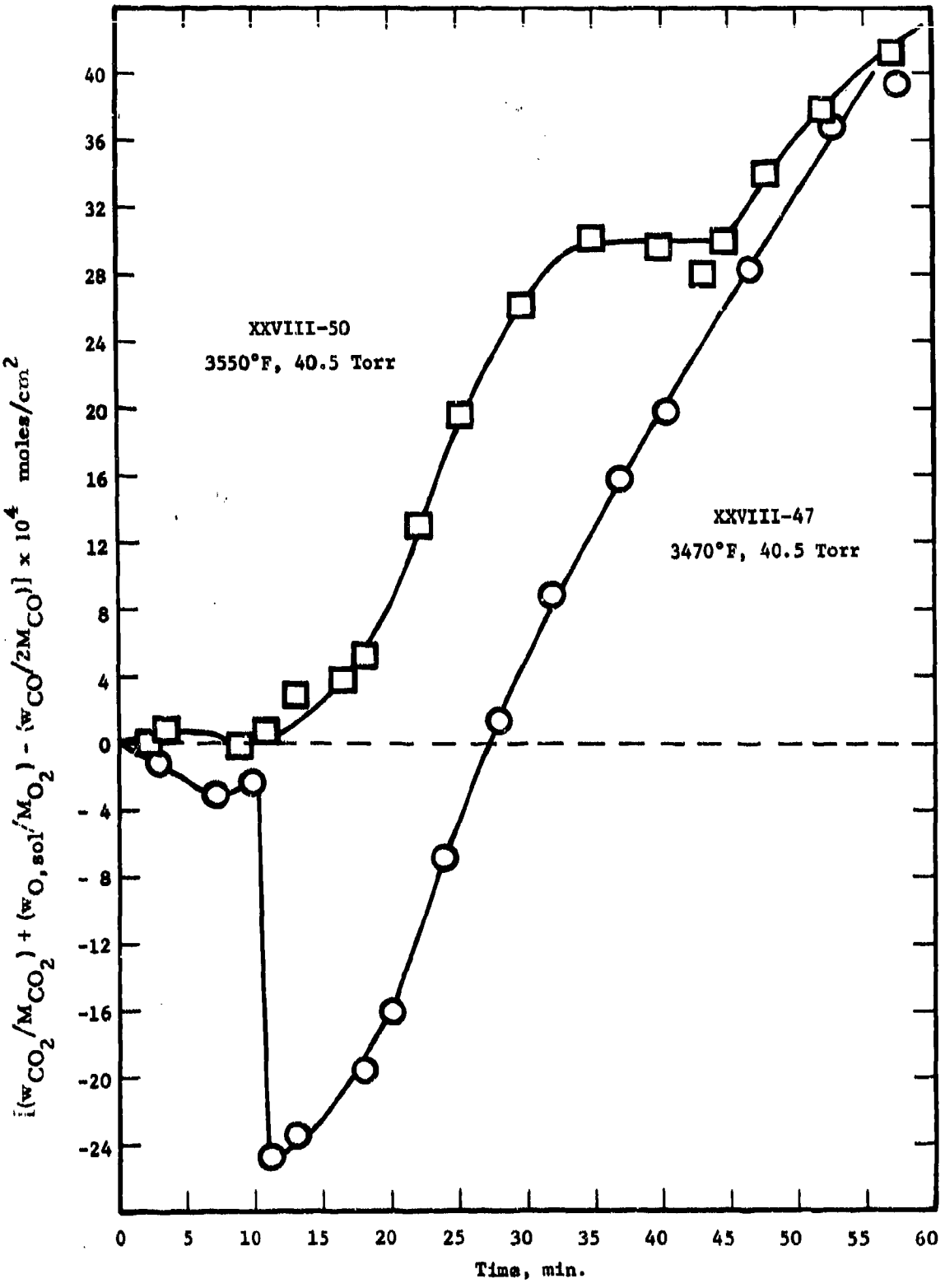

Figure 90. Oxidation of JT0992 (C-HfC-SiC) (F-15) Composite as a Function of Time at 3470°F and 3550°F.

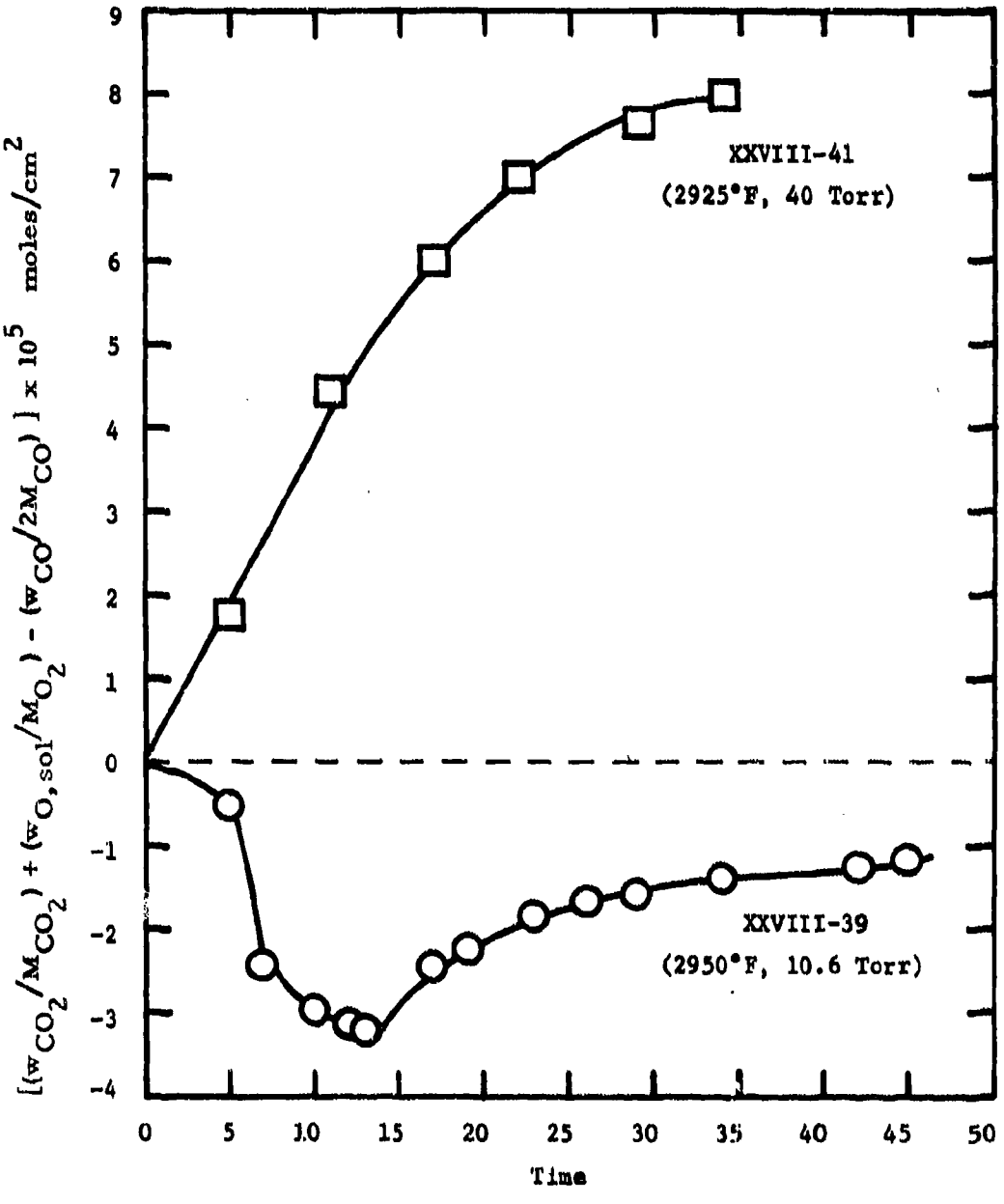

Figure 91. Oxidation of JT0981 (C-ZrC-SiC) (F-16) Composite as a Function of Time at 2925°F and 2950°F.

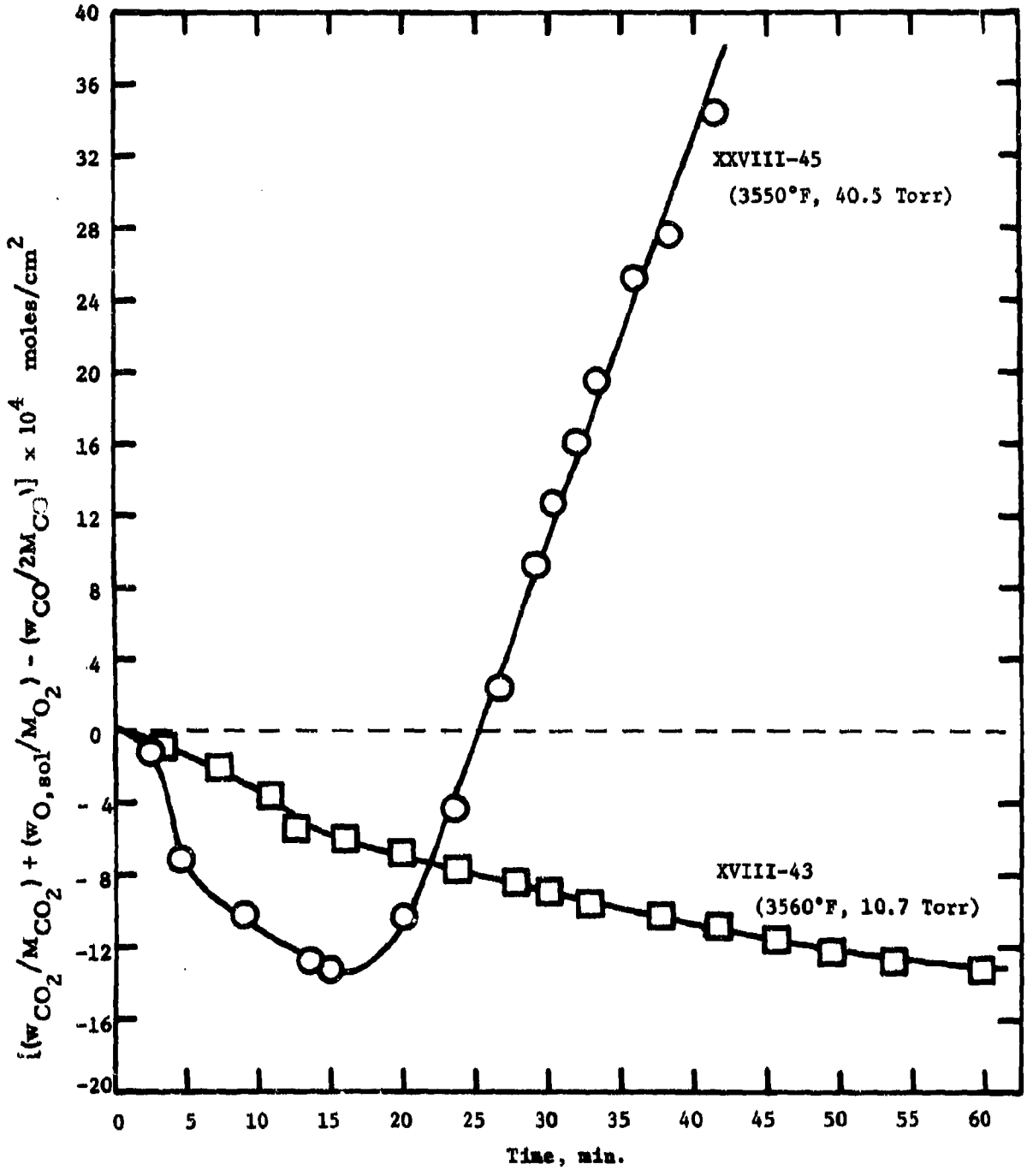

Figure 92. Oxidation of JT0981 (C-ZrC-SiC) (F-16) Composite as a Function of Time at 3550°F and 3560°F.

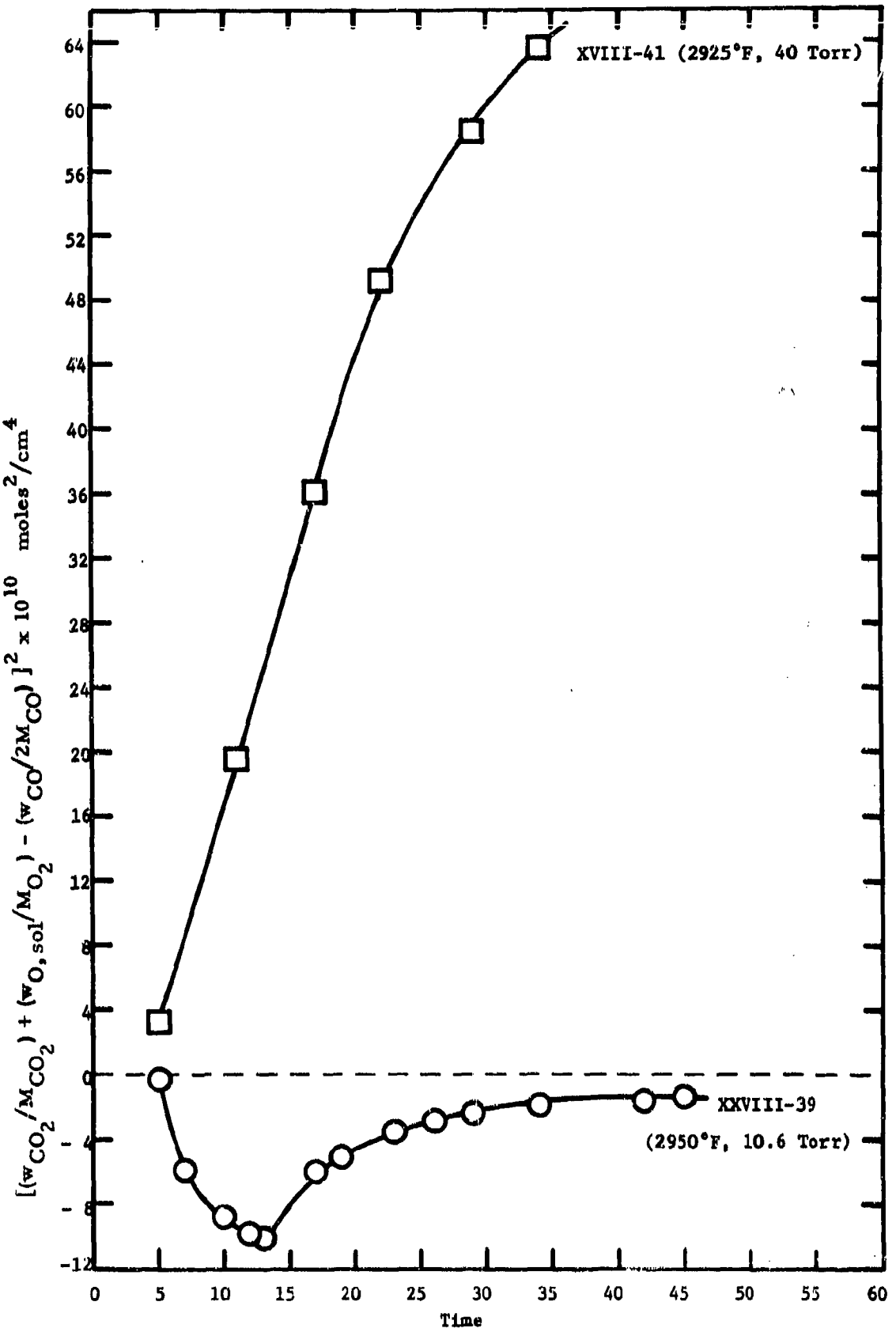

Figure 93. Parabolic Representation of Oxidation of JT0981 (F-16).

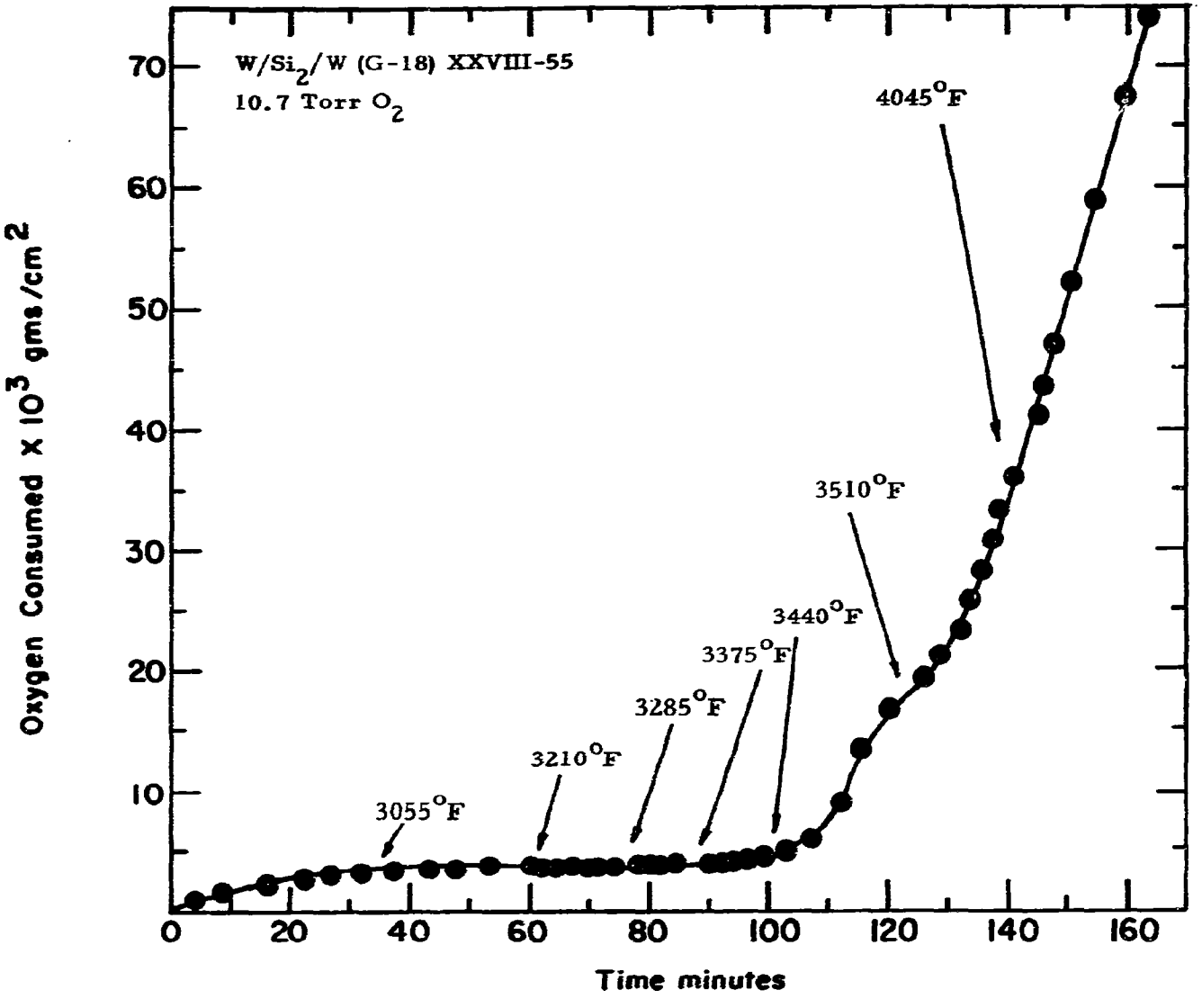

Figure 94. Oxygen Consumed as a Function of Time for WSi_2/W (G-18) at a Oxygen Partial Pressure at 10.7 Torr.

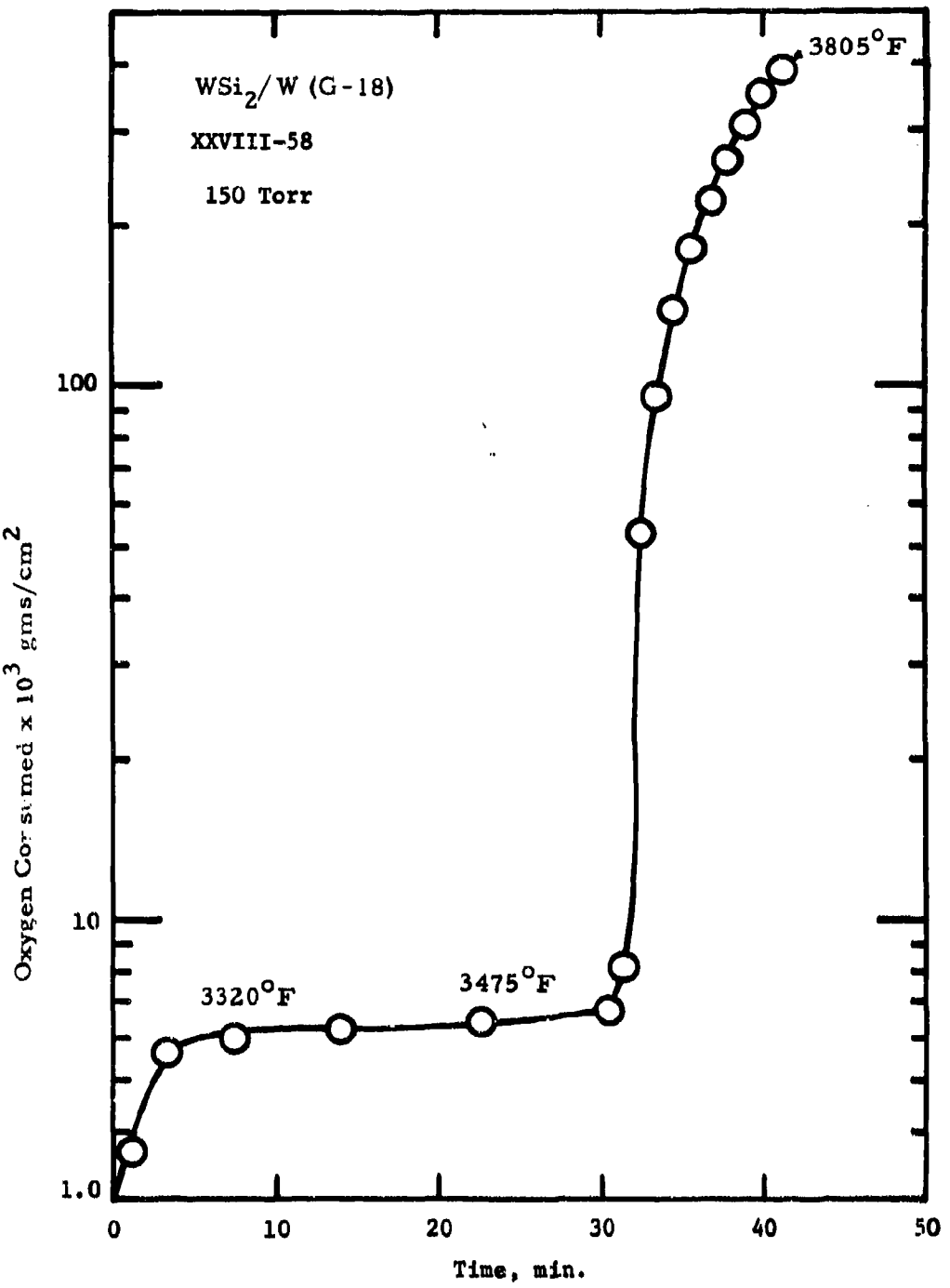

Figure 95. Oxygen Consumed as a Function of Time for WSi_2/W (G-18) at an Oxygen Partial Pressure of 150 Torr.

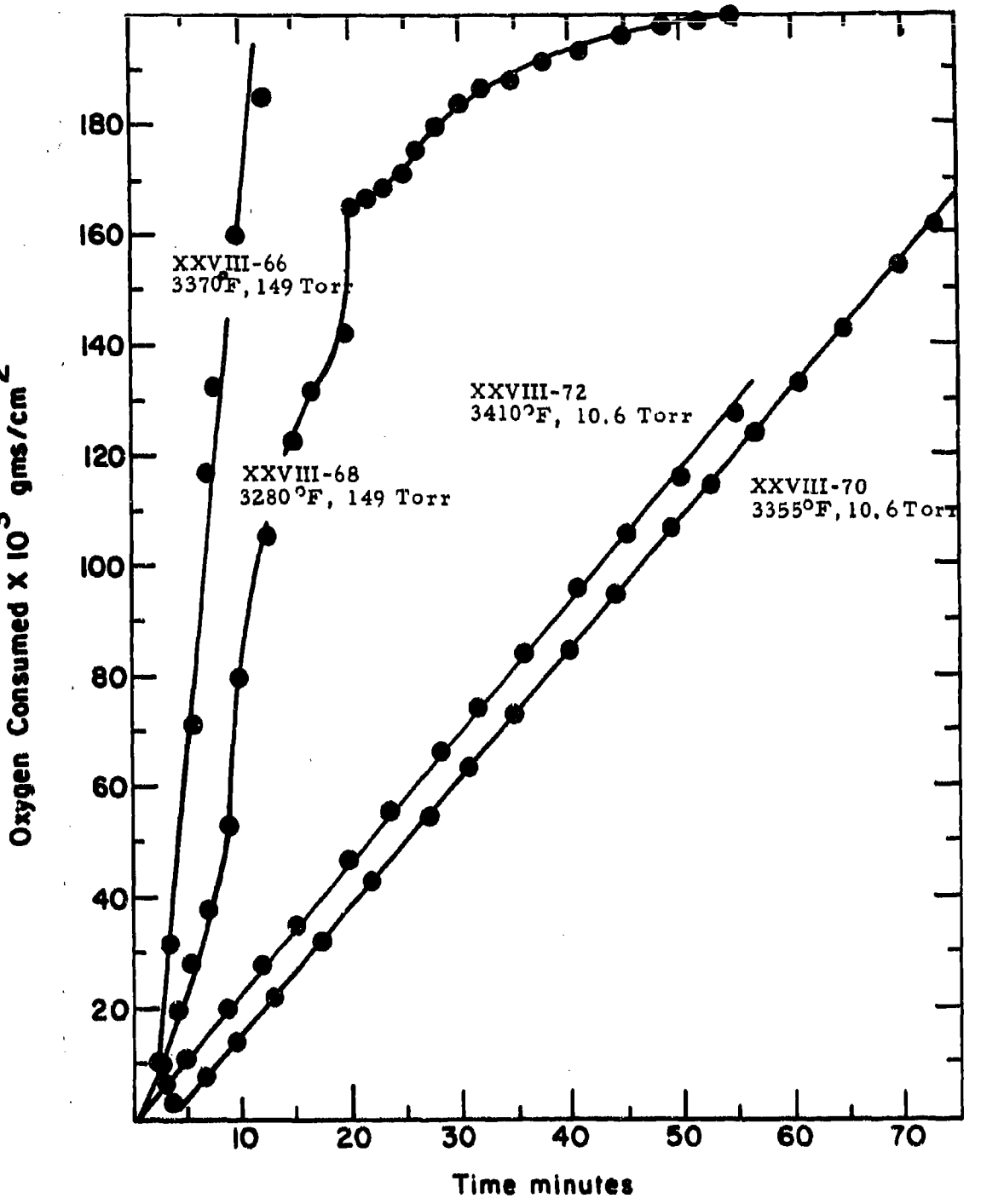

Figure 96. Oxygen Consumption as a Function of Time at Oxygen Partial Pressures of 10.6 and 149 Torr for WSi_2/W (G-18) near 3500°F.

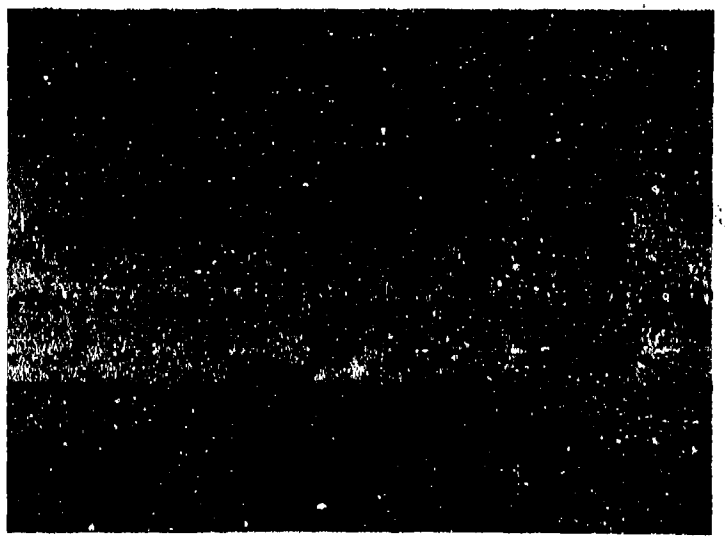

Plate No. 1-5390

Figure 97. Macrophotograph of WSi_2/W(G-18) Coated Samples Exposed at a Partial Pressure of 10 Torr O_2 at 3070(#37), 3180(#38), 3250(#41), 3380(#42) and 3460°F (#43), Respectively for One Hour.

Plate No. 1-5404

Etched with Murakami's Reagent X200

Figure 98. Coating on WSi_2/W(G-18) Test XXIX-42 after One Hour at 3380°F in 10 Torr O_2. Width of W_5Si_3 Zone is 3.55 Mils.

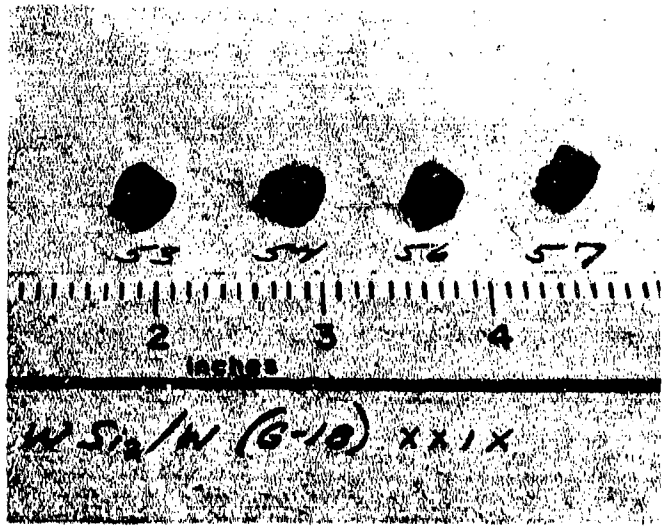

Plate No. 1-6886

Figure 99. Macrophotograph of WSi_2/W(G-18) Coated Samples Exposed at a Partial Pressure of 149 Torr at 3460 (#53), 3560(#54), 3560(#56) and 3500°F(#57), Respectively for One Hour.

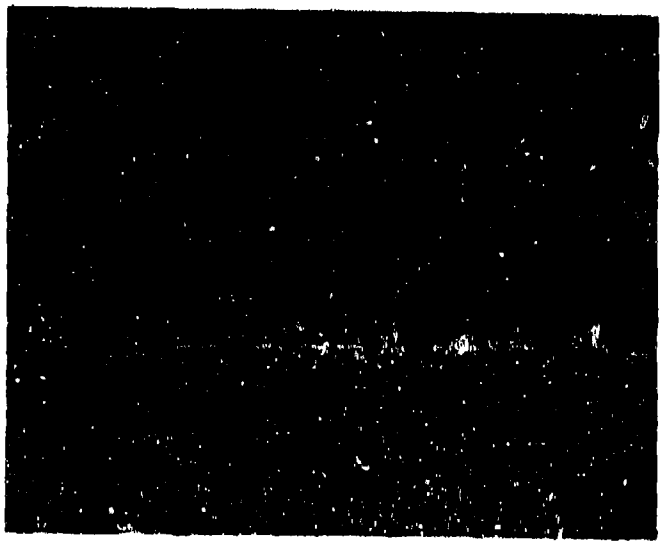

Plate No. 1-6883

Etched with Murakami's Reagent X250

Figure 100. Coating on WSi_2/W(G-18) Test XXIX-48 after One Hour at 3370°F at 149 Torr O_2. Width of W_5Si_3 Zone is 3.55 Mils.

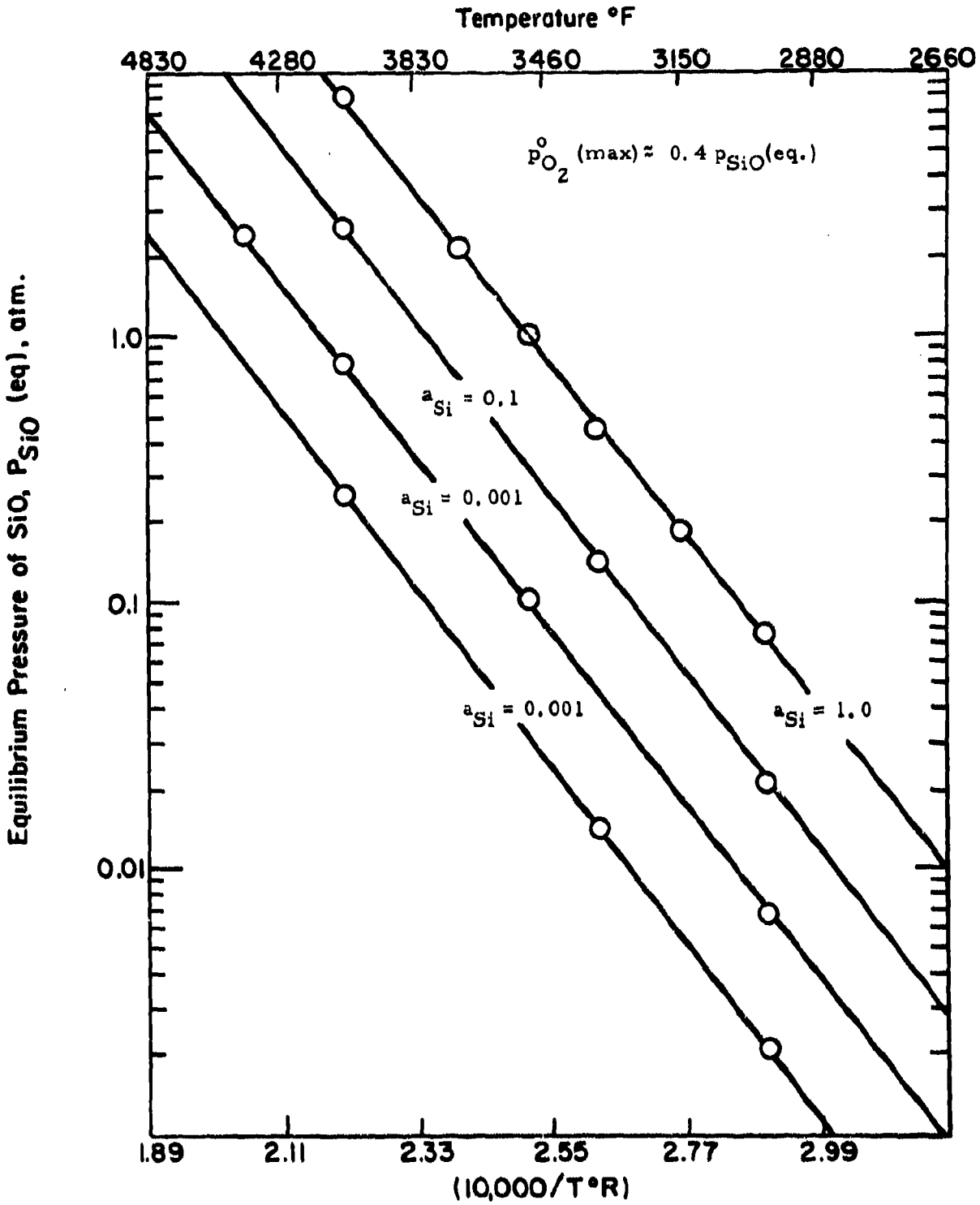

Figure 101. Pressure of SiO in Equilibrium with SiO_2 and Si as a Function of Temperature and Silicon Activity (a_{Si}).

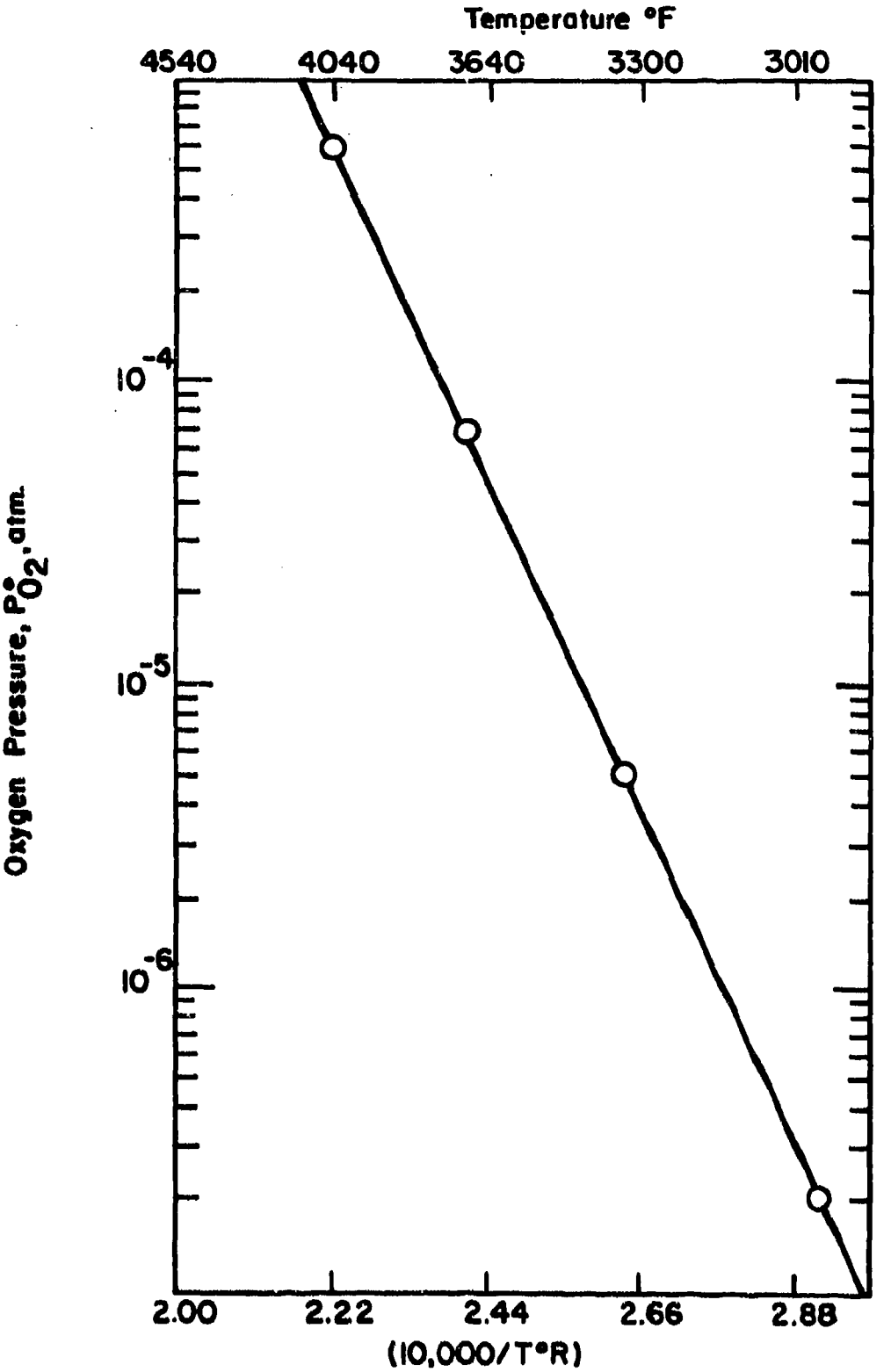

Figure 102. Minimum Oxygen Pressure at which Solid SiO is Stable as a Function of Temperature.

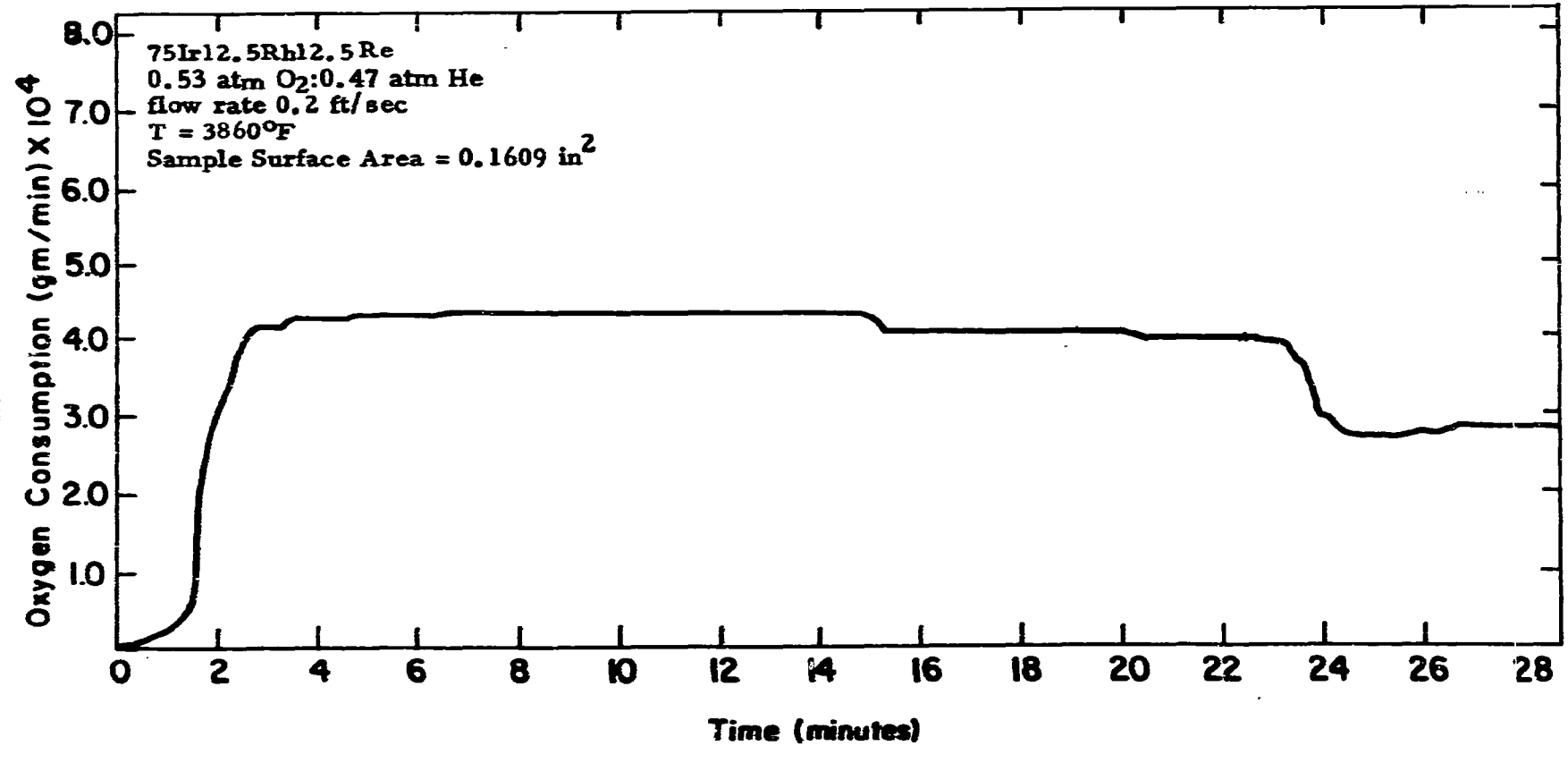

Figure 103. Oxygen Consumption Vs. Time for 75Ir12.5Rh12.5Re at 3860°F.

TABLE I

CANDIDATE MATERIALS INVESTIGATED

Material	Code No.	Supplier
$HfB_{2.1}$	A-2	Carborundum Co., Niagara Falls, New York
ZrB_2	A-3	Carborundum Co., Niagara Falls, New York
HfB_2 + 20 v/o SiC	A-4	Carborundum Co., Niagara Falls, New York
Boride Z	A-5	Carborundum Co., Niagara Falls, New York
$HfB_{2.1}$	A-6	ManLabs-Avco AF33(615)-3671
$HfB_{2.1}$ + 20v/o SiC	A-7	ManLabs-Avco AF33(615)-3671
$ZrB_{2.1}$ + 20v/o SiC	A-8	ManLabs-Avco AF33(615)-3671
$HfB_{2.1}$ + 35v/o SiC	A-9	ManLabs-Avco AF33(615)-3671
ZrB_2 + 14v/o SiC + 30v/o C	A-10	ManLabs-Avco AF33(615)-3671
RVA	B-5	Union Carbide Corp., New York, New York
PG	B-6	General Electric Co., Detroit, Michigan
BPG	B-7	High Temperature Materials, Lowell, Mass.
Si/RVC	B-8	Union Carbide Corp., New York, New York
PT0178	B-9	Union Carbide Corp., New York, New York
Poco Graphite (AXF-5Q)	B-10	Poco Graphite Inc., Garland, Texas
Glassy Carbon	B-11	Lockheed M/S Co., Palo Alto, California
HfC + C	C-11	Battelle Memorial Institute, Columbus, Ohio
ZrC + C	C-12	Battelle Memorial Institute, Columbus, Ohio
JTA (C + ZrB_2 + SiC)	D-13	Union Carbide Corp., New York, New York
KT-SiC	E-14	Carborundum Co., Niagara Falls, New York
JT0992 (C + HfC + SiC)	F-15	Union Carbide Corp., New York, New York
JT0981 (C + ZrC + SiC)	F-16	Union Carbide Corp., New York, New York
WSi_2/W	G-18	General Electric Co., Cleveland, Ohio (Type MK-W) TRW, Cleveland, Ohio (WSi_2 coating)
Sn-Al/Ta-W	G-19	National Research Corp., Newton, Mass. (Ta-10W) GT&E, Hicksville, New York (Sn-Al coating)
W-Zr-Cu	G-20	Rockeydyne, Canoga Park, California
W-Ag	G-21	Wah Chang Corp., Albany, Oregon
SiO_2 + 68.5 w/o W	H-22	Bjorksten Research Labs, Madison, Wisconsin
SiO_2 + 60 w/o W	H-23	General Electric Co., Willoughby, Ohio
SiO_2 + 35 w/o W	H-24	General Electric Co., Willoughby, Ohio
Hf-20Ta-2Mo	I-23	Wah Chang Corp., Albany, Oregon
Ir/Graphite	I-24	Battelle Memorial Institute, Columbus, Ohio General Technologies Corp., Reston, Virginia

TABLE 2

SUMMARY OF AIR OXIDATION RESULTS FOR $HfB_{2.1}$ (A-2) AND ZrB_2 (A-3)

$HfB_{2.1}$ (A-2)

Test No. (Velocity-ft/sec)	Time (min)	T°F	L_o(mils) initial	D_o(mils) initial	L_f(mils) final	D_f(mils) final	d(mils) length/diam
268 (0.9)	60	3200	402	500	371	472	16/14
269 (0.9)	60	2993	406	500	385	487	11/7
270 (0.9)	60	3374	402	500	366	471	18/15
271 (0.9)	60	3546	410	502	327	362	42/70
273 (0.9)	60	3722	397	500	324	344	37/70
303 (0.9)	60	3776	395	500	339	324	28/88
328 (1.8)	60	3533	404	499	319	329	43/85
331 (3.6)	60	3533	404	499	---	387	--/71
341 (7.2)	60	3627	404	499	310	303	49/98
344 (1.8)	60	3740	401	503	303	311	49/96
354 (0.9)	60	3950	4[illegible]	500	288	331	59/85
355 (7.2)	60	3938	4[illegible]	503	289	317	59/92
377 (0.9)	60	2825	400	499	391	490	5/5
379 (0.9)	60	3023	403	499	386	486	9/7
381 (0.9)	60	3209	402	499	396	493	3/5
417 (1.8)	2 x 30	3637	406	502	284	386	61/73
418 (1.8)	2 x 60	3632	399	499	241	375	79/162
493 (7.2)	120	3605	398	499	188	357	108/171
488 (1.8)*	15	3617	381	499	314	435	19/32
489 (1.8)*	30	3617	381	499	305	415	39/42
490 (1.8)*	60	3617	403	499	312	382	46/89
491 (1.8)*	120	3617	408	499	257	334	74/133
552 (1.8)°	15	3831	408	499	377	470	14/15
553 (1.8)°	30	3831	409	499	394	409	28/49
554 (1.8)°	60	3837	413	499	336	414	39/43
555 (1.8)°	120	3831	418	499	390	438	36/31
564 (1.8)†	15	3380	386	498	374	490	6/5
563 (1.8)†	30	3380	391	500	375	466	8/18
564 (1.8)†	60	3380	390	499	340	446	20/17
565 (1.8)†	120	3380	399	499	348	451	26/24
678 (1.8)	60	3985	278	499	146	322	66/89
858 (1.8)	4 x 30	3490	486	499	262	267	112/116
863 (1.8)	60	1203	98	500	100	499	-1/1
866 (1.8)	60	1723	102	500	100	500	1/0
867 (1.8)	60	2221	101	500	97	497	2/2
868 (1.8)	60	2703	103	500	85	490	9/5
879 (1.8)*	15	3548	377	400	335	337	21/32
880 (1.8)*	30	3540	375	400	308	331	34/35
881 (1.8)*	60	3544	376	400	261	285	56/58
882 (1.8)*	120	3542	377	400	224	220	77/90
889 (1.8)**	15	3640	377	401	315	335	31/33
890 (1.8)**	30	3636	376	400	288	287	61/57
891 (1.8)**	60	3640	377	400	163	208	107/96
892 (1.8)**	120	3640	376	400	113	142	132/124
1283 (1.8)	60	4100	406	500	288	311	74/99
1325 (1.8)	15	3300	352	400	310	362	21/19
1326 (1.8)	30	3300	352	401	292	316	30/43
1327 (1.8)	60	3300	353	401	255	241	59/79
1332 (1.8)	120	3300	349	500	308	340	61/80
1333 (1.8)	15	3600	352	401	292	338	30/33
1334 (1.8)	30	3600	352	401	247	289	53/71
1335 (1.8)	88	3596	353	401	233	264	60/69
1336 (1.8)	120	3600	357	500	302	284	78/108
1384 (1.8)	15	3700	352	401	291	343	31/29
1385 (1.8)	30	3700	353	400	240	281	47/60
1386 (1.8)	60	3700	352	500	235	330	59/85
1387 (1.8)	120	3700	373	499	274	302	100/99
1428 (1.8)	15	4000	432	500	396	362	30/42
1429 (1.8)	30	4000	445	500	343	394	50/61
1430 (1.8)	60	4000	481	500	316	345	69/78
1431 (1.8)	120	4000	498	500	283	280	108/110

The symbols °, †, *, ** all denote simultaneous runs in large furnace

ZrB_2 (A-3)

Test No. (Velocity-ft/sec)	Time (min)	T°F	L_o(mils) initial	D_o(mils) initial	L_f(mils) final	D_f(mils) final	d(mils) length/diam
175 (0.9)	2 x 30	3488	508	491	281	317	114/87
176 (0.9)	60	3497	523	492	306	263	109/115
177 (0.9)	30	3497	520	492	435	351	-43/71
178 (0.9)	2 x 30	3794	515	492	239	317	148/88
180 (0.9)	60	3488	528	492	312	297	108/98
185 (0.9)	30	3506	527	492	439	359	44/67
186 (0.9)	2 x 30	3415	523	492	212	192	156/150
187 (0.9)	60	3776	527	492	192	211	168/141
188 (0.9)	30	3785	522	492	341	278	91/107
189 (0.9)	2 x 30	3794	521	492	210	209	156/144
211 (0.9)	30	4118	518	492	439	188	40/82
213 (0.9)	2 x 30	4100	515	491	351	246	92/173
214 (0.9)	120	3506	499	491	181	141	159/175
259 (0.9)	60	3506	491	511	173	113	159/184
264 (0.9)	240	3490	499	492	ALL GONE		>246
275 (0.9)	60	3985	494	491	332	393	81/99
277 (0.9)	60	4190	517	492	306	226	116/133
307 (1.8)	60	3410	520	420	406	245	57/84
342 (1.8)	60	3409	524	492	438		48
346 (1.8)	60	3605	503	491	346		79
347 (1.8)	60	3800	464	491	292		87
601 (1.8)°	15	3509	323	491	272	428	26/33
602 (1.8)°	30	3509	325	491	ALL GONE		>162
603 (1.8)°	60	3469	326	491	ALL GONE		>163
604 (1.8)°	120	3469	330	491	ALL GONE		>165
605 (1.8)°	240	3469	331	491	ALL GONE		>165
684 (1.8)	60	3985	328	490	123	154	101/168
686 (1.8)	60	3875	328	491	196	344	66/74
730 (1.8)	60	3998	330	492	69	---	131/---
732 (1.8)	60	3998	334	492	ALL GONE		>167
829 (1.8)*	15	3424	324	491	283	431	21/30
830 (1.8)*	30	3438	326	491	250	384	38/19
831 (1.8)*	30	3438	335	491	287	392	24/50
832 (1.8)*	60	3440	324	491	190	318	67/87
837 (1.8)**	15	3245	354	481	313	442	21/20
838 (1.8)**	30	3236	342	482	272	385	35/49
839 (1.8)**	60	3236	354	482	248	371	53/56
840 (1.8)**	120	3236	344	481	233	379	56/51
900 (1.8)	60	1220	101	491	100	491	1/1
902 (1.8)	60	1738	101	495	98	487	2/4
904 (1.8)	60	2216	93	494	82	476	6/9
905 (1.8)	60	2717	102	492	72	448	15/24
908 (1.8)†	15	3574	330	491	264	381	33/34
909 (1.8)†	30	3560	340	491	222	342	59/78
910 (1.8)†	60	3556	359	491	214	196	73/148
911 (1.8)†	120	3556	340	492	ALL GONE		>170
934 (1.8)	4 x 30	3206	318	492	238	422	40/35
964 (1.8)	60	2914	127	493	107	466	10/14
969 (1.8)	60	3087	426	401	388	364	19/19
970 (1.8)	60	3128	426	401	402	369	12/16
977 (0.9)	60	3243	426	400	392	371	17/15
978 (0.9)	60	3349	426	401	321	304	53/49
1010 (1.8)	15	3263	452	400	426	386	14/7
1011 (1.8)	30	3263	453	400	433	376	10/12
1012 (1.8)	60	3263	452	400	421	371	16/15
1013 (1.8)	120	3263	452	400	407	347	23/27
1314 (1.8)	15	3400	326	491	279	440	24/26
1315 (1.8)	30	3400	357	491	289	429	34/31
1316 (1.8)	60	3400	336	491	217	358	60/67
1317 (1.8)	120	3400	332	491	ALL GONE		>166
1318 (1.8)	15	3500	426	401	374	336	26/33
1319 (1.8)	30	3500	426	401	346	278	40/52
1320 (1.8)	60	3500	452	401	260	224	96/89
1121 (1.8)	15	3300	427	401	411	385	8/8
1122 (1.8)	30	3300	427	401	403	377	12/12
1123 (1.8)	60	3300	452	401	407	348	23/22
1124 (1.8)	120	3300	452	401	364	314	44/44

The symbols °, †, *, ** all denote simultaneous runs

TABLE 3

SUMMARY OF AIR OXIDATION RESULTS FOR HfB_2 + 20%SiC(A-4) AND (A-4-2)

HfB_2 + 20%SiC (A-4)

Test No. (Velocity-ft/sec)	Time (min)	T°F	L_o(mils) initial dimensions	D_o(mils) initial dimensions	L_f(mils) final dimensions	D_f(mils) final dimensions	d(mils) length/diam
322 (0.9)	60	3300	462	505	462, 462*	505, 502*	0/0, (0/2)*
323 (0.9)	60	3416	390	505	394, 367*	499, 498*	2/3, (6/4)*
324 (0.9)	60	3670	373	506	361, 350*	499, 496*	6/3, (12/5)*
325 (0.9)	60	3630	466	504	466, 466*	504, 504*	0/0, (0/0)*
334 (0.9)	60	3725	393	505	379, 273*	495, 372*	7/5, (60/67)*
410 (0.9)	60	3695	406	505	386, 240*	489, 301*	10/9, (83/102)*
411 (0.9)	60	3674	402	505	346, 201*	474, 312*	28/16, 101/97)*
412 (0.9)	60	3732	409	505	396, 315*	495, 427*	6/5, (47/39)*
413 (0.9)	60	4065	399	503	360, 119*	463, 207*	20/51, 140/149)*
400 (1.0)	60	3636	394	504	371, 226*	483, 243*	12/26, (84/130)*
401 (1.0)	120	3631	502	503	443, 0*	455, 0*	30/24, (>250)*
514 (1.0)	15	3795	436	504	416, 373*	484, 439*	10/9, (31/32)*
515 (1.0)	30	3795	522	504	480, 427*	486, 414*	21/9, (48/45)*
536 (1.0)*	15	3575	456	492	452, 437*	481, 467*	2/5, (10/12)*
537 (1.0)*	30	3575	461	492	448, 419*	484, 448*	7/4, (21/22)*
538 (1.0)*	60	3575	480	505	473, 407*	496, 443*	4/5, (37/31)*
539 (1.0)*	120	3575	484	506	474, 376*	477, 433*	5/4, (54/39)*
544A (1.0)+	15	3600	450	477	440, 414*	469, 449*	5/4, (18/14)*
545 (1.0)+	30	3600	459	477	456, 384*	457, 390*	2/10, (38/44)*
546 (1.0)+	60	3600	486	504	464, 374*	493, 386*	10/6, (56/60)*
547 (1.0)+	120	3600	487	505	469, 0*	464, 0*	9/21, (>250)
572 (1.0)‡	120	3620	466	505	430, 309*	494, 321*	8/6, (48/88)*
573 (1.0)‡	240	3620	475	506	276, [illegible]	310, [illegible]	100/98, [illegible]
[illegible] (1.0)	60	3671	368	487	356, 333*	480, 427*	6/4, (16/22)*
891 (1.0)	60	3664	396	487	130, 0*	476, 0*	9/5, >170*
893 (1.0)	60	3632	375	474	196, 0*	346, 0*	90/107, >188*
994 (1.0)**	120	3646	366	470	326, 0*	484, 0*	20/27, >183*
995 (1.0)**	240	3646	361	480	ALL GONE, 0*	0*	>191, >191*
996 (1.0)**	400	3646	377	477	ALL GONE, 0*	0*	>189, >189*

*Depletion zone dimensions.
The symbols *, +, ‡, ** all denote simultaneous runs in large furnace.

HfB_2 + 20 v/o SiC (A-4-2)

Test No. (Velocity-ft/sec)	Time (min)	T°F	L_o(mils) initial dimensions	D_o(mils) initial dimensions	L_f(mils) final dimensions	D_f(mils) final dimensions	d(mils) length/diam
489* (1.0)	15	3540	349	477	346, 325*	474, 454*	2/3, (11/12)*
660* (1.0)	30	3540	352	474	344, 278*	466, 454*	4/4, (37/24)*
661 (1.0)	60	3570	355	487	345, 273*	471, 382*	5/8, (41/53)*
662* (1.0)	120	3570	356	477	350, 0*	430, 0*	8/24, (>183)*
663** (1.0)	15	3730	---	474	---	444, 444*	--/3, (--/15)*
664** (1.0)	30	3730	362	474	360, 312*	474, 393*	1/0, (35/41)*
665** (1.0)	60	3725	362	487	345, 180*	481, 272*	19/18, (91/108)*
666** (1.0)	120	3730	389	477	240, 0*	234, 0*	75/122, (>195)*
679 (1.0)	60	3880	304	477	166, 0*	370, 0*	80/80, (>152)*
681 (1.0)	60	3905	349	477	223, 0*	324, 0*	63/75, (>175)*
726 (1.0)	60	3990	346	477	139, 0*	410, 0*	104/130, (>173)*
728 (1.0)	60	3990	378	477	174, 0*	206, 0*	100/135, (>189)*
847+ (1.0)	15	3902	313	488	264, 180*	427, 338*	25/31, (67/75)*
848 (1.0)	30	3894	314	478	235, 102*	368, 290*	40/55, (104/199)*
849 (1.0)	60	3894	349	474	172, 0*	301, 0*	99/87, (>185)*
850 (1.0)	120	3894	381	478	212, 0*	322, 0*	84/78, (>191)*
917 (1.0)	60	1859	103	498	103, 103*	491, 491*	0/4, (0/4)*
919 (1.0)	60	1724	101	496	101, 101*	492, 492*	0/2, (0/2)*
920 (1.0)	60	2197	99	504	97, 97*	502, 502*	1/1, (1/2)*
921 (1.0)	60	2697	100	482	99, 87*	477, 462*	1/3, (7/10)*
939** (1.0)	15	4018	340	503	303, 257*	416, 357*	23/44, (46/72)*
940** (1.0)	30	3998	312	499	207, 120*	369, 237*	53/70, (91/131)*
941** (1.0)	60	4099	340	488	157, 0*	143, 0*	[illegible], (>170)*
942** (1.0)	120	4000	337	502	ALL GONE		>168, (>160)*
952 (1.0)	4 x 30	3994	380	477	113, 0*	226, 0*	120/126, (>190)*
966 (1.0)	60	3363	195	501	190, 174*	476, 479*	3/3, (11/14)*
956 (1.0)	60	3363	368	478	341, 324*	471, 460*	4/4, (22/14)*
967 (1.0)	60	3469	348	478	344, 307*	473, 438*	2/3, (21/22)*
968 (1.0)	60	3544	367	474	360, 301*	470, 450*	2/8, (42/29)*
1041 (1.0)	4 x 30	3499	350	478	300, 301*	424, 362*	25/27, (75/58)*

*Depletion zone dimensions.
The symbols *, **, + and ** all denote simultaneous runs.

TABLE 4

SUMMARY OF AIR OXIDATION RESULTS FOR $HfB_{2.1}$+20v/oSiC(A-7), $ZrB_{2.1}$+20v/oSiC(A-8), $HfB_{2.1}$+35v/oSiC(A-9) AND ZrB_2+14v/oSiC+30v/oC(A-10)

$HfB_{2.1}$ + 20 v/o SiC(A-7)

Test No. (Velocity-ft/sec)	Time (min)	T°F	L_o(mils) initial	D_o(mils) initial	L_f(mils) final	D_f(mils) final	d(mils) length/diam
384 (0.9)	60	3720	300	351	245 0*	344 0*	3/4 (>60)*
387 (0.9)	60	3660	301	351	296 231*	342 243*	3/5 (36/54)*
396 (0.9)	60	3660	359	351	255 195*	346 257*	2/3 (32/47)*
427 (0.9)	60	3675	300	351	192 265*	339 304*	4/6 (18/24)*
442 (0.9)	60	3595	300	350	294 248*	344 271*	3/4 (26/40)*
492 (0.9)	60	3270	299	350	298 292*	349 341*	1/1 (4/5)*
493 (0.9)	60	3270	301	351	299 294*	350 344*	1/1 (4/4)*
494 (0.9)	60	3270	350	350	347 342*	348 340*	2/1 (4/5)*
496 (0.9)	60	3250	299	301	297 281*	349 343*	1/1 (4/4)*
498 (0.9)	60	3240	350	350	337 212*	342 261*	7/4 (69/45)*
500 (0.9)	60	3740	350	350	345 324*	338 294*	3/5 (13/28)*
524 (0.9)	60	3830	300	350	268 0*	297 0*	14/27 (>150)*
525 (0.9)	60	3815	301	351	280 0*	324 0*	10/14 (>151)*
1482 (1.8)	15	3534	270	436	266 259*	432 419*	2/2 (6/9)
1483 (1.8)	30	3550	277	436	267 255*	417 413*	5/10 (11/12)
1489 (1.8)	60	3550	333	436	330 309*	421 400*	2/8 (12/18)
1490 (1.8)	120	3550	463	435	450 428*	417 392*	7/9 (19/22)
1491 (1.8)	15	3750	333	428	333 291*	419 371*	0/5 (21/29)
1492 (1.8)	30	3750	394	428	388 318*	416 382*	3/6 (38/53)
1493 (1.8)	60	3750	387	427	352 249*	413 262*	3/7 (84/83)
1494 (1.8)	120	3750	380	426	363 0*	413 0*	9/7 (>190)
1495 (1.8)	15	3900	393	429	378 291*	411 319*	0/9 (51/89)
1496 (1.8)	30	3900	396	429	396 385*	418 349*	5/9 (92/90)
1497 (1.8)	60	3900	421	429	386 ---*	385 126*	18/34 (---/128)
1498 (1.8)	120	3900	442	438	306 0*	383 0*	68/28 (>219)

*Depletion zone dimensions.

ZrB_2 + 20 v/o SiC(A-8)

Test No. (Velocity-ft/sec)	Time (min)	T°F	L_o(mils) initial	D_o(mils) initial	L_f(mils) final	D_f(mils) final	d(mils) length/diam
383 (0.9)	60	3560	297	351	270 225*	314 287*	14/19 (36/32)*
389 (0.9)	60	3290	300	351	297 271*	348 328*	2/2 (15/12)*
398 (0.9)	60	3720	300	351	188 0*	202 0*	84/74 (>150)*
399 (0.9)	60	3735	300	351	150 0*	219 0*	75/64 (>150)*
430 (0.9)	60	3465	300	351	283 169*	342 281*	9/8 (68/56)*
432 (0.9)	60	3450	300	351	292 234*	337 327*	4/7 (32/62)*
437 (0.9)	60	3540	301	350	281 240*	336 344*	10/12 (31/42)*
438 (0.9)	60	3560	299	351	279 255*	336 281*	10/13 (22/36)*
631 (0.9)	60	3335	351	351	348 326*	346 332*	2/3 (6/10)*
635 (0.9)	60	3940	351	351	302 0*	256 0*	33/48 (>176)*
903 (0.9)	60	3575	333	350	296 245*	332 304*	19/9 (36/33)*
913 (0.9)	60	3865	333	350	167 0*	188 0*	83/121 (>167)*
918 (0.9)	60	3890	333	350	335 300*	344 328*	4/3 (17/14)*
1499 (1.8)	15	3518	345	426	389 347*	416 403*	5/5 (9/12)
1500 (1.8)	30	3518	364	426	349 334*	400 387*	8/9 (18/20)
1501 (1.8)	60	3518	424	426	385 364*	407 384*	20/9 (30/40)
1502 (1.8)	120	3518	403	426	367 323*	404 363*	18/11 (40/32)
1504 (1.8)	15	3518	346	426	332 322*	415 401*	7/6 (18/13)
1507 (1.8)	30	3600	377	426	350 329*	407 389*	14/16 (34/19)
1510 (1.8)	60	3600	383	426	376 345*	413 391*	9/7 (19/19)
1511 (1.8)	120	3600	406	426	361 332*	401 368*	13/13 (37/39)
1513 (1.8)	15	3700	362	426	349 324*	415 393*	10/6 (19/17)
1518 (1.8)	30	3700	373	426	351 331*	408 378*	11/11 (26/27)
1519 (1.8)	60	3700	404	426	383 340*	424 368*	11/9 (22/29)
1520 (1.8)	120	3700	441	426	411 391*	426 347*	10/10 (40/40)
1537 (1.8)	15	3850	492	438	466 468*	496 539*	13/17 (42/50)
1538 (1.8)	30	3850	501	438	463 377*	376 285*	19/31 (62/74)
1539 (1.8)	60	3850	486	438	482 391*	384 271*	42/86 (98/83)
1540 (1.8)	120	3848	506	438	ALL GONE		>219 (>219)

*Depletion zone dimensions.

TABLE 4 (CONT)

SUMMARY OF AIR OXIDATION RESULTS FOR $HfB_{2.1}$+20v/oSiC(A-7), $ZrB_{2.1}$+20v/oSiC(A-8), $HfB_{2.1}$+35v/oSiC(A-9) AND ZrB_2 + 14v/oSiC+30v/oC(A-10)

$HfB_{2.1}$ + 35 v/o SiC (A-9)

Test No. (Velocity-ft/sec)	Time (min)	T°F	L_o(mils) initial	D_o(mils) dimensions	L_f(mils) final	D_f(mils) dimensions	d(mils) length/diam
368 (0.9)	60	3270	299	351	297 ---	348 336*	1/2 (-/8)*
383 (0.9)	60	3560	299	352	286 230*	350 253*	7/1 (38/46)*
388 (0.9)	60	3810	299	351	294 0*	347 0*	3/2 (>150)*
431 (0.9)	60	3900	299	351	283 0*	325 0*	8/13 (>180)*
443 (0.9)	60	3840	300	350	297 146*	349 204*	2/1 (77/73)*
484 (0.9)	60	3270	300	350	294 286*	345 337*	3/3 (7/7)*
499 (0.9)	60	3595	299	351	291 191*	348 230*	4/2 (54/60)*
503 (0.9)	60	3670	300	350	283 181*	348 271*	9/1 (40/40)*
511 (0.9)	60	3760	300	350	295 84*	344 ---	3/3 (108/--)*

ZrB_2 + 14 v/o SiC + 30 v/o C (A-10)

Test No. (Velocity-ft/sec)	Time (min)	T°F	L_o(mils) initial	D_o(mils) dimensions	L_f(mils) final	D_f(mils) dimensions	d(mils) length/diam
1128 (0.9)	60	3526	401	351	356 301*	294 247*	23/28 (50/52)*
1129 (0.9)	60	2941	401	351	399 399*	347 347*	1/2 (1/2)*
1130 (0.9)	60	3144	401	351	396 388*	347 338*	3/2 (7/7)*
1131 (0.9)	60	3724	401	351	318 0*	238 0*	44/57 (>176)*
1132 (0.9)	60	3335	402	351	378 354*	340 317*	12/6 (24/17)*
1133 (1.8)	60	3232	401	351	396 376*	344 321*	3/5 (13/15)*
1134 (1.8)	60	3427	401	351	365 350*	313 298*	8/9 (26/27)*
1135 (1.0)	60	3042	400	351	398 392*	349 344*	1/1 (4/4)*
1136 (1.8)	60	3623	401	351	250 149*	212 120*	76/70 (126/110)*
1137 (1.8)	60	3524	657	438	530 498*	409 377*	14/15 (30/31)*
1138 (1.8)	60	3738	544	438	472 335*	308 236*	36/66 (56/101)*
1139 (1.8)	60	3913	544	438	ALL GONE		>219 (>219)*
1259 (1.8)	60	1806	431	418	426	418	3/0
1260 (1.8)	60	2204	427	416	430	415	-3/1
1246	60	2800	479	434	476	431	2/2
1546 (1.8)	15	3500	500	440	266	401	17/20
1547 (1.8)	30	3400	504	440	231	364	37/38
1548 (1.8)	60	3500	400	351	346	279	27/36
1549 (1.8)	120	3500	383	439	252	302	66/69
1551 (1.8)	30	3650	339	432	295	343	42/44
1552 (1.8)	15	3650	199	438	169	409	17/14
1553 (1.8)	60	3650	401	351	315	244	43/54
1554 (1.8)	120	3650	496	440	94	155	201/143
1555 (1.8)	15	3764	328	440	306	420	11/10
1556 (1.8)	30	3764	401	350	382	321	15/10
1557 (1.8)	60	3764	389	439	**	**	--/--
1558 (1.8)	120	3764	566	438	ALL GONE		>219

*Depletion zone dimensions

**Specimen broke prior to measurement

TABLE 5

SUMMARY OF AIR OXIDATION RESULTS FOR BORIDE Z(A-5), $HfB_{2.1}$(A-6), RVA(B-5), PG(B-6), BPG(B-7), PT0178(B-9) AND AXF-5Q Poco (B-10)

BORIDE Z(A-5)

Test No. (Velocity-ft/sec)	Time (min)	T°F	L_o(mils) initial dimensions	D_o(mils)	L_f(mils) final dimensions	D_f(mils)	d(mils) length/diam
1166 (1.8)	60	3920	523	491	101	95	311/198
1167 (1.8)	60	2984	297	488	287	477	5/4
1168 (1.8)	60	3245	312	490	291	467	11/12
1169 (1.8)	60	3454	383	488	356	453	14/16
1174 (1.8)	60	3628	373	490	327	434	23/28
1179 (1.8)	60	3736	513	491	389	287	62/52
1284 (1.8)	60	3124	479	490	480	491	-1/-1
1285 (1.8)	60	2806	555	490	549	491	3/-1

$HfB_{2.1}$(A-6)

Test No. (Velocity-ft/sec)	Time (min)	T°F	L_o(mils) initial dimensions	D_o(mils)	L_f(mils) final dimensions	D_f(mils)	d(mils) length/diam
321 (0.9)	60	3295	300	350	277	327	12/12
329 (0.9)	60	3205	302	351	280	329	11/11
338 (0.9)	60	3690	301	351	167	179	67/86
349 (0.9)	60	3090	288	351	248	342	5/5
351 (0.9)	60	3090	267	352	259	341	4/6
360 (0.9)	60	3100	281	351	249	340	6/6
363 (0.9)	60	3270	281	352	260	327	11/13
366 (0.9)	60	3285	258	351	235	327	12/12
367 (0.9)	60	3490	266	352	178	261	44/46
369 (0.9)	60	3490	281	351	201	278	40/37
428 (0.9)	60	3670	281	351	157	188	62/82
455 (0.9)	60	3450	300	350	266	310	17/20
456 (0.9)	60	3450	301	351	266	298	18/27
468 (0.9)	60	3470	300	350	253	297	24/27
507 (0.9)	60	3670	300	350	151	176	75/87
510 (0.9)	60	3730	300	350	192	207	54/72
1180 (0.9)	60	3072	353	352	343	338	5/7
1181 (0.9)	60	3279	353	352	328	324	12/14
1182 (0.9)	60	3450	353	352	315	289	19/33
1183 (0.9)	60	3573	352	352	274	247	39/53
1184 (0.9)	60	3081	350	351	333	331	9/10
1185 (0.9)	60	3450	350	351	300	298	25/27
1186 (0.9)	60	3281	350	351	310	306	20/23
1187 (0.9)	60	3637	350	351	245	229	53/61
1221 (0.9)	60	3092	476	439	467	---	5/--
1222 (0.9)	60	3278	474	437	449	402	13/13
1223 (0.9)	60	3440	481	439	416	396	33/22
1224 (0.9)	60	3627	484	424	332	309	62/58

RVA (B-5)

Test No. (Velocity-ft/sec)	Time (min)	T°F	L_o(mils) initial dimensions	D_o(mils)	L_f(mils) final dimensions	D_f(mils)	d(mils) length/diam
146 (0.9)	10	2851	493	488	331	319	81/85
147 (0.9)	10	3119	493	487	314	322	90/83
148 (0.9)	10	3470	505	486	349	366	78/60
150 (0.9)	10	3884	511	486	335	332	88/77
152 (0.9)	10	4288	513	487	330	323	92/82
173 (3.6)	10	3794	508	488	241	274	132/107
195 (0.9)	10	2858	513	487	420	342	47/73
196 (1.8)	10	2813	528	486	427	390	51/48
197 (3.6)	10	2795	515	487	407	---	54/--
198 (7.2)	10	2813	538	487	325	213	106/137
199 (9.0)	10	2786	524	486	286	179	119/154

PG (B-6)

Test No. (Velocity-ft/sec)	Time (min)	T°F	L_o(mils) initial dimensions	D_o(mils)	L_f(mils) final dimensions	D_f(mils)	d(mils) length/diam
140 (0.9)	10	2795	531	486	493	427	19/30
141 (0.9)	10	3182	546	486	488	426	29/30
142 (0.9)	10	3515	560	487	483	408	38/40
151 (0.9)	10	3875	562	486	428	421	67/33
153 (0.9)	10	4190	568	487	389	392	90/48
161 (3.6)	10	3677	570	486	398	399	86/44
200 (0.9)	10	2876	555	487	518	434	19/27
201 (1.8)	10	2828	558	488	510	357	24/14
202 (3.6)	10	2810	548	484	490	363	23/12
203 (7.2)	10	2786	513	481	437	316	43/86
204 (9.0)	10	2939	517	487	388	327	97/80
1272 (1.8)	10	3180	563	486	468	373	51/57
1273 (1.8)	10	3480	590	486	[illegible]	460	[illegible]

BPG (B-7)

Test No. (Velocity-ft/sec)	Time (min)	T°F	L_o(mils) initial dimensions	D_o(mils)	L_f(mils) final dimensions	D_f(mils)	d(mils) length/diam
143 (0.9)	10	2831	500	486	438	423	36/32
144 (0.9)	11	3144	500	484	417	418	43/36
148 (0.9)	10	3515	501	488	468	396	47/46
149 (0.9)	10	3839	501	488	376	384	64/52
154 (0.9)	10	4190	502	487	437	443	33/22
174 (3.6)	10	3735	500	486	426	378	40/104
206 (0.9)	10	2871	503	486	461	411	21/40
207 (1.8)	10	2884	504	486	467	415	19/36
208 (3.6)	10	2841	504	486	469	371	23/58
209 (7.2)	10	2884	491	485	410	349	41/68
210 (9.0)	10	2812	514	485	469	343	27/71
1276 (1.8)	10	3100	506	483	407	407	50/38
1277 (1.8)	10	3407	546	486	396	355	75/66
1278 (1.8)	10	3784	565	486	404	360	81/59

PT0178 (B-9)

Test No. (Velocity-ft/sec)	Time (min)	T°F	L_o(mils) initial dimensions	D_o(mils)	L_f(mils) final dimensions	D_f(mils)	d(mils) length/diam
1059 (1.8)	10	3030	489	496	ALL GONE		>239
1060 (1.8)	10	2760	453	491	No Measurements		200
1061 (1.8)	5	2856	443	496	321	366	61/75
1062 (1.8)	5	3083	441	496	285	334	78/81
1063 (1.8)	5	3360	435	496	280	329	78/84
1065 (1.8)	5	3641	438	496	369	336	63/81
1066 (1.8)	5	3741	436	497	291	334	68/71
1068 (0.9)	5	3027	440	496	346	382	48/57
1077 (0.9)	5	3402	397	496	296	358	51/52
1180 (7.2)	5	3184	400	497	244	296	114/103
1279 (0.9)	5	3484	408	496	276	349	65/74
1280 (7.2)	5	3164	447	497	211	[illegible]	[illegible]

Poco Graphite (AXF-5Q)(B-10)

Test No. (Velocity-ft/sec)	Time (min)	T°F	L_o(mils) initial dimensions	D_o(mils)	L_f(mils) final dimensions	D_f(mils)	d(mils) length/diam
1070 (1.8)	10	2712	304	502	281	311	48/47
1071 (1.8)	10	3013	415	502	220	292	98/98
1072 (1.8)	10	3125	403	501	214	296	134/114
1073 (1.8)	10	3480	404	500	249	292	121/196
1074 (1.8)	10	3436	460	502	237	206	117/149
1075 (7.2)	10	2784	403	502	294	230	128/134
1076 (7.2)	10	3004	419	503	240	[illegible]	130/207
1077 (7.2)	5	3335	416	502	ALL GONE		>207
1274 (1.8)	10	3000	393	502	134	[illegible]	104/131
1275 (1.8)	10	3180	467	502	280	355	94/75

TABLE 6

SUMMARY OF AIR OXIDATION RESULTS FOR Si/RVC(B-8), HfC+C(C-11), ZrC+C(C-12) AND KT-SiC(E-14)

Si/RVC (B-8)

Test No. (Velocity-ft/sec)	Time (min)	T °F	L_o(mils)	D_o(mils)	L_f(mils)	D_f(mils)	d(mils)
770 (1.0)	60	3048	402	516	380	488	12/4
771 (1.0)*	60	3212	420	517	Too Distorted to Measure		
780 (1.0)*	15	3486	409	514	ALL GONE		>205
781 (1.0)*	15	3444	428	516	ALL GONE		>214
845 (1.0)	120	2994	420	518	393	474	14/23
846 (1.0)	4 x 30	2976	420	511	406	501	7/5
1048 (1.0)	60	2806	429	509	414	512	8/-2
1049 (1.0)	60	2847	426	514	418	493	4/8
1050 (1.0)	60	2943	410	511	398	496	6/8
1051 (1.0)	60	3008	426	514	393	499	15/8
1052 (1.0)	60	3050	408	511	390	515	9/-2
1053 (1.0)**	60	3121	407	503	251	499	156/2
1054 (1.0)*	15	3188	420	504	ALL GONE		>210
1101 (1.0)+	4 x 30	3098	414	515	....	....	---/---
1102 (1.0)**	120	3102	406	513	228	500	139/7
1103 (1.0)	30	3108	420	509	397	485	12/12
1104 (1.0)	60	3108	407	511	388	507	10/2
1105 (1.0)	15	3108	409	513	391	501	6/9
1110 (1.0)	15	3020	399	507	387	486	6/10
1111 (1.0)	30	3016	414	506	418	485	7/11
1112 (1.0)	60	3016	414	504	397	509	9/9
1113 (1.0)	120	3016	407	510	401	514	3/-2

*Coating failure.
**Partial coating failure.
+Coating failed on fourth cycle.

ZrC + C (C-12)

Test No. (Velocity-ft/sec)	Time (min)	T °F	L_o(mils)	D_o(mils)	L_f(mils)	D_f(mils)	d(mils)
976 (1.0)	60	3267	380	452	257	308	62/72
981 (0.9)	60	3484	469	452	357	335	81/59
982 (0.9)	60	3679	440	452	390	328	70/64
983 (0.9)	60	3982	470	452	301	269	85/102
984 (0.9)	60	4001	455	452	277	248	89/105
985 (0.9)	60	4084	435	452	185	175	125/139
988 (1.0)	60	3058	474	452	271	295	92/77
992 (1.0)	60	1193	477	453	425	342	26/51
993 (1.0)	60	1719	400	464	346	309	27/78
994 (1.0)	60	3444	278	464	188	164	45/80
995 (1.0)	60	2238	475	464	364	309	56/78
996 (1.0)	60	3630	278	464	160	116	59/74
997 (1.0)	60	2719	396	464	276	308	60/78
998 (1.0)	60	3678	390	464	233	190	79/92
999 (1.0)	60	4070	471	464	338	188	118/138
1031 (7.2)	60	3465	497	439	385	328	86/86
1035 (7.2)	60	3681	397	439	267	316	65/62
1037 (7.2)	60	3871	489	440	302	334	78/77
1119 (1.0)	15	3389	365	443	319	394	23/25
1120 (1.0)	4 x 30	3396	419	439	298	308	61/67
1121 (1.0)	30	3393	413	440	345	372	34/68
1122 (1.0)	60	3389	409	440	269	344	45/48
1123 (1.0)	120	3389	407	441	326	326	64/68
1124 (1.0)	15	3401	413	440	378	391	19/23
1125 (1.0)	30	3407	398	439	338	361	30/39
1126 (1.0)	60	3407	379	440	370	318	55/61
1127 (1.0)	120	3407	468	439	278	285	93/92
1129 (1.0)	240	2804	483	464	....	....	230*
1130 (1.0)	60	2804	432	463	290	291	71/84
1131 (1.0)	30	2804	389	463	312	384	39/40
1132 (1.0)	15	2804	395	463	363	392	28/31
1418 (1.0)	15	3100	370	427	304	321	33/33
1417 (1.0)	30	3100	344	426	260	323	43/52
1418 (1.0)	60	3100	350	426	183	238	84/94
1419 (1.0)	120	3100	369	426	196	237	87/98
1420 (1.0)	15	3800	364	439	321	378	22/31
1421 (1.0)	30	3800	401	463	292	329	55/62
1422 (1.0)	60	3800	459	463	278	282	91/91
1423 (1.0)	120	3800	483	464	178	194	153/134

*Estimate

HfC + C (C-11)

Test No. (Velocity-ft/sec)	Time (min)	T °F	L_o(mils)	D_o(mils)	L_f(mils)	D_f(mils)	d(mils)
971 (1.0)	60	3684	486	478	394	412	31/32
972 (1.0)	60	3682	388	478	368	407	33/33
973 (1.0)	60	3879	474	478	184	378	48/50
974 (1.0)	60	3884	491	478	398	360	46/58
975 (1.0)	60	3833	481	476	380	361	51/68
986 (1.0)	60	4006	491	478	388	388	53/60
987 (1.0)	60	4064	441	478	312	344	65/66
1080 (1.0)	60	1190	484	489	483	458	1/1
1081 (1.0)	60	1734	484	489	394	352	45/54
1083 (1.0)	60	2232	484	489	394	347	45/56
1084 (1.0)	60	2788	483	489	347	333	48/43
1024 (7.2)	60	3459	488	485	338	326	62/68
1026 (7.2)	60	3794	481	486	370	380	49/53
1027 (7.2)	60	3907	488	485	367	337	48/59
1030 (1.0)	60	1212	448	447	440	447	1/0
1106 (1.0)	15	3592	388	483	341	394	21/30
1107 (1.0)	30	3691	417	483	383	385	32/34
1108 (1.0)	60	3691	447	483	370	373	39/40
1109 (1.0)	120	3592	498	483	389	335	53/59
1114 (1.0)	4 x 30	3592	418	483	296	339	50/57
1115 (1.0)	15	3782	389	482	342	398	24/27
1116 (1.0)	30	3832	444	483	399	384	34/34
1117 (1.0)	60	3792	477	483	381	374	48/60
1118 (1.0)	120	3792	506	483	404	382	51/51
1234 (1.0)	15	2804	433	483	388	397	23/28
1235 (1.0)	30	2794	389	483	290	377	35/38
1236 (1.0)	60	2804	434	483	332	327	51/66
1237 (1.0)	120	2804	449	483	239	200	105/127
1424 (1.0)	15	3200	384	427	336	368	24/30
1425 (1.0)	30	3200	358	427	289	330	35/49
1426 (1.0)	60	3200	346	427	256	266	55/81
1427 (1.0)	120	3200	352	426	201	242	76/92
1428 (1.0)	15	4000	382	427	285	368	34/30
1429 (1.0)	30	4002	375	426	295	349	40/39
1430 (1.0)	60	4000	381	427	240	295	71/66
1431 (1.0)	120	4000	367	427	183	244	92/92

KT-SiC (E-14)

Test No. (Velocity-ft/sec)	Time (min)	T °F	L_o(mils)	D_o(mils)	L_f(mils)	D_f(mils)	d(mils)
240 (0.9)	60	3191	503	488	503	486	0/1
247 (0.9)	60	2984	489	490	486	491	3/-1
248 (0.9)	60	2876	506	490	504	490	1/0
260 (0.9)	60	3290	483	491	477	489	3/1
261 (0.9)	60	3497	487	489	356	304	66/43
262 (0.9)	60	3380	491	489	480	460	6/15
571 (1.8)	60	3450	487	490	451	449	18/21
570 (1.8)**	9	3640	498	490	Rapid attack + melting		
575 (1.8)**	22	3610	505	488	Rapid attack + melting		
658 (1.8)*	15	3470	504	489	482	468	26/16
686 (1.8)*	30	3464	508	489	No Measurements		
657 (1.8)*	60	3470	511	489	320	286	96/102
656 (1.8)*	120	3470	519	489	ALL GONE		>245
869 (1.8)	120	3813	504	489	398	452	53/19
871 (1.8)	120	3446	502	490	462	410	20/40
870 (1.8)	4 x 30	3394	488	491	400	402	44/45
1170 (1.8)	15	3393	472	490	458	476	7/7
1171 (1.8)	30	3393	503	490	490	472	7/9
1172 (1.8)	60	3393	475	491	449	470	13/11
1173 (1.8)	120	3391	523	488	496	460	14/14
1175 (1.8)	15	3482	507	490	483	460	12/15
1176 (1.8)	30	3482	510	490	502	473	4/9
1177 (1.8)	60	3482	511	490	469	427	21/32
1178 (1.8)	120	3482	561	490	496	336	33/77
1328 (1.8)	15	3200	182	491	171	490	6/1
1329 (1.8)	30	3200	240	489	271	491	-16/-1
1330 (1.8)	60	3200	256	489	252	490	2/-1
1331 (1.8)	120	3200	290	488	289	488	1/0
1337 (1.8)	15	3400	259	488	256	484	2/2
1338 (1.8)	30	3400	284	486	275	477	9/5
1339 (1.8)	60	3400	299	490	286	465	7/13
1340 (1.8)	120	3400	356	488	298	456	29/16
1350 (1.8)	15	3491	297	490	268	464	15/13
1351 (1.8)	30	3500	405	490	373	442	16/14
1352 (1.8)	60	3500	359	485	298	394	34/46
1353 (1.8)	120	3500	535	489	362	333	87/71

**Inserted into hot furnace.
*Simultaneous run in large furnace.

TABLE 7

SUMMARY OF AIR OXIDATION RESULTS FOR JTA(D-13) AND JT0992(F-15)

JTA (D-13)

Test No. (Velocity-ft/sec)	Time (min)	T°F	L_o(mils)	D_o(mils)	L_f(mils)	D_f(mils)	d(mils)
			Initial Dimensions		Final Dimensions		Length/Diam.
219 (0.9)	60	3709	475	489	ALL GONE		>238
228 (0.9)	60	4081	465	488	ALL GONE		>233
230 (0.9)	60	3542	507	489	314	200	97/145
241 (0.9)	60	3709	537	489	ALL GONE		>245
244 (0.9)	60	3272	508	489	446	432	30/29
251 (0.9)	70	3494	502	489	ALL GONE		>245
276 (0.9)	60	3587	404	488	-10	---	-237/--
302 (1.8)	60	3402	490	488	272	264	109/112
336 (0.9)	60	3232	419	488	293	355	63/67
337 (3.6)	60	3237	494	488	354	330	70/79
339 (7.2)	60	3247	384	488	164	246	108/121
362 (1.8)	60	3649	816	991	542	671	137/210
364 (1.8)	60	3973	850	990	475	572	188/209
378 (1.8)	60	4046	817	993	587	607	115/193
548 (1.8)*	15	3364	414	497	371	431	22/33
549 (1.8)*	30	3361	412	498	311	342	51/78
550 (1.8)*	60	3361	432	498	164	224	133/137
551 (1.8)*	120	3361	432	498	ALL GONE		>216
581 (1.8)°	15	3247	314	488	226	374	44/57
582 (1.8)°	30	3247	405	498	200	252	103/123
583 (1.8)°	60	3247	406	498	-70	---	-146/--
584 (1.8)°	120	3247	411	498	ALL GONE		>205
667 (1.8)°	15	3575	783	993	714	892	35/51
668 (1.8)°	30	3575	796	993	648	706	74/144
669 (1.8)°	60	3600	853	993	484	663	118/165
670 (1.8)°	120	3600	972	993	573	410	200/292
710 (1.8)	60	3035	381	488	360	472	11/8
713 (1.8)	60	3015	396	490	376	475	10/8
714 (1.8)	60	3125	401	490	381	470	10/10
715 (1.8)	60	3204	387	489	317	447	30/21
716 (1.8)	60	3254	407	489	357	421	25/34
717 (1.8)	60	3910	392	489	ALL GONE		>196
720 (1.8)	60	3912	389	491	ALL GONE		>195
723 (1.8)	60	3990	402	488	ALL GONE		>201
788 (1.8)**	15	3240	396	513	356	433	20/40
789 (1.8)**	30	3255	402	514	237	263	83/126
790 (1.8)**	60	3240	392	515	150	166	122/175
791 (1.8)**	120	3235	418	515	ALL GONE		>209
859 (1.8)	60	1193	489	499	---	499	---/0
					---	453+	(---/23)+
860 (1.8)	60	1701	486	498	476	500	-9/-1
					348+	390+	(64/59)+
861 (1.8)	60	2199	451	499	455	512	-4/-7
					432+	477+	(10/11)+
862 (1.8)	60	2703	461	500	462	506	-1/-3
					464+	480+	(9/10)+
907 (1.8)	120	2905	486	489	369	468	59/11
944 (1.8)	120	2894	511	489	498	480	6/5
945 (1.8)	4 x 30	2894	395	488	378	464	14/12
1042 (1.8)	60	3096	489	524	446	480	7/22
1043 (1.8)	60	3084	458	524	435	476	12/24
1082 (1.8)	15	3054	345	435	335	428	5/4
1083 (1.8)	30	3054	352	438	338	430	7/4
1084 (1.8)	60	3054	416	436	396	427	10/4
1085 (1.8)	15	3250	312	436	278	410	17/13
1086 (1.8)	30	3250	309	434	278	408	16/13
1087 (1.8)	60	3258	403	436	350	372	26/32
1088 (1.8)	15	3350	325	438	280	394	24/22
1089 (1.8)	30	3350	319	439	251	355	34/42
1090 (1.8)	60	3350	387	435	329	351	29/42
1403 (1.8)	15	3200	167	489	125	427	21/9
1404 (1.8)	30	3122	390	489	368	467	11/11
1405 (1.8)	60	3200	414	487	351	434	32/27
1406 (1.8)	120	3200	401	488	344	425	29/32
1407 (1.8)	15	3400	209	489	168	423	21/33
1408 (1.8)	30	3400	404	489	341	407	32/41
1409 (1.8)	60	3400	397	489	110	265	140/112
1410 (1.8)	120	3400	404	490	290	330	57/80
1411 (1.8)	15	3500	331	437	220	337	56/50
1412 (1.8)	30	3500	400	437	241	243	80/97
1413 (1.8)	60	3500	525	438	299	173	113/133
1414 (1.8)	120	3500	531	435	ALL	GONE	>218
1416 (1.8)	30	3200	314	433	242	360	36/37

+Depletion zone dimensions.
The symbols *,**,O all denote simultaneous runs in large furnace.

JT0992 (F-15)

Test No. (Velocity-ft/sec)	Time (min)	T°F	L_o(mils)	D_o(mils)	L_f(mils)	D_f(mils)	d(mils)
			Initial Dimensions		Final Dimensions		Length/Diam.
223 (0.9)	60	3784	491	488	430	160	36/64
224 (0.9)	60	4086	533	488	ALL GONE		>244
225 (0.9)	60	3156	495	488	490	478	3/5
226 (0.9)	60	3806	527	488	485	441	21/24
227 (0.9)	60	3003	550	490	331	218	110/136
249 (0.9)	60	3848	500	489	ALMOST GONE		~245
250 (0.9)	60	3969	489	489	ALL GONE		>245
252 (0.9)	60	3290	536	489	517	488	10/16
278 (0.9)	60	3785	543	490	317	164	113/163
279 (0.9)	60	3089	394	489	379	484	8/3
282 (0.9)	60	3016	389	488	362	484	2/2
284 (0.9)	60	3767	396	488	311	309	42/90
297 (1.8)	60	3705	520	489	427	423	47/33
298 (1.8)	60	3795	483	491	332	318	34/88
299 (1.8)	60	3862	394	489	ALL GONE		>196
319 (1.8)	60	3586	401	488	346	442	30/23
320 (3.6)	60	3594	419	489	345	410	37/40
326 (7.2)	60	3531	488	488	288	348	72/72
370 (1.8)	60	3949	1021	993	818	747	105/123
380 (1.8)	60	4035	926	993	650	782	133/121
520 (1.8)*	15	3476	396	499	382	484	7/7
521 (1.8)*	30	3476	392	479	339	444	27/26
522 (1.8)*	60	3476	397	488	346	428	26/37
523 (1.8)*	120	3476	396	498	314	408	41/46
566 (1.8)°	15	3603	390	487	348	431	24/28
567 (1.8)°	30	3603	393	488	334	404	30/42
568 (1.8)°	60	3623	488	486	346	384	28/50
569 (1.8)°	120	3563	416	487	354	434	30/27
682 (1.8)	60	3585	366	485	309	324	29/83
683 (1.8)	60	3868	394	488	363	324	64/82
688 (1.8)	60	4055	394	499	ALL GONE		>250
705 (1.8)	60	3912	393	489	350	469	22/10
706 (1.8)	60	3862	401	488	394	486	4/1
707 (1.8)	60	3298	410	488	380	483	15/10
708 (1.8)	60	3900	397	487	ALL GONE		>199
711 (1.8)	60	3962	398	490	ALL GONE		>199
712 (1.8)	60	4000	398	488	ALL GONE		>199
808 (1.8)*	15	3540	390	489	363	447	14/21
809 (1.8)*	30	3515	480	489	364	410	28/36
810 (1.8)*	60	3520	404	488	354	362	26/63
811 (1.8)*	120	3515	390	490	305	363	43/64
817 (1.8)**	15	3616	371	487	319	430	26/29
818 (1.8)**	30	3616	371	489	294	352	38/66
819 (1.8)**	60	3616	408	489	252	287	78/101
820 (1.8)**	120	3616	409	489	138	150	136/166
846 (1.8)	60	1210	490	487	368	358	60/65
852 (1.8)	60	1690	500	489	242	238	129/127
853 (1.8)	60	2195	492	489	288	256	120/117
856 (1.8)	60	2710	491	488	370	333	60/78
914 (1.8)	4 x 30	3518	518	489	416	363	51/63
1375 (1.8)	15	3450	190	488	174	470	8/9
1376 (1.8)	30	3445	191	488	161	463	15/13
1378 (1.8)	60	3450	371	489	327	452	22/19
1380 (1.8)	120	3450	397	490	347	440	25/25
1381 (1.8)	15	3596	194	488	163	463	16/13
1383 (1.8)	30	3591	189	489	146	451	21/19
1384 (1.8)	60	3600	324	488	284	444	20/22
1386 (1.8)	120	3600	359	489	297	425	29/32
1391 (1.8)	15	3690	269	489	236	450	16/20
1392 (1.0)	30	3700	293	488	244	457	24/16
1393 (1.8)	60	3695	832	488	484	388	38/50
1394 (1.8)	120	3700	512	489	372	304	70/93

The symbols *,o,** all denote simultaneous runs in large furnace.

TABLE 8

SUMMARY OF AIR OXIDATION RESULTS FOR JT0981(F-16), WSi_2/W(G-18) AND Sn-Al/Ta-W(G-19)

JT0981 (F-16)

Test No. (Volts-Hr-T/Sec)	Time (Min)	T°F	L_o(mils)	D_o(mils)	L_f(mils)	D_f(mils)	d(mils)
233 (0.9)	60	2804	488	489	430	360	49/70
234 (0.9)	60	2802	485	489	472	472	7/9
237 (0.9)	60	2804	519	488	441	349	39/50
242 (0.9)	60	2804	488	486	ALL GONE		>243
243 (0.9)	60	2760	524	488	ALL GONE		>243
254 (0.9)	60	2801	474	488	386	407	44/41
256 (0.9)	60	2801	538	488	387	460	14/14
257 (0.9)	60	2805	491	487	487	458	32/35
258 (0.9)	60	2807	391	490	384	474	5/8
280 (0.9)	60	2803	401	489	389	477	6/6
281 (0.9)	60	2807	484	489	ALL GONE		>203
283 (0.9)	60	2804	414	489	350	373	38/58
288 (1.0)	60	2804	398	489	ALL GONE		>196
301 (1.0)	60	3410	437	489	367	418	35/56
310 (1.0)	60	3409	388	489	338	431	24/29
313 (0.9)	60	3411	514	490	471	484	22/18
315 (1.0)	60	3431	421	488	346	402	28/47
327 (1.0)	60	3803	999	994	858	794	72/100
328 (1.0)	60	3648	483	489	314	321	45/54
404 (1.0)	60	3760	487	488	ALL GONE		>204
407 (1.0)	60	3808	398	489	333	315	33/37
408 (1.0)	60	3435	482	487	399	431	12/36
409 (1.0)	60	3385	481	499	444	477	4/11
416 (1.0)*	15	3386	484	499	416	448	26/29
417 (1.0)*	30	3386	484	499	407	422	27/39
418 (1.0)*	60	3388	490	499	407	419	31/40
419 (1.0)*	120	3386	481	499	406	401	10/4
435 (1.0)°	15	3673	398	488	354	401	10/4
433 (1.0)°	30	3673	399	489	328	414	40/50
434 (1.0)°	60	3673	488	491	343	403	50/44
489 (1.0)	15	3785	437	499	314	338	44/51
490 (1.0)	30	3410	488	499	396	408	30/46
491 (1.0)	60	3807	469	499	ALL GONE		>130
700 (1.0)	15	3860	391	489	389	464	16/13
701 (1.0)	30	3850	416	489	397	451	10/19
704 (1.0)	60	3783	398	488	368	379	46/107
734 (1.0)	60	3648	830	991	696	772	72/110
735 (1.0)	60	3643	718	1017	991	894	64/88
736 (1.0)	60	3731	488	994	838	778	88/146
737 (1.0)	60	3788	1068	1023	844	734	21/17
784 (1.0)°	15	3371	396	488	388	489	27/27
785 (1.0)°	30	3389	414	489	360	438	38/48
786 (1.0)°	60	3398	409	489	333	396	50/63
787 (1.0)°	120	3398	414	489	314	363	36/50
788 (1.0)°°	15	3632	395	489	344	388	64/78
789 (1.0)°°	30	3632	384	489	337	340	>196
790 (1.0)°°	60	3632	407	488	ALL GONE		>212
791 (1.0)°°	120	3632	423	486	ALL GONE		107/121
823 (1.0)	60	1230	975	488	361	347	137/142
825 (1.0)	60	1780	818	489	366	208	147/163
826 (1.0)	60	2219	820	489	186	164	51/64
827 (1.0)	60	2700	496	485	394	350	57/70
842 (1.0)	4 x 30	3486	389	489	276	330	0/2
1346 (1.0)	15	3400	174	489	158	486	17/15
1347 (1.0)	30	3400	203	490	169	461	21/25
1348 (1.0)	60	3400	382	489	341	440	30/52
1349 (1.0)	120	3400	391	490	316	387	11/12
1358 (1.0)	15	3500	184	489	162	466	16/21
1359 (1.0)	30	3500	315	489	280	448	32/26
1360 (1.0)	60	3500	389	489	325	437	47/48
1361 (1.0)	120	3500	401	489	308	393	19/16
1362 (1.0)	15	3600	321	489	184	457	26/38
1363 (1.0)	30	3600	387	489	338	414	58/46
1364 (1.0)	60	3600	400	490	298	398	96/93
1365 (1.0)	120	3600	412	488	220	302	

The symbols *, **, ° all denote simultaneous runs in large furnace.

WSi_2/W (G-18)

Test No. (Volts-Hr-T/Sec)	Time (Min)	T°F	L_o(mils)	D_o(mils)	L_f(mils)	D_f(mils)	d(mils)
476 (1.8)	60	2896	529	504	526	512	2/-4
477 (1.8)	60	3109	509	504	509	503	0/1
478 (1.8)	60	3329	512	503	510	492	1/6
485 (1.8)*	60	3532	511	503	458	508	--/--
499 (1.8)*	93	3682	516	504	ALL GONE		>152
577 (1.8)*	60	3518	513	503	No Measurement		--/--
578 (1.8)*	60	3508	509	503	No Measurement		--/--
579 (1.8)*	60	3574	512	503	No Measurement		--/--
580 (1.8)	60	3450	510	503	494	486	6/9
671 (1.8)*	15	3448	501	504	498	464	2/10
672 (1.8)*	30	3448	509	503	508	488	1/8
673 (1.8)*	60	3448	510	503	510	489	0/7
674 (1.8)*	120	3448	511	504	510	488	1/8
687 (1.8)	60	3109	506	503	493	479	7/12
688 (1.8)	60	3434	516	503	510	468	3/21
749 (1.8)	60	3200	523	504	516	499	4/3
750 (1.8)	60	3200	510	504	498	503	8/1
751 (1.8)+	60	3416	531	504	No Measurements		
752 (1.8)	60	3421	506	504	495	496	9/7
753 (1.8)+	60	3505	490	504	No Measurements		
870 (1.8)	120	3410	513	505	510	479	2/13
887 (1.8)	4 x 30	3440	528	504	514	492	1/6
1044 (1.8)+	2 x 30	3511	509	504	No Measurements		
1045 (1.8)	4 x 30	3476	511	504	510	495	1/5
1145 (1.8)	15	3484	518	504	508	484	2/10
1146 (1.8)	30	3484	516	504	493	493	13/6
1147 (1.8)	60	3484	517	503	500	480	9/13
1148 (1.8)	120	3484	528	504	508	484	9/10

*Simultaneous run.
+Coating failure.

Sn-Al/Ta-W (G-19)

Test No. (Volts-Hr-T/Sec)	Time (Min)	T°F	L_o(mils)	D_o(mils)	L_f(mils)	D_f(mils)	d(mils)
390 (1.8)	60	2684	530	516	506	509	12/3
392 (1.8)	60	2718	512	519	492	511	10/6
394 (1.8)	60	2831	526	517	498	506	14/10
395 (1.8)	60	2930	516	515	501	501	8/7
397 (1.8)	60	3002	525	520	507	501	9/10
400 (1.8)	60	3092	508	516	490	506	8/8
439 (1.8)+	60	3173	522	517	342	204	--/--
693 (1.8)	60	3173	526	514	510	503	8/6
744 (1.8)+	60	3101	527	516	512	502	8/7
872 (1.8)+	20	3020	503	515	No Measurements		
877 (1.8)	120	2938	523	515	526	505	-2/5
883 (1.8)	4 x 30	2932	534	515	546	506	-6/6
1069 (1.8)	4 x 30	2990	518	516	527	502	-8/7
1140 (1.8)	15	2981	525	518	510	505	8/7
1141 (1.8)	30	2979	527	518	518	504	6/7
1142 (1.8)	60	2982	526	518	508	505	8/7
1143 (1.8)	120	2979	529	516	518	504	7/6
1192(1.8)	60	3207	522	519	505	505	9/7
1193 (1.8)+	27	3317	530	518	No Measurements		--/--

+Coating failure.

TABLE 9

SUMMARY OF AIR OXIDATION RESULTS FOR SiO_2-68.5%W(H-22), SiO_2-60%W(H-23), SiO_2-35%W(H-24) AND Hf-20Ta-2Mo(I-23)

SiO_2-68.5% W (H-22)

Test No (Velocity-ft/sec)	Time (min)	T°F	L_o(mils) initial	D_o(mils) dimensions	L_f(mils) final	D_f(mils) dimensions	d(mils) length/diam
1034 (1.8)	60	3276	503	507	297	505	3/1
1036 (1.8)	60	3490	328	507	325	501	2/3
1038 (1.8)	60	3691	335	507	328	492	4/8
1041 (1.8)	60	3924	282	507	206	476	38/16
1044 (1.8)	60	3837	327	507	300	465	14/16
1066 (1.8)	60	3998	325	507	187	*	*
1153 (1.8)	4 x 30	3834	469	508	514	444	78/32
1158 (1.8)	15	3682	264	508	257	497	4/6
1159 (1.8)	30	3682	284	509	280	500	2/5
1160 (1.8)	60	3682	339	509	328	499	6/5
1161 (1.8)	120	3682	373	508	344	479	18/15
1162 (1.8)	15	3839	209	509	178	500	17/5
1163 (1.8)	30	3839	220	509	169	496	26/7
1164 (1.8)	60	3839	265	508	171	489	48/16
1165 (1.8)	120	3829	262	509	187	463	38/25

*Specimen badly deformed due to viscous flow.

SiO_2-60%W (H-23)

Test No. (Velocity-ft/sec)	Time (min)	T°F	L_o(mils) initial	D_o(mils) dimensions	L_f(mils) final	D_f(mils) dimensions	d(mils) length/diam
619 (1.8)	60	3412	392	505	375	504	9/1
620 (1.8)	60	3618	400	505	No Measurements		
622 (1.8)	60	3618	391	505	349	499	11/1
640 (1.8)	60	3873	401	506	391	485	8/10
1023 (1.8)	60	3186	410	506	406	506	2/0
1025 (1.8)	60	3382	394	506	398	503	0/4
1029 (1.8)	60	3571	409	506	406	497	2/5
1032 (1.8)	60	3692	397	507	395	491	1/8
1042 (1.8)	60	3819	403	506	386	471	9/18
1043 (1.8)	60	3907	422	508	362	461	30/19
1067 (1.8)	60	4036	328	506	203	*	*
1144 (1.8)	4 x 30	3843	412	506	337	460	48/21
1149 (1.8)	15	3672	178	506	170	507	4/-1
1150 (1.8)	30	3672	193	506	181	504	6/1
1151 (1.8)	60	3672	192	506	184	498	5/6
1152 (1.8)	120	3672	206	506	178	497	6/5
1154 (1.8)	15	3846	173	506	156	488	9/4
1155 (1.8)	30	3846	188	506	161	495	4/6
1156 (1.8)	60	3846	438	506	430	491	4/8
1157 (1.8)	120	3846	506	506	518	498	-6/4
1239 (1.8)	60	2708	528	506	502	503	13/2
1240 (1.8)	60	2812	339	506	304	475	18/16
1241 (1.8)	60	1716	339	506	318	481	12/11
1242 (1.8)	60	2613	560	506	520	489	20/24
1243 (1.8)	60	1418	178	506	173	502	1/2
1281 (1.8)	60	3500	323	505	320	500	2/1
1282 (1.8)	60	3803	358	508	334	484	14/11

*Specimen badly deformed due to viscous flow.

SiO_2-35%W (H-24)

Test No. (Velocity-ft/sec)	Time (min)	T°F	L_o(mils) initial	D_o(mils) dimensions	L_f(mils) final	D_f(mils) dimensions	d(mils) length/diam
1040 (1.8)	60	3254	247	505	397	509	*
1045 (1.8)	60	3256	252	505	273	514	*
1046 (1.8)	60	3486	300	506	Melting		*
1047 (1.8)	60	1042	226	506	244	441	*

*Material deforms due to viscous flow at all temperatures studied.

Hf-20Ta-2Mo (I-23)

Test No. (Velocity-ft/sec)	Time (min)	T°F	L_o(mils) initial	D_o(mils) dimensions	L_f(mils) final	D_f(mils) dimensions	d(mils) length/diam
290 (0.9)	60	3220	401	500	367	473	17/14
291 (0.9)	60	3020	390	492	379	487	6/3
292 (0.9)	60	2886	402	503	389	495	7/4
293 (0.9)	60	3434	407	501	321	423	43/39
294 (0.9)	60	3886	447	503	60	---	204/---
296 (0.9)	60	3606	401	497	128	136	137/181
386 (1.2)	60	3821	393	501	80	---	187/---
414 (0.9)	60	3119	410	500	363	491	24/25
415 (0.9)	60	3318	409	501	346	416	32/45
413 (1.8)	60	3147	319	505	498	488	11/9
414 (1.8)	60	3196	319	490	469	424	28/33
415 (1.8)	60	3388	501	505	444	430	29/36
416 (1.8)	60	3386	503	492	449	394	27/30
417 (1.8)	120	3410	525	491	321	319	102/86
418 (1.8)	2 x 30	3417	407	507	297	374	55/67
621 (1.8)	4 x 30	3423	506	505	402	545	58/71
651 (1.8)*	15	3371	428	504	360	424	34/40
652 (1.8)*	30	3376	519	502	349	311	85/96
653 (1.8)*	60	3380	521	490	349	260	102/120
654 (1.8)*	120	3384	524	494	371	330	77/82
655 (1.8)	60	3542	401	498	353	306	74/96
656 (1.8)	60	3542	408	502	379	484	13/9
658 (1.8)	62	3620	411	501	196	276	108/113
659 (1.8)	60	3706	408	502	ALL GONE		>405
792 (1.8)**	15	3125	507	501	359	479	24/11
793 (1.8)**	30	3328	418	504	400	488	6/23
794 (1.8)**	60	3328	559	498	308	421	24/37
795 (1.8)**	120	3328	481	501	319	409	86/46
797 (1.8)	15	3440	706	504	631	409	37/48
798 (1.8)	30	3409	784	506	669	306	47/100
799 (1.8)	60	3409	743	508	601	281	72/112
800 (1.8)	120	3400	736	499	Too Distorted to Measure		
893 (1.8)	4 x 30	3318	810	505	269	344	121/81
927 (1.8)	60	1232	100	502	100	500	0/1
928 (1.8)	60	1728	94	503	90	498	2/3
929 (1.8)	60	2271	97	508	92	503	3/0
931 (1.8)	60	2707	95	509	84	468	6/21
1006 (1.8)	15	3400	243	512	213	490	19/11
1007 (1.8)	30	3400	114	504	370	469	21/19
1008 (1.8)	60	3400	466	511	378	407	47/52
1009 (1.8)	120	3400	564	507	446	406	51/59
1055 (1.8)	15	3479	419	503	381	448	19/28
1056 (1.8)	30	3479	447	501	393	446	21/28
1057 (1.8)	60	3479	452	504	376	371	38/67
1058 (1.8)	120	3479	582	503	408	396	87/84
1474 (1.8)	15	3450	479	501	436	342	22/25
1475 (1.8)	30	3450	481	503	427	329	27/32
1476 (1.8)	60	3450	495	507	406	270	45/59
1477 (1.8)	120	3450	498	500	ALL GONE		>195
1478 (1.8)	15	3430	503	500	432	317	36/37
1479 (1.8)	30	3435	509	500	402	241	54/75
1480 (1.8)	60	3435	495	508	77	96	209/146
1481 (1.8)	120	3448	517	500	ALL GONE		>195

*Simultaneous run.
**Simultaneous run.

TABLE 10

SUMMARY OF ARGON INERT TEST RESULTS

Material (Code)	Test No.	Time (Min)	T°F	L_o (mils)	D_o (mils)	L_f (mils)	D_f (mils)	d(mils)	Weight (grams)
M/RVC(B-6)									
	1233	60	3400	340	330	344	328	0/0	0.6161/0.6161
	1234	60	3574	338	330	338	328	0/0	0.6473/0.6318
	1237	60	3648	343	333	343	331	1/1	0.6649/0.6490
	1238	60	4001	347	331	347	321	1/9	0.6736/0.6477
PT6176(B-9)									
	1194	60	2998	448	498	448	498	0/0	---
	1196	60	3485	433	498	433	498	0/0	---
	1198	60	3798	416	498	416	498	0/0	---
	1201	60	4013	461	496	460	494	1/1	---
JTA(D-13)									
	1195	60	3507	424	489	425	489	-1/0	---
	1197	60	3798	417	490	418	490	-1/0	---
	1199	60	4013	410	489	410	489	0/0	---
	1200	60	4000	397	490	376	446	11/22	---
	1202	60	4176	388	490	396	491	-8/-1	---
JT6958(F-15)									
	1204	60	3503	386	489	389	486	1/1	5.3364/5.1482
	1206	60	3813	405	488	406	488	-1/0	5.3220/5.4875
	1208	60	4190	384	488	389	488	-1/0	4.7618/4.7166
	1210	60	4197	488	489	483	486	-1/2	5.4990/5.1939
JT6958(F-16)									
	1213	60	3600	484	489	485	489	-1/0	5.3339/5.4859
	1214	60	3949	389	490	389	490	0/0	5.3790/5.3120
	1215	60	4012	488	490	483	488	-1/2	5.7149/5.5963
	1216	60	4194	481	488	483	488	-1/3	5.5082/5.2793
WSi_2/W(G-16)									
	1203	60	3101	371	291	371	291	0/0	5.1784/5.1751
	1205	60	3288	371	313	371	313	0/0	6.0094/6.0044
	1207	60	3804	317	313	291	307	3/3	5.6137/5.4140
	1209	60	3990	264	307	265	305	-1/1	5.6141/5.3838
	1211	60	3998	272	298	274	286	-1/1	5.1237/4.4710
	1212	60	4018	264	312	267	319	-2/-4	5.7984/5.4078
SiO_2+40[a]/eW(M-23)									
	12187	60	3934	309	506	280	445	15/31	4.6481/5.4212
	12198	60	3992	313	504	237	43240	36/37	4.7963/5.3718
	12208	60	3812	339	504	328	48400	9/26	5.2330/4.4435
	1204	60	3000	367	504	366	508	1/0	4.1882/4.7360
	1247	60	3389	346	506	347	505	-1/1	5.4040/5.3083
	1248	60	3688	356	506	360	490	-3/8	5.8493/5.2315

[a] Loose tungsten particles on surface due to sublimation of SiO_2.

[aa] Specimen badly cracked.

TABLE 11

SUMMARY OF OXYGEN PICKUP, GAS ANALYSIS AND METALLOGRAPHIC DATA ON JTA(C-ZrB_2-SiC) (D-13) COMPOSITE

Oxidation No.	Initial Dimensions Diam./Height	Initial Surface Area Initial Weight (cm^2/gm)	T ϵ=0.75 at λ=0.65μ (^oF)	P_{O_2} Flow Rate (torr/ft/sec)	Exposure Time (min)	Weight Loss Carbon Consumed (gms/gms)
XXVIII-28	301/113	1.609/0.3887	2900	11.9/0.20	60	0.0828/0.0935
XXVIII-31	293/135	1.668/0.4380	3740	11.9/0.20	12*	------/0.059?
XXVIII-33	294/103	1.481/0.3227	2910	40.4/0.20	60	0.0716/0.0846
XXVIII-52	300/251	2.42 /0.8458	+++	41 /0.20	60	------/0.0525
XXVIII-60	300/278	2.59 /0.9591	**	149 /0.20	30	***/0.0479+
XXVIII-74	299/248	2.41 /0.8419	3663	149 /0.20	17	***/0.0263+
XXIX-8(D-13)	300/244	2.40 /0.8338	3663	149 /0.20	10	------/0.331
XXIX-12	300/262	2.50 /0.9021	3663	149 /0.20	12	------/0.344
XXIX-17	300/243	2.38 /0.8238	3663	149 /0.20	5	------/0.252
XXIX-20	300/253	2.45 /0.8594	3663	149 /0.20	11	------/0.197
XXIX-22	300/247	2.41 /0.8462	3614	149 /0.20	20	------/0.364

% Carbon Consumed	w_{CO_2} w_{CO} w_{O_2} 44 56 32	Oxidation No.	Calculated Recession Rate (mils/hr)	Observed Metallographically: Final Dimensions Diam./Height (mils)	Observed Metallographically: Recession Rate (mils/hr)
50	1.07/38.4/18.0	XXVIII-28	19.7	265/80	18/17
28.5	----/----/----	XXVIII-31	55.5++	225/70	160/170
54.8	5.70/32.4/10.0	XXVIII-32	19.7	244/68	25/18
13.0	----/----/----	XXVIII-52	6.4	255/189	23/31
10.4+	----/----/----	XXVIII-60	----	73/85	227/193
6.5+	----/----/----	XXVIII-74	----	All Gone	More than 500 mils/hr
83.0	----/----/----	XXIV-8(D-13)	370	---/---	---/---
74.0	----/----/----	XXIX-12	260	180/175	300/218
65.6	----/----/----	XXIX-17	500	234/209	396/204
47.8	----/----/----	XXIX-20	150	218/165	223/240
90.0	----/----/----	XXIX-22	220	149/104	226/216

* Signs of melting and possible reaction with ThO_2.

** Temperature varied between 3100°F and 3975°F.

*** Sample to badly oxidized to obtain weight change.

+Ascarite may be exhausted.

++Extrapolated based on linear rate.

+++Temperature dropped continuously from 3665°F to 2850°F.

TABLE 12

SUMMARY OF OXYGEN PICKUP, GAS ANALYSIS AND METALLOGRAPHIC DATA ON JT0992 (C-HfC-SiC) (F-15) COMPOSITE

Oxidation No.	Initial Dimensions Diam/Height	Initial Surface Area Initial Weight (cm^2/gm)	T ϵ=0.75 at λ=0.65μ (^oF)	P_{O_2} Flow Rate (torr/ft/sec)	Exposure Time (min)	Weight Loss Carbon Consumed (gms/gms)
XXVIII-35	298/117	1.609/0.6177	2900	10.3/0.2	15*	0.0100/0.0092
XXVIII-37	298/109	1.560/0.5725	2950	40.1/0.2	60	0.0107/0.0189
XXVIII-47	287/252	2.30 /1.2401	3470	40.5/0.2	60	***/0.1790
XXVIII-50	298/206	2.14 /1.0972	3550	40.5/0.2	60	***/0.1462
XXVIII-62	307/277	2.60 /1.4781	3580	149/0.2	31	***/0.0533

% Carbon Consumed	$\frac{w_{CO_2}}{44}$ / $\frac{w_{CO}}{56}$ / $\frac{w_{O_2}}{32}$ (gms x 10^{-4})	Oxidation No.	Calculated Recession Rate (mils/hr)	Observed Metallographically: Final Dimensions Diam/Height (mils)	Observed Metallographically: Recession Rate (mils/hr)
4.7	1.36/ 3.16/ 2.08	XXVIII-35	3.0**	295/116	1.0/ 3.0
10.4	2.72/ 6.50/ 3.53	XXVIII-37	3.4	296/105	1.0/ 2.0
30.0	99.5 /24.9 /63.4	XXVIII-47	14.7	204/185 Irr.Shape	42/34
41.8	- / - / -	XXVIII-50	-	103/- Irr.Shape	98/-
11.3+	- / - / -	XXVIII-62	-	0/0	>2"7

*Whisker formation.

**Extraploation based on parabolic rate law (actual rate may be lower).

***Sample too badly oxidized to determine weight loss.

+Ascarite may have been exhausted.

TABLE 13

SUMMARY OF OXYGEN PICKUP, GAS ANALYSIS AND METALLOGRAPHIC DATA ON JT0981 (C-ZrC-SiC) (F-16) COMPOSITE

Oxidation No.	Initial Dimensions Diam/Height	Initial Surface Area Initial Weight (cm^2/gm)	T $\epsilon = 0.75$ at $\lambda = 0.65\mu$ (^oF)	P_{O_2} Flow Rate (torr/ft/sec)	Exposure Time (min)	Weight Loss Carbon Consumed (gms/gms)
XXVIII-39	300/112	1.598/0.3961	2950	10.6/0.2	60	0.0274/0.0336
XXVIII-41	300/ 95	1.490/0.3380	2925	40.1/0.2	60	0.0153/0.0260
XXVIII-43	301/229	2.31 /0.8319	3558	10.7/0.2	60*	**
XXVIII-45	300/227	2.30 /0.8191	3547	40.5/0.2	60	**
XXVIII-64	296/225	2.24 /0.7816	3550	149 /0.2	45	**
XXIX - 1	295/261	2.44 /0.8993	3652	149 /0.2	40	**

111

% Carbon Consumed	$^wCO_2/44$	$^wCO/56$	$^wO_2/32$	Oxidation No.	Calculated Recession Rate (mils/hr)	Observed Metallographically: Final Dimensions Diam/Height (mils)	Observed Metallographically: Recession Rate (mils/hr)
	gms x 10^{-4}						
17.6	6.00/10.99/ 4.85			XXVIII-39	6.0	291/103	4.5/ 4.5
16.0	5.60/ 8.00/ 3.52			XXVIII-41	4.9	298/91	1.0/ 2.0
26.9	3.02/43.4 /10.3			XXVIII-43	13.5	260/205	21/12
72.4	113.8 /62.3 /85.1			XXVIII-45	47	Sample Melted	
11.9+	- / - / -			XXVIII-64	-	173/151	82/50
5.5+	- / - / -			XXIX - 1	-	- / -	- / -

*Temperature dropped to 2900°F during the last 20 minutes of the run.
**Sample was too badly oxidized to obtain weight changes.
+Ascarite may have been exhausted.

TABLE 14

SUMMARY OF OXYGEN PICKUP AND METALLOGRAPHIC DATA FOR WSi_2/W (G-18)

(WSi_2 Coating Initially 5 mils Thick)

Oxidation No.	Initial Dimensions Diam/Height	Initial Surface Area Initial Weight (cm^2/gm)	T $\epsilon = 0.60$ at $\lambda = 0.65\mu$ (^oF)	P_{O_2} Flow Rate (torr/ft/sec)	Exposure Time (min)	Weight Loss Oxygen Consumed (gms/gms)
XXVIII-54	309/174	2.05/3.7371	3465	Sample reacted with ThO_2 support rod on degassing.		
XXVIII-55	306/168	1.99/3.5356	3055	10.7/0.2	60	-----/0.006790
			3210		13	-----/0.000585
			3285		13	-----/0.000106
			3375		13	-----/0.003150
			3440		24	-----/0.032900
			3510		13	-----/0.0350
			3590		2	-----/------
			4045		18	-----/0.0793
			2995		13	-----/------

Calculated Recession (mils)	Calculated Recession Based on Equation	Oxidation No.	Observed Metallographically: Final Dimensions Diam/Height (mils)	Observed Metallographically: Recession (mils)	Comments
-----	----	XXVIII-54	----	----	Extensive Reaction
0.310	(11)	XXVIII-55			
0.013	(12)				
0.002	(12)				
0.060	(12)				
2.1	(8)				
2.2	(8)				
---	---				
5.1	(8)		272/141	17/13.5	Coating Failed
---	---				

TABLE 14 (CONT)

SUMMARY OF OXYGEN PICKUP AND METALLOGRAPHIC DATA FOR WSi_2/W (G-18)

(WSi_2 Coating Initially 5 mils Thick)

Oxidation No.	Initial Dimensions Diam/Height	Initial Surface Area Initial Weight (cm^2/gm)	T ϵ = 0.60 at λ = 0.65μ (°F)	P_{O_2} Flow Rate (torr/ft/sec)	Exposure Time (min)	Weight Loss Oxygen Consumed (gms/gms)
XXVIII-58	308/164	1.98/3.5030	3320	150/0.2	14	-----/0.01235
			3475		16	-----/0.00083
			3805		10	-----/0.716
XXVIII-66	307/118	1.69/2.9885	3370	149/0.2	13	0.469/0.424
XXVIII-68	309/183	2.11/3.8975	3280	149/0.2	55	0.188/0.421
XXVIII-70	298/157	1.84/3.0910	3355	10.6/0.2	90	0.781/0.386
XXVIII-72	313/159	2.00/3.4278	3410	10.6/0.2	60	0.458/0.281

Calculated Recession (mils)	Calculated Recession Based on Equation	Observed Metallographically: Oxidation No.	Final Dimensions Diam/Height (mils)	Recession (mils)	Comments
0.570	(11)	XXVIII-58			
0.018	(12)				
42.0	(8)		214/73	47/46	Coating Failed
31.8	(8)	XXVIII-66	158/128	75/--	Irregular Height (Failure)
18.1	(11)	XXVIII-68	251/143	29/20	Irregular Diam (Failure)
26.6	(8)	XXVIII-70	206/140	46/9	Coating Failed
17.8	(8)	XXVIII-72	252/127	32/16	Coating Failed

TABLE 15

SUMMARY OF OXYGEN PICKUP AND METALLOGRAPHIC DATA ON WSi_2/W (G-18) MATERIAL

Oxidation No.	Initial (Diam/Height) (mils)	Initial (Area/Weight) cm^2/gms	Temperature Time $^oF/min$ ($\epsilon_\lambda = 0.65 \approx 0.60$)	Oxidation Mode	Width of W_5Si_3 Zone (mils)
XXIX - 28*	300/268	----/5.4503	----/--	coating damaged during degassing	----
- 37*	308/264	2.62/5.6732	3070/60	protective	1.95
- 38*	307/259	2.58/5.5104	3180/40	protective	2.15
- 41*	307/249	2.50/5.2991	3280/60	protective	2.15
- 42*	310/253	2.57/5.5118	3380/60	protective	3.55
- 43*	308/257	2.57/5.5208	3460/60	onset of failure	----
- 44*	308/259	2.58/5.5630	3560/10	linear	----
- 45*	313/255	2.67/5.6551	3560/60	linear	----
- 46°	310/251	2.55/5.4632	3280/60	protective	2.75
- 48°	307/256	2.54/5.4227	3370/60	protective	3.55
- 52°	299/272	----/5.5034	3465/--	sample fell off mount	----
- 53°	300/262	2.49/5.2678	3465/60	protective	4.70
- 54°	306/248	----/5.2436	3550/--	sample overheated	----
- 56°	307/269	2.63/5.7858	3550/5	failure	----
- 57°	296/262	2.56/5.1660	3500/23	failure	----

*Oxygen pressure equal to 10 torr.
°Oxygen pressure equal to 149 torr.

TABLE 16

SUMMARY OF OXIDATION EXPERIMENTS OF IRIDIUM BASE ALLOYS

(0.53 atm O_2-0.47 atm He, flow rate = 0.2 ft/sec)

Alloy Test No.	Initial Height Diam. mils	Initial Weight gms	Melting Temperature °F (20)	Melting Temperature Carbon Present °F (20)	Oxidation+ Temperature °F	Exposure Time (min) Weight Loss (gms)	Surface Area in^2	Initial Rate of Oxidation mils/hr
Ir* XXVIII-1	111.2 252	2.0215	4430	4175	4030	40 0.2721	0.1875	5.9
Ir* XXVIII-5	91.5 236	1.4401	4430	4175	4030	38 0.2508	0.1544	7.0
Ir XXVIII-11	52.5 198.8	0.5489	4430	4175	3840	57 ------	0.0946	7.2
75Ir25Pt XXVIII-13	95.8 221.7	1.3522	3940	3800	3860	60 0.3120	0.1440	5.5
75Ir25Rh XXVIII-15	92.8 248	1.6064	4060	3865	3860	57 0.3415	0.1690	3.2
90Ir10Re XXVIII-17	105.6 224	1.5006	4425	4255	3860	19 0.2111	0.1527	5.4
75Ir12.5Rh 12.5Re XXVIII-20	107.8 230	1.6204	4450	4150	3860	24 0.0875	0.1609	6.8
75Ir25Os XXVIII-22	113.8 230	1.7192	4595	4370	3860	32 ------	0.1652	13.7
75Ir12.5Os 12.5Pt XXVIII-24	95.1 217	1.2857	4230	3980	3860	32 ------	0.1378	13.2
75Ir12.5Os 12.5Rh XXVIII-26	81.8 217.5	1.1000	4240	4055	3860	30 ------	0.1297	6.2

*Flow rate = 0.1 ft/sec.
+Based on emittance = 0.30 at $\lambda = 0.65\mu$.

TABLE 17

SUMMARY OF DIMENSIONAL CHANGES FOR IRIDIUM BASE ALLOYS

(0.53 atm O_2 - 0.47 atm He, flow rate = 0.2 ft/sec)

Alloy Test No.	Initial Height Diam. (mils)	T ϵ=0.30 at λ=0.65μ ^{o}F	Exposure Time (min)	Final Height Diameter (mils)	Calculated* Rate of Oxidation (mils/hr)	Observed** Rate of Oxidation (mils/hr)
75Ir25Pt XXVM-13	95.8 / 221.7	3860	60	86 / ----	5.5	4.8 / ---
75Ir25Rh XXVIII-15	92.8 / 248	3860	57	79 / 233	3.2	6.9 / 7.5
90Ir10Re XXVIII-17	105.6 / 224	3860	19	91 / 212	5.4	23 / 19
75Ir12.5Rh 12.5 Re XXVIII-20	107.8 / 230	3860	24	96 / 218	6.8	15 / ---
75Ir12.5 Os 12.5Pt XXVIII-24	95.1	3860	32	87 / ----	13.4	12.4 / ----
75Ir12.5 Os 12.5Pt XXVIII-26	81.8 / 217.5	3860	30	75 / ----	6.2	6.8 / ----

*Based on oxygen pickup.

**Based on initial and final dimensions.

TABLE 18

COMPARISON OF IRIDIUM OXIDATION RESULTS

T	P_{O_2} atm	Flow Rate ft/sec	Recession Rate mils/hr	Reference
3450	0.53	400.00	51.00	Cricione et. al. (23)
3970	0.53	0.20	7.20	Present Investigation
4040	0.20	0.03	0.28	Krier and Jaffee (24)
4040	0.02	0.25	1.20	Kuriakose, Kent and Margrave (25)
4040	0.20	1.71	15.00	Kuriakose, Kent and Margrave (25)
4040	0.19	200.00	22.00	Rexer (26)
4040	0.93	416.75	240.00	Rexer (26)
4050	0.53	equilibrium	510.00	Alcock and Hooper (27)
4030	0.53	0.10	6.5 ± 0.5	Present Investigation

TABLE 19

SPECTRAL EMITTANCE OF PLATINUM GROUP METALS (22)

(BARE SURFACE)

	ϵ at λ = 0.65μ	
Element	Solid	Liquid
Iridium	0.30	----
Palladium	0.33	0.37
Platinum	0.30	0.38
Rhodium	0.24	0.30
90 Pt-10Rh	0.27	----

UNCLASSIFIED

Security Classification

DOCUMENT CONTROL DATA - R & D

(Security classification of title, body of abstract and indexing annotation must be entered when the overall report is classified)

1. ORIGINATING ACTIVITY (Corporate author) ManLabs, Inc. 21 Erie Street Cambridge, Massachusetts 02139	2a. REPORT SECURITY CLASSIFICATION UNCLASSIFIED 2b. GROUP N/A

3. REPORT TITLE

Stability Characterization of Refractory Materials under High Velocity Atmospheric Flight Conditions, Part III Volume I: Experimental Results of Low Velocity Cold Gas/Hot Wall Tests

4. DESCRIPTIVE NOTES (Type of report and inclusive dates)

Technical Documentary Report, April 1966 to July 1969

5. AUTHOR(S) (First name, middle initial, last name)

Larry Kaufman
Harvey Nesor

6. REPORT DATE December 1969	7a. TOTAL NO. OF PAGES 118	7b. NO. OF REFS 27
8a. CONTRACT OR GRANT NO. AF33(615)-3859 b. PROJECT NO. 7312 Task 731201 c. 7350 Tasks 735001 and 735002 d.	9a. ORIGINATOR'S REPORT NUMBER(S) N/A 9b. OTHER REPORT NO(S) (Any other numbers that may be assigned this report) AFML-TR-69-84, Part III Volume I	

10. DISTRIBUTION STATEMENT

This document is subject to special export controls and each transmittal to foreign governments or foreign nationals may be made only with prior approval of the Air Force Materials Laboratory (MAMC), Wright-Patterson AFB, Ohio 45433.

11. SUPPLEMENTARY NOTES N/A	12. SPONSORING MILITARY ACTIVITY Air Force Materials Laboratory (MAMC) Air Force Systems Command Wright-Patterson Air Force Base, Ohio

13. ABSTRACT

Furnace oxidation results in flowing air at 0.9 to 7.2 ft/sec for times up to four hours at temperatures between 1150°C and 4200°F are presented for 30 candidate materials including the most refractory borides, carbides, boride composites, boride-graphite composites (JTA), JT composites, carbide-graphite composites, pyrolytic and bulk graphite, PT graphite, coated refractory metal/alloys, oxide-metal composites, oxidation-resistant refractory metal alloys and coated graphites. Temperature limits for coated materials, viscous flow of metal-oxide composites and effects of cyclic heating and cooling exposures are reported. Results are presented for exposures in flowing argon between 3000° and 4200°F. These data are complemented by the results of oxygen pickup and gas analysis tests on JT composites, silicide coated tungsten and a series of binary and ternary iridium-base alloys which were heated by induction in oxygen-helium mixtures flowing at 0.2 ft/sec. Failure conditions were established for the silicide coating on tungsten at oxygen partial pressures of 0.031 and 0.20 atmospheres.

This abstract is subject to special export controls and each transmittal to foreign governments or foreign nationals may be made only with prior approval of the Air Force Materials Laboratory (MAMC), Wright-Patterson Air Force Base, Ohio 45433.

DD FORM 1 NOV 68 1473 REPLACES DD FORM 1473, 1 JAN 64, WHICH IS OBSOLETE FOR ARMY USE.

UNCLASSIFIED

Security Classification

14. KEY WORDS	LINK A		LINK B		LINK C	
	ROLE	WT	ROLE	WT	ROLE	WT
oxidation						
refractory borides						
graphites						
JT composites						
hypereutectic carbide-graphite composites						
refractory metals						
coated refractory metals						
metal-oxide composites						
iridium coated graphites						
furnace tests						
flowing air						
temperatures between 1150° and 4200°F						
failure conditions						